Computational insights into charged dopant-vacancy defect complexes in graphane for nanotechnology applications

by

Hezekia Mapingire

submitted in partial fulfilment of the requirement

for the degree

Doctor of Philosophy (PhD) in Physics

in the Faculty of natural and Agricultural Sciences

University of Pretoria

Supervisor: Dr Refilwe Edwin Mapasha

17 February 2025

UNIVERSITEIT VAN PRETORIA
UNIVERSITY OF PRETORIA
YUNIBESITHI YA PRETORIA

UNIVERSITY OF PRETORIA

DECLARATION OF ORIGINALITY

This document must be signed and submitted with every essay, report, project, assignment, dissertation and/or thesis.

Full names of student: Hezekia mapingire

Student number: U29059195

Personnel number: U04408705

Declaration

1. I understand what plagiarism is and am aware of the University's policy in this regard.
2. I declare that this thesis is my own original work. Where other people's work has been used (either from a printed source, Internet or any other source), this has been properly acknowledged and referenced in accordance with departmental requirements.
3. I have not used work previously produced by another student or any other person to hand in as my own.
4. I have not allowed, and will not allow, anyone to copy my work with the intention of passing it off as his or her own.

SIGNATURE OF STUDENT.....

SIGNATURE OF SUPERVISOR.....

SIGNATURE OF HEAD OF DEPARTMENT.....

Declaration

I sincerely and truthfully declare that this thesis is my bona-fide original contribution that was carried out at Pretoria university from 2020 to 2024. This research was done under the supervision of Dr Refilwe Edwin Mapasha.

Acknowledgements

My sincere gratitude to the Almighty who gave me the strength to commence and finish this project. In God I have faith. I am greatly indebted to my supervisor Dr Refilwe Edwin Mapasha who guided and encouraged me all the way until I crossed the line. Thank you for your patience, wisdom and understanding. It was such an honour having you as my supervisor. Many thanks go to my wife, Memory Mapingire nee Machingauta. I will forever cherish your support and for being there with me all the way.

Contents

1 Introduction **13**

1.1 Significance of Research 14

1.2 Problem Identification 14

1.3 Research Aims and Objectives 15

1.4 Expected Research Output 17

1.5 Synopsis 17

2 Literature Review **19**

2.1 Graphene 19

2.2 Graphane 22

2.3 Defects in Graphane 27

2.3.1 Point defects 27

2.3.2 Formation energy 33

2.3.2.1 Hydrogen vacancy (V_H) 33

2.3.2.2 Carbon vacancy (V_C) 34

2.3.2.3 Carbon-hydrogen vacancy (V_{CH}) 34

2.3.3 U-parameter 35

2.3.4 Charge transition levels 36

2.3.5 Binding energy 37

2.3.6 Literature Review on: vacancy point defects, substitutional point defects and point defect complexes in graphane 37

3 Material Property Derivation 43

3.1 Wave Function Theory 43

3.1.1 Variational Principle 45

3.1.2 The Many-Body System Hamiltonian 45

3.2 Born-Oppenheimer Approximation 47

3.3 Hartree's Independent Electron Approximation 49

3.4 Hartree-Fock Approximation 50

3.4.1 Short-comings of the Hartree theory 50

3.4.2 The Slater Determinant 51

3.5 *ab initio* Density Functional Theory 53

3.5.1 Thomas-Fermi model 54

3.5.2 Hohenberg- Kohn Theorems (HK I and HK II) 54

3.5.2.1 Hohenberg and Kohn's First Theorem and Proof 55

3.5.2.2 Hohenberg and Kohn's Second Theorem and Proof . . . 58

3.5.3 Kohn-Sham Equations 59

3.6 Solving Kohn-Sham Equations Self-consistently 62

3.6.1 Symmetry transformation and Brillouin zone 63

3.6.2 Bloch's Theorem 66

3.6.3 Kinetic energy cut-off 67

3.6.4 Convergence testing 68

3.6.5 Pseudo-potential approximation 69

3.6.5.1 PKA Pseudo-potential 70

3.6.5.2 Norm-conserving Pseudo-potential 71

3.7 Local Density Approximation 73

3.7.1 Exchange and Correlation 74

3.7.2 Spin-free Local Density Approximation 76

3.7.3 Local Spin Density Approximation 77

3.7.4 Limitations of LDA/LSDA 78

3.8 Generalised Gradient approximation 78
3.9 Hybrid functionals 80

4 Results and Discussion: Published paper 1 82

5 Results and Discussion: Published paper 2 96

6 Results and Discussion: Published paper 3 112

7 Results and Discussion: Published paper 4 144

8 Further Discussion and Conclusion 160

8.1 Formation energy 160
8.2 U-parameter 164
8.3 Charge transition levels 166
8.4 Density of states 167
8.5 Charge distribution for nitrogen-vacancy complexes 168
8.6 Nitrogen-vacancy complexes binding energy 168
8.7 Li-doped divacancies in graphane 170
8.8 Summary 171
8.9 Challenges 174
8.10 Future work 175

List of Figures

2.1 Graphene two-dimensional material. The red spheres represent the carbon atoms that are covalently bonded to each other to form hexagonal carbon rings comprising of six identical atoms. The carbon atoms are $sp^2 - hybridized$ and each carbon atom has four covalent bonds. 21

2.2 Graphane two-dimensional material. The red and yellow spheres represent the carbon and hydrogen atoms respectively. The carbon and hydrogen atoms are covalently bonded to each other forming sp^3 hybridization. The hydrogen atoms are chemi-sorbed to the carbon atoms on either side in an alternating way. 23

2.3 Different graphane isomers: chair, stirrup, twist-boat, boat-1, boat-2 and tricycle.[1] 24

2.4 Vacancy point defect in the graphane two-dimensional material. The red spheres represent carbon atoms while the yellow spheres represent hydrogen atoms. The carbon atom was removed from its lattice site leaving a single unattached hydrogen atom. 30

2.5 Nitrogen substitutional point defect in the graphane two-dimensional material. The red spheres represent carbon atoms, while the blue sphere represent the impurity nitrogen atom that has displaced a carbon atom from its normal site. The yellow spheres denote the hydrogen atoms that are covalently bonded to the carbon atoms. 32

2.6 Point defect complex which is formed by a combination of two or more point defects. The two point defects are the substitutional sulphur atom (shown by the orange sphere) which is adjacent to a hydrogen vacancy. The hydrogen atoms are represented by the yellow spheres while the carbon atoms are represented by the red spheres. 33

3.1 Convergence testing: (a) total energy versus cut-off kinetic energy (b) total energy versus K-points (c) total energy versus lattice constant . . . 70

3.2 Schematic representation of the Pseudo-potential approximation. 73

8.1 Formation energy for the point defect complexes of the type: $N_C V_H$, $N_C V_{CH}$, $N_{CH} V_H$ and $N_{CH} V_{CH}$ in the graphane two-dimensional material when the Fermi-level is (a) 0 eV (b) -3.5 eV and (c) 3.5 eV. 163

8.2 Charge distribution in the nitrogen dopant-vacancy defect complexes in graphane: (a) $N_C V_H^0$ and (b) $N_C V_H^{+1}$. The grey and green spheres respectively represent carbon and hydrogen atoms. The dark blue non-uniform spheres shows the charge distribution which is more pronounced around the light blue nitrogen dopant atoms. 169

8.3 Binding energy and U-parameter values for nitrogen-vacancy complexes in graphane 170

List of Tables

2.1 Table 2.1: Structural properties of the six main graphane stereo isomers: chair, tricycle, stirrup, boat-1, boat-2 and twist-boat[1]. 28

3.1 Recordings of the fundamental steps for solving the Kohn-Sham equations in a self-consistent manner. 63

Abstract

In this contribution, we present a detailed analysis of the effects of the presence of substitutional nitrogen-vacancy complexes in the two-dimensional material - graphane. We critically examine the derived formation energies, transition energy levels and U-parameters. In order to do this, we commence by systematically characterizing substitutional nitrogen point defects of the form N_C, N_H and N_{CH} in graphane. We also do a detailed investigation of vacancy point defects of the type V_C, V_H and V_{CH} in this graphene derivative two-dimensional material. We comprehensively derive the formation energies of these point defects giving the material science research community invaluable information about the stability aspects of these point defects in graphane. This investigation extends to fundamental aspects of density of states, defect level diagrams and activation energies, leading to a deeper understanding of the stability landscape of the point defects as well as the host material at play. In the second part of this investigation, we thoroughly examine the intricate relationship that exist when we combine these point defects to form the nitrogen-vacancy complexes of the form N_CV_H, N_CV_{CH}, $N_{CH}V_H$ and $N_{CH}V_{CH}$. We unravel the paramount information and the subtle influences that nitrogen-vacancy complexes have on graphane. We meticulously explore the fundamental effects of the presence of nitrogen-vacancy complexes on the structural and electronic properties of hydrogenated graphene. Our detailed analysis provides a pivotal ground work on the potential applications of point defect modified graphane in nanotechnology. Information on the defect energy levels are scrutinized to unravel the electronic dynamics while the calculated defect induced band gaps offer valuable

insights into graphane's potential applications in band gap engineering as well as in quantum computing. Furthermore, this investigation sheds light on the intricate stability patterns of point defect modified graphane. Our findings contribute to the critical comprehension of the interplay that exist between fundamental defect parameters of formation energies, defect transition energy levels, U-parameters as well as binding energies. Our results are of critical importance in terms of paving the way for technological advancement in the use of two-dimensional materials for nano-technology applications.

Chapter 1

Introduction

The presence of point defects in the two-dimensional material graphane, makes it an apt candidate for nanotechnology and other suitable applications. The electronic and structural properties of graphane can be considerably altered by the introduction of point defects as well as point defect complexes [2][3][4]. This study is centred on understanding the impact of substitutional nitrogen and vacancy point defects and their complexes in modifying the properties of graphane. This current contribution is imperative in terms of the use of nitrogen-vacancy point defect-modified graphane for quantum computer applications as well as the making of nanotechnology devices. It is also one aim of this contribution to study the local properties of graphane once a substitutional nitrogen point defect or a vacancy or a combination of these point defects is introduced in the material. We comprehend the material's new properties after the introduction of nitrogen-vacancy class of point defects by way of studying the modified system using Density Functional Theory (DFT) [5][6]. Among other uses, a positive outcome of this work has the potential to open new ground for defect-modified graphane as a very important material for the fabrication of nanodevices for nanotechnology uses as well as for memory and information keeping in quantum computers.

1.1 Significance of Research

Two-dimensional materials such as graphane are attracting research interest because of their unique properties such as high electron mobility, large surface area and wide bandgap. These properties make the crystals suitable for various technological applications. Modification of their nano-level electron behaviour can increase their applications in the fabrication of modern nano-technology devices. An indepth knowledge of point defects in graphane can possibly lead to the making of electron-spin based nano-devices as well as energy and memory storage devices. The research output can possibly have a positive impact on quantum information processing, quantum metrology and teleportation [7][8][9][10]. This study can also give rise to a new knowledge of quantum point defects in new host materials. Current research on graphane and other similar two-dimensional materials is aimed at understanding the positive and negative impact of defects on their properties. Therefore, the output of this study can possibly have a positive impact to the research community at large.

1.2 Problem Identification

One of the main point defects in three-dimensional materials is the negatively charged nitrogen vacancy center (NV^{-1}) embedded in the diamond lattice [11][12][13][14]. This point defect complex in diamond has various fundamental applications, which among others include: quantum information processing, magnotometry, signal detection and metrology as well as biomedical applications. The unique and innovative applications of the nitrogen-vacancy center in diamond crystal have prompted researchers to actively seek new point-defects complexes as well as new host materials that can be utilized in the fabrication of ingenious nano-devices for a wide range of applications like quantum computing, science of measurement as well as in nano-electronics. The world-over, there is an apparent shift from bulk electronic instruments to extremely tiny accessories which are made up of very few atoms. Graphane is one of the two-dimensional materials

that have suitable electronic and structural properties which make these materials apt for use in technological devices that require size reduction. The electron properties in graphane can be modified by pertubations such as point defects introduced into the material. In order to comprehend the properties of a many-body systems, we study the compound's defect and electron behaviour by using periodic computer simulation techniques [15][16][17][18]. In this contribution, we do a comprehensive examination of the effects of the presence of nitrogen-vacancy point defect centers in graphane using Quantum Espresso package for electronic structure calculations. We also thoroughly analyse how this class of point defects modifies the local properties of hydrogenated graphene. An in-depth understanding of the positive as well as negative effects of point defects in graphane can open a new window of application for such two-dimensional materials.

1.3 Research Aims and Objectives

The broad aim of this research is to intensively study various types of nitrogen-vacancy point defects complexes in graphane for nano-technology applications. In particular, we carry out this research project in order to:

- Do *ab initio* Quantum Espresso electronic structure calculations of pristine graphane and point defect modified graphane;
- Calculate the formation energies of pristine graphane and graphane with substitutional nitrogen and vacancy point defects;
- Investigate the thermodynamic stability of substitutional nitrogen point defects, vacancy point defects and their respective combinations in graphane;
- Explore the suitability of substitutional nitrogen point defects, vacancy point defects and the point defects complexes in graphane for the making of nanotechnology devices;

- Characterize a nitrogen atom substituting a hydrogen atom (N_H) , a nitrogen atom substituting a carbon atom (N_C) and a nitrogen atom substituting both a carbon and a hydrogen atom (N_{CH}) in the graphane chair conformer.
- Understand how N_H , N_C and N_{CH} point defects in graphane modify the local properties of graphane chair conformer for electronic and nano-technology applications;
- Characterize a hydrogen vacancy (V_H), a carbon vacancy (V_C) and a carbon vacancy adjacent to a hydrogen vacancy (V_{CH}) in graphane chair conformer.
- Comprehend the various aspects of how V_H , V_C and V_{CH} vacancy centers in graphane alter the local properties of graphane for nanotechnology applications;
- Systematically study: a substitutional nitrogen impurity that is adjacent to hydrogen vacancy (N_CV_H), a dopant nitrogen atom which is adjacent to a carbon-hydrogen vacancy (N_CV_{CH}), a nitrogen atom substituting both a carbon and hydrogen atom contiguous with a hydrogen vacancy ($N_{CH}V_H$) and a nitrogen dopant atom substituting both carbon and hydrogen atoms from their lattice sites, adjacent to a carbon-hydrogen vacancy ($N_{CH}V_{CH}$).
- Do a comparison of how N_CV_H, N_CV_{CH}, $N_{CH}V_H$ and $N_{CH}V_{CH}$ point defect complexes in graphane alter the electronic and structural properties of graphane at nano-level;
- Compare the outcome of this study with the current existing theoretical and experimental work within the same research area;
- Study the adsorption mechanisms of Li dopant atoms on graphane with several CH divacancies (v12, v13, and v14) configurations;
- Systematically perform density functional theory calculations in order to comprehend the energetic stability, structural and electronic properties of Li dopnats on graphane.

1.4 Expected Research Output

Positive outcomes of this work have the potential to make graphane a very important material for the making of electronic devices. The fabrication of defect-modified graphane nanodevices is another anticipated positive outcome of this work. The size reduction of electronic devices for memory and information keeping using graphane is another door that this research study can open. We hope to have an incremental input to the existing body of knowledge of point defects in the graphane two-dimensional material. We also anticipate the publication of at least three academic papers that precedes a PhD dissertation.

1.5 Synopsis

The rest of this dissertation is arranged as follows: In Chapter 2 we do a brief literature review of the material graphene followed by a detailed review of graphane. In this chapter, we also briefly study the concepts of point defects in materials before analysing the existing literature of the proto-type nitrogen vacancy center point defect in diamond. In the next Chapter we look at the electronic structure methods that have been developed over many years in order to derive the properties of many-body systems. In Chapters 4 , we present a published paper entitled **"Thermodynamic stability and formation energies of hydrogen and carbon vacancy centers in hydrogenated graphene"**. In this paper, we make use of the Quantum Espresso code to derive formation energies, effective U-parameters and thermodynamic transition levels of the mono-vacancies V_H, V_C as well as V_{CH}. In Chapter 5, we present another published paper with the title **" First principles characterization of nitrogen substitutional point defects in graphane (CH)"**. In this contribution, we characterize nitrogen substitutional point defects of the type N_H, N_C and N_{CH} embedded in the two-dimensional material - graphane. Chapter 6 is another published paper on the comparative study of nitrogen-vacancy complexes in graphane. The paper is entitled **"First principles exploration**

of N-V point defect complexes in graphane: analysis of energetic stabilities and electronic properties". In this publication, we comprehensively characterize defect complexes of the form $N_C V_H$, $N_C V_{CH}$, $N_{CH} V_H$ and $N_{CH} V_{CH}$. Chapter 7 is also another published paper that explores the possibility of the use of defect modified graphane in nano-technology. In this contribution, we specifically explore the use of graphane with point defects as an electrode material. The article is entitled **"Lithium on CH Divacancy Self-Healed Graphane: A First-Principles Study."** The last Chapter of this dissertation gives an overview of the results of the research study as well as possible future studies.

Chapter 2

Literature Review

2.1 Graphene

Graphane material is derived from graphene by way of various hydrogenation processes. Therefore, in the next section, we briefly explore these fabrication processes as well as some fundamental concepts that are entwined in graphene. We will then systematically analyze the graphane material.

Graphene is a two dimensional material[1] that was discovered in 2004 by Novoselov and Geim at the University of Manchester [19]. The isolation and characterization of graphene culminated in Novoselov and Geim winning the Nobel Prize in 2010. Graphene is composed of carbon atoms only. The carbon atoms are covalently bonded in such a way that they form a hexagonal structure or a honey-comb structure. This material has no band gap but it has some properties that are extremely interesting. In their detailed overview Sahin et al [20] commenced from the isolation and characterization of the 2-dimensional material graphene in 2004 at the University of Manchester [21]. Graphene was isolated from graphite using the now famous scotch-tape method. The initial stage in micro-mechanical cleavage of graphene is the attaching of skotch-tape to highly ordered and pyrolytic graphite [22][21]. Using the skotch-tape a layer of the

[1]For a two dimensional material we can only use two measurements or dimensions to describe any point within the material, hence electrons can only move in two directions in the material.

graphite[2] is peeled and deposited on a substrate such as silicon dioxide (SiO_2). The peeling of the graphite layer is repeated until a mono-layer of the material is produced. This initial method used to synthesis graphene was very important in terms of the isolation and characterization of graphene but the disadvantage of this method is that one cannot produce large quantities of any material in this way. Better methods of synthesizing graphene have since been developed.

Among others, chemical vapour deposition (CVD) is one method that is used to produce large quantities of graphene as compared to the micro-mechanical cleavage of graphene method [23]. To kick-start the process, atoms of carbon are deposited on a metal surface, for instance a copper surface. The temperature of the surface is then increased so that the carbon atoms form graphene layers. Apt layers of polymer are then deposited on the graphene layers. In the next stage of this process both the polymer and graphene layers are simultaneously removed. The last stage of CVD involves the dissolving of the polymer so that the graphene layers are left behind on a suitable substrate [23]. Among other unique features, graphene has unique properties [20][24][3][25][26] such as:

- an atom-thin material;
- strongest and stiffest material;
- has massless dirac fermions at the fermi surface;
- best material for electrical conduction;
- semi-metalic

The absence of a band gap in graphene has limited its direct application in nano-electronics [27]. A number of material researchers are seeking apt ways of creating a band gap in graphene in order to open new ground of application for two-dimensional materials. Some researchers [20] proposed dimensionality reduction and the use of functionalization to create a band gap in graphene. The former is done by cutting graphene

[2]Graphite is a trigonal planar three dimensional structure made of carbon atoms only. The carbon atoms are sp^2 hybridized and are covalently bonded by both σ and π bonds. The covalent bonds are strong as compared to the weak van Der Waal forces between the graphite layers hence graphite is slippery.

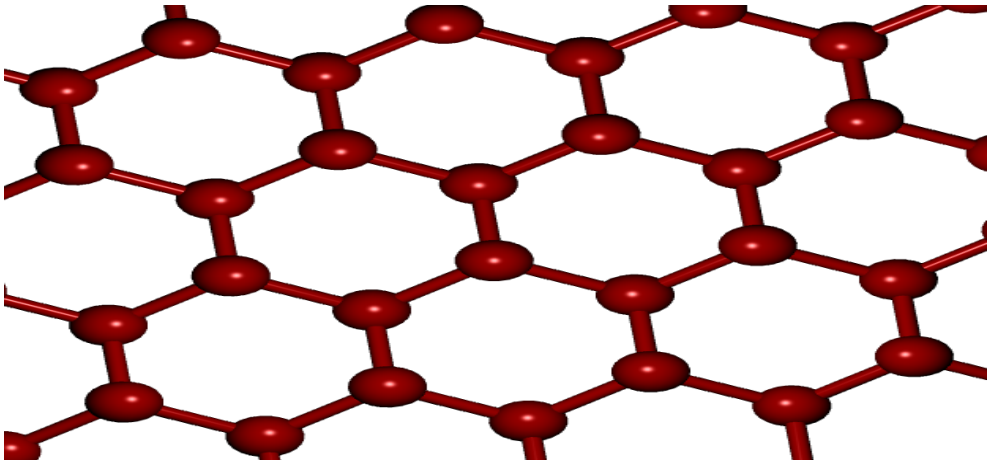

Figure 2.1: Graphene two-dimensional material. The red spheres represent the carbon atoms that are covalently bonded to each other to form hexagonal carbon rings comprising of six identical atoms. The carbon atoms are $sp^2 - hybridized$ and each carbon atom has four covalent bonds.

to create ribbons or flakes while the later gets rid of the π-bonds. Functionalization can be achieved by substituting carbon atoms in the graphene layer by using suitable foreign atoms such as nitrogen and boron. Alternatively, one can adsorb molecules or functional groups onto a graphene layer. These two methods can give rise to charge doping and the opening up of an electronic band gap. Charge doping is brought about by physisorption even though it leaves the graphene structure virtually the same. However, chemisorption can give rise to pronounced graphene structural changes. This can be brought about by the adsorption of radicals such as hydroxyl functional groups. Two-dimensional materials that are synthesized from graphene in more or less similar ways as discussed above are referred to as graphene derivative materials [20]. Among others, we have fluorographene which is fluorinated graphene as well as chlorographene or chlorinated graphene [28]. Graphene hydrogenation gives rise to graphane which has a direct band gap at the Brillouin zone centre. In the section that follows, we do an indepth analysis of the graphane material.

2.2 Graphane

Graphane material is derived from graphene by way of various hydrogenation processes. Therefore, in the next section, we briefly explore these fabrication processes as well as some fundamental concepts that are entwined in graphene. We will then systematically analyze the graphane material.

The existence of graphane was first predicted by Sluiter and Kawazoe in 2003 [29]. Four years later, Sofo et al [28] used first-principles total energy calculations to give weight to the existence of graphane. Graphane is a two-dimensional material just like graphene. It is derived from pristine graphene by way of attaching hydrogen atoms onto the carbon atoms. Graphane is thus made up of covalently-bonded hydrogen and carbon atoms only- it is thus a hydrocarbon whose formula is CH. This material is composed of single bonds only, hence it is a completely saturated hydrocarbon. The carbon atoms are bonded in such a way that they form a ring or a hexagonal structure as shown by figure 2.1. The attachment of hydrogen atoms to the carbon atoms is a transition from sp^2 to sp^3 hybridization for the carbon atoms [20]. The numerous isomers and many interesting properties of graphane emanate from the various ways in which the carbon and hydrogen atoms are bonded.

The different ways in which the hydrogen atoms can be adsorbed onto the carbon atoms determine the atomic structure of graphane [30] as shown by figure 2.3. We first analyse the atomic structure of the chair configuration which is considered to be the most stable. This graphane isomer has four atoms in each unit cell, that is two hydrogen atoms and two carbon atoms. Each carbon ring has a similar pattern of three hydrogen atoms facing upwards and three facing downwards in a repeating pattern [1] as depicted by figure 2.3. The hydrogen atoms are attached to the carbon atoms on both sides in an alternating manner. Each carbon atom has four covalent bonds and is sp^3 hybridized. The $C-C$ bond length for the chair conformer is 1.52 $\AA$, while the $C-H$ bond length is 1.11 $\AA$ [28]. The binding energy as determined by Sofo et al is 6.56 eV[28].

According to the contribution by Sahin et al [20][30], the next stable graphane isomer

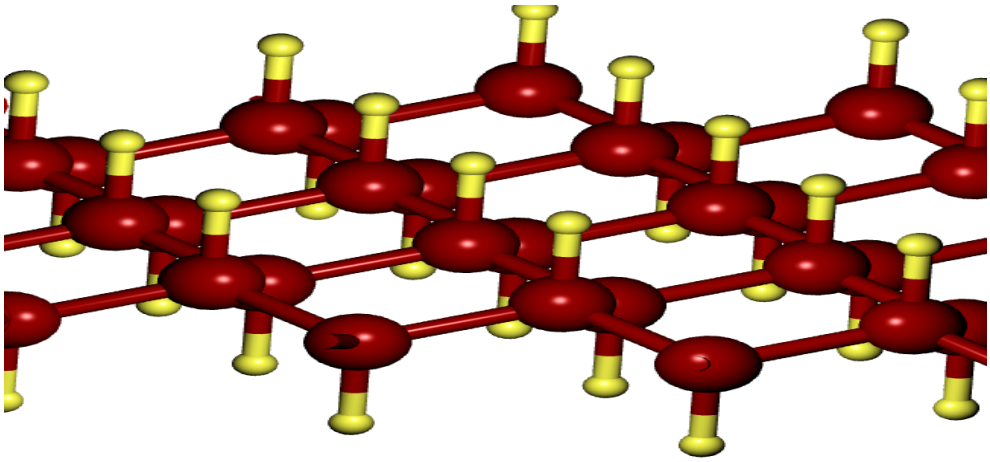

Figure 2.2: Graphane two-dimensional material. The red and yellow spheres represent the carbon and hydrogen atoms respectively. The carbon and hydrogen atoms are covalently bonded to each other forming sp^3 hybridization. The hydrogen atoms are chemi-sorbed to the carbon atoms on either side in an alternating way.

after the chair is the stirrup conformer. This graphane allotrope is also referred to as the zigzag or washboard configuration. The hydrogen atoms are chemisorbed to the carbon atoms in such a way as to form zigzag patterns that are alternating. The stirrup conformation has three hydrogen atoms below and above the carbon layer in a given carbon ring [1]. For this conformer, the $C-C$ and $C-H$ bond lengths are respectively $1.544\mathring{A}$ and $1.105\mathring{A}$ [1].

After the stirrup allotrope, the boat configuration is considered to be the most stable. For this conformation, the hydrogen atoms that are adsorbed to the carbon atoms alternate in pairs. We have the so called $boat-1$ and $boat-2$ graphane stereo isomers as illustrated by figure 2.3. The boat conformer has eight atoms in a unit cell. The repulsion between the pair of hydrogen atoms on the same side decreases the stability of this allotrope. As a result of this repulsion, the $C-C$ bond length can vary between 1.52 $\mathring{A}$ and 1.56 $\mathring{A}$ while the binding energy is 6.50 eV.

Sofo et al [28], used first-principles derivation of total energy to predict the existence and stability of graphane (CH) as a semi-conductor hydrocarbon which is completely saturated. They compared the binding and formation energy of graphane to other hydro-carbons like benzene, polyethylene and cyclohexane. DFT calculations were run

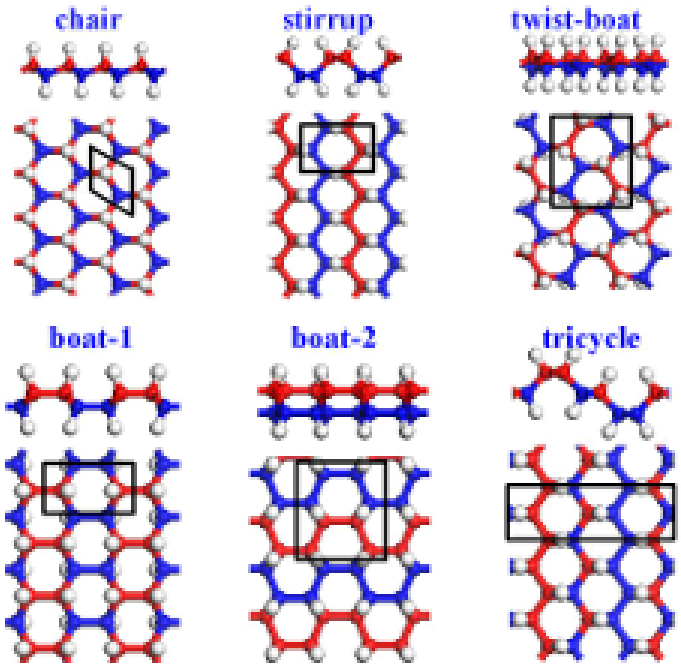

Figure 2.3: Different graphane isomers: chair, stirrup, twist-boat, boat-1, boat-2 and tricycle.[1]

using the CASTEP code [28]. The pseudopotential approximation was used for the inner electrons while Perdew, Burke and Ernzerhof's generalized gradient approximation (GGA) was utilised for the determination of exchange and correlation terms [31][32]. Sofo et al [28] also compared the stability of graphane with it's fluorinated counterpart , CF. They found out that the chair and boat configurations are the conformations favoured by graphane. The stability of the chair is better than the boat conformer because of the repulsion of the hydrogen atoms alternating in pairs on either side of the graphene sheet for the boat configuration. They proposed methods of synthesizing graphane as well possible applications in nano-electronics and hydrogen storage for fuel cells.

In their review article, Pumera and Wong [33] discussed the possible methods of synthesizing graphane and partially hydrogenated graphene. Two main approaches are used, that is top-down and bottom-up methods. The well known method of chemical vapour deposition [23] falls under the bottom-up approach. Among others, these meth-

ods can further be divided into different categories such as gas phase hydrogenation and liquid phase hydrogenation [23]. The properties of the structural isomers of graphane were reviewed in this contribution [33]. The extent of graphene hydrogenation give rise to a tunable band gap that can be exploited for nanotechnology applications such as transistors. Partially hydrogenated graphene exhibits ferro-magnetic and magnetic properties which can be exploited for spintronics applications [33].

In their work, Reshak and Auluck [34] derived and compared the electronic and optical properties of two graphane conformations, namely chair and boat-1. They utilized the Full Potential Linear Augumented Plane Wave (FPLAPW) computational method based on the WIEN2k code [35]. The exchange and correlation functionals were determined using the local density approximation (LDA) following the procedure of Ceperley and Alder [36]. For the purpose of comparison, the same functionals were deduced by way of Perdew, Burke and Ernzerhof's widely used generalized gradient approximation (GGA) [31]. Similar calculations were further done in line with the generalized gradient approximation of Engel and Vosko [37]. In addition to some other fundamental findings, Reshak and Auluck [34] calculated density of states which depicted strong $s-p$ orbital hybridization between the carbon and hydrogen atoms.

In 2014 Zhou et al [38] reported the structures of graphane isomers that have been theoretically derived. The structures of the six main allotropes of graphane- chair, stirrup, boat-1, boat-2, tricycle and twist-boat- depends on the ways in which the hydrogen atoms are attached to the carbon atoms in each carbon hexagonal carbon ring. The chair conformer is the most stable with the UDUDUD hydrogenation pattern. U and D respectively represents up and down ways of attaching the hydrogen atoms on a graphene monolayer. The stirrup isomer that has the zigzag pattern of UUUDDD is second in stability. The other allotropes, boat-1, boat-2, tricycle and twist-boat have the following respective hydrogenation pattern: UUDDUU, UUUUDD, UUUDUD, and UUDUDD [1].

Zhou et al [38] also discussed the different properties of graphane that have been

reported in literature. Among other properties the review article reported: mechanical, thermal, optical, electronic and magnetic properties of graphane. The methods of graphane single layer fabrication discussed by Zhou et al [38] include exposing graphene monolayer to hydrogen plasma, chemical vapour deposition that is plasma-assisted as well as thermal vapour deposition. Their review article also encompassed possible significant applications of graphane such as nano-electronics, transistor, nano-composites, nano-sensors, hydrogen storage and electron-phonon superconductors [38].

In their contribution, Sahin et al [20] discussed in detail the various properties of graphane- that is structural, electronic, magnetic, vibrational and mechanical properties. The different properties of graphane come into play because of the different configurations. In their work, Sahin et al [20] states that the most stable allotropes of graphane are the chair, the boat and the stirrup. The other graphane stereo isomers that have been proposed in research articles include: the armchair; the twist-boat; the twist boat-chair and the tricycle which comes from the chair and stirrup combination [1].

Sahin et al [20] discussed a number of methods that can be used to synthesize graphane. The prominent ones are: the exposure of graphene to hydrogen plasma, plasma-assisted chemical vapour deposition (CVD), the apt use of high temperatures and pressure to thermally exfoliate graphene oxides, electron-assisted dissociation of the inorganic compounds that belong to the hydrogen silsesquioxane (HSQ) family and the use of scanning tunnelling microscope (STM) to hydrogenate graphene. Various suitable applications of graphane were discussed by Sahin et al [20]. These include hydrogen storage and release for energy devices, making of nano-sensors that can find their use in medical fields as well as for the detection of explosives. Graphane can also find important applications in piezoelectricity as well as thermoelectricity.

In their overview, He et al [1] used first principles energy calculations under the density functional theory framework to predict the existence of another graphane isomer called the tricycle. They also determined the structural properties of the other five

graphane allotropes whose existence was already known. They used generalized gradient approximation (GGA) under the Vienna ab initio Simulation Package (VASP) [39] for the determination of the exchange and correlation energy. Their description of the nucleus and valence electrons interactions was done using the Projector Augumented Wave method (PAW) . In the tricycle conformer, each carbon ring is composed of four hydrogen atoms on one side and two hydrogen atoms on the other side of a monolayer of carbon atoms. The four- up and two- down arrangement of the hydrogen atoms in this conformer is different from the boat-1 and boat-2 configurations. The similarity is limited to the number of hydrogen atoms below and above a given graphene sheet. According to He et al [1], the cohesive energy of the tricycle conformer is -5.21 eV and this makes it the next stable isomer from the chair. The electronic properties of the tricycle stereo isomer is more or less the same as the other five configurations. He et al [1] proposed the atomic properties for tricycle as summarised in the table 2.1.

The structural and electronic properties of graphane can be considerably influenced by the presence of point defects in the material. In the section that follows, we systematically analyse the effects of point defects on some properties of materials.

2.3 Defects in Graphane

2.3.1 Point defects

The properties of a material can be considerably altered by the introduction of defects or impurities. Defects can make a material useful for electronic applications or can negatively affect the usefulness of a given material. In many cases, defects are able to induce energy states in a host material and these states can be an advantage for device applications. If we are able to control the incorporation of defects into materials and measure as well as manipulate the defect-induced properties, then it will be probably possible to derive positive electronic applications of the defects.

We can classify defects into two classes- intrinsic and extrinsic. Intrinsic defects are

Table 2.1: Table 2.1: Structural properties of the six main graphane stereo isomers: chair, tricycle, stirrup, boat-1, boat-2 and twist-boat[1].

Graphane isomer	Chair	Tricycle	Stirrup	Boat-1	Boat-2	Twist boat
Space group	P-3m1(164)	Pbcm(57)	Pmna(53)	Pmmn(59)	Pbcm (57)	Pcca(54)
Cohesive energy per atom(eV)	-5.222	-5.210	-5,194	-5.171	-5.155	-5.147
Lattice constant	a=b=2.504 c=15.000	a=15.000 b=7.681 c=2.544	a=2.549 b = 15.000 c=3.828	a=2.529 b=4.309 c=15.000	a=15.000 b=4.585 c=4.328	a=4.417 b=15.000 c=4.987
C-C bond length (Å)	1.537	1.539 1.541 1.540	1.544	1.537 1.570	1.542 1.548 1.573	1.542 1.548 1.562
C-H bond length (Å)	1.110	1.108 1.109	1.105	1.105	1.103	1.106
Band gap (eV)	3.491	3.446	3.340	3.374	3.412	3.529
Carbon atoms sites	C: (0.333 0.667 0.515)	C1: (0.498 0.056 0.250) C2: (0.573 0.193 0.250)	C: (0.000 0.364 0.462)	C: (0.500 0.182 0.522)	C: (0.462 0.594 0.432)	C: (0.090 0.479 0.615)
Hydrogen atoms sites	H: (0.333 0.667 0.589)	H1: (0.433 0.124 0.250) H2: (0.636 0.119 0.250)	H: (0.000 0.398 0.509)	H: (0.500 0.256 0.592)	H: (0.399 0.493 0.504)	H: (0.122 0.408 0.561)

also referred to as native defects since they only involve atoms of the host material [40]. No foreign atoms take part in the formation of the defect at play. Extrinsic defects encompass impurities or foreign atoms embedded in the host material. There are some defects that are able to donate free electrons to the host material while others accept electrons from the material in which they are embedded. These defects are respectively referred to as donors and acceptors [41]. Donor states are located close to the conduction band minimum while acceptor states are located close to the valence band edge. For a given element on the periodic table, atoms on the left side of the element are acceptors while those on the right side are donors. For instance, consider carbon which is a group four element. Elements such as boron in group three have one valence electron less than carbon. A substitutional boron atom on a carbon host site will be an acceptor. However, elements such as nitrogen on the right side of carbon are donors since they have one extra valence electron more than carbon. There are some donors and acceptors that can donate or accept multiple electrons depending on the host crystal in which they are. If a foreign substitutional atom replaces a host atom that has the same number of valence electrons, we refer to that center as isovalent or isoelectronic [42]. The atoms at play have to be in the same group for the center to form, for instance, a carbon atom replacing a germanium atom give rise to the formation of an isovalent center in the host material.

Imperfections in crystals can further be categorised into point and line defects [43]. Line defects are distortions in a crystal that encompass a significant number of atoms in rows or lines as the name suggests. Some line defects render devices useless in terms of application because it is extremely difficult to control or manipulate such imperfections- for example grain boundaries, dislocations and stacking faults [44]. Point defects are localised imperfections in a crystal and they entwine a few isolated atoms in the host material . A number of point defects may combine to form what is called a complex. We will focus on point defects only in this work because unlike many of the line defects, there are some point defects whose properties can be easily measured, manipulated and

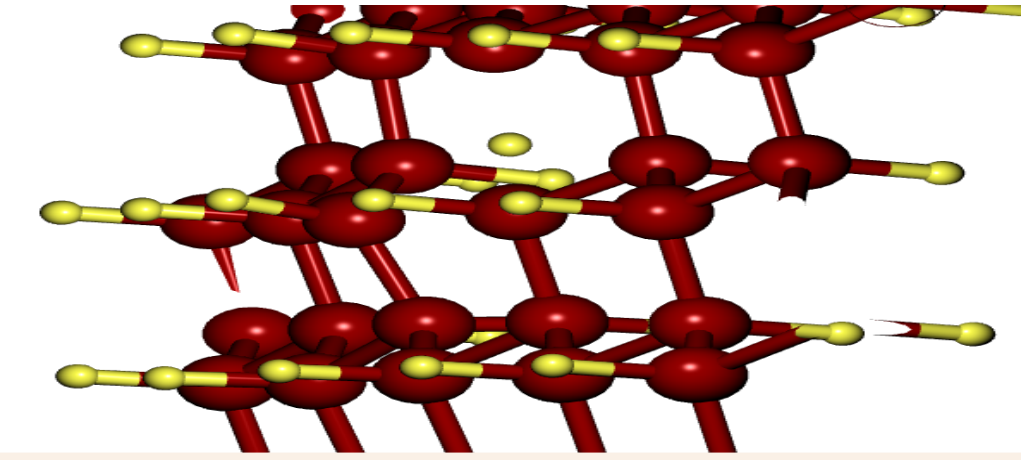

Figure 2.4: Vacancy point defect in the graphane two-dimensional material. The red spheres represent carbon atoms while the yellow spheres represent hydrogen atoms. The carbon atom was removed from its lattice site leaving a single unattached hydrogen atom.

controlled. We can put point defects into a number of classes such as: presence of a vacancy, atom occupying an interstitial site, substitutional atom or impurity in the host material , host atoms swapping positions or anti-site and Frenkel defect pair complex [45]. If there is an atom, A, missing from its site in the host material, a vacancy defect, V_A, is created at that particular position as shown by figure 2.4. A vacancy can have a positive or a negative or a neutral charge state[3]. During the formation phenomena of two-dimensional materials, vacancy point defects can form. Lattice vacancies can form because of the high possibility of imperfect packing of atoms or molecules during the process of crystallization. It is also a possibility that atoms can be shifted and subsequently displaced from their exact equilibrium sites as a result of extremely high temperatures [43]. The extreme temperatures increase the average kinetic energies of the species within the material and this signicantly increases the phonons or atomic vibrations within the material. Another possible source of lattice vacancies is thermal effects and radiation damage during the different stages of the growth processes [43]. Any crystal structure will always have vacancies, hence comprehending their behaviour

[3]In this case vacancy charge state refers to the number of electrons in the dangling bonds that surrounds the vacancy [40]

is of extreme importance so that we can take advantage of the aspects that we can utilise positively. Moreover, knowledge of the negative effects of vacancy point defects can also assist material engineers to mitigate their unwanted interference in the operation of technological devices. Patterson and Bailey [43] presented a convincing argument of the importance of analysing and comprehending possible properties of vacancy point defects in materials.

To cement their argument, they considered, the Schottky and Frenkel defects which are vacancy-related point defects. A crystal structure that comprises N atoms and v vacancies of this type, has W as the total number of vacancies distributed in the material under consideration. W is given by equation 2.1

$$W = \left[\frac{N!}{(N-v)!v!}\right] \tag{2.1}$$

The entropy , S, can be deduced from the expression

$$S = k_B l_v W \tag{2.2}$$

where k_B represents the Boltzmann constant at an apt temperature of equilibrium, T. The system's free energy is given by equation 2.3

$$\triangle F = \triangle U - T\triangle S \tag{2.3}$$

where $\triangle U$ denotes the system's internal energy which is given by

$$\Delta U = vE_{vac} \tag{2.4}$$

The term E_{vac} represents the energy required to create a single vacancy. For v vacancies in a given lattice structure, we have the expression given by equation 2.5

$$\triangle F = vE_{vac} - Tk_B ln\left[\frac{N!}{(N-v)!v!}\right] \tag{2.5}$$

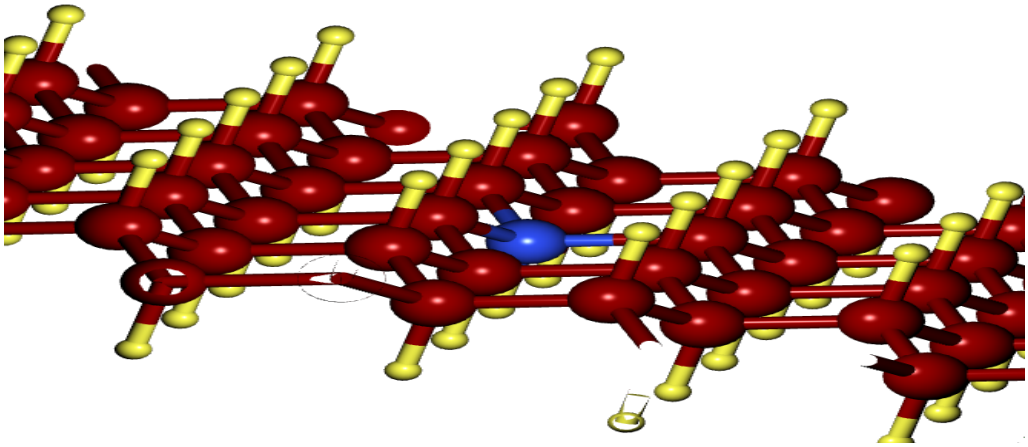

Figure 2.5: Nitrogen substitutional point defect in the graphane two-dimensional material. The red spheres represent carbon atoms, while the blue sphere represent the impurity nitrogen atom that has displaced a carbon atom from its normal site. The yellow spheres denote the hydrogen atoms that are covalently bonded to the carbon atoms.

The expression $\triangle F = \triangle U - T\triangle S$ has a minimum value in a state of equilibrium. The value of $\triangle U$ will be considerably increased by the vacancies, causing some form of disorder and a subsequent increase in the system's entropy, $\triangle S$. At a temperature that is high enough, an increase in the value of $\triangle U$ is likely to be compensated by a decrease in $-T\triangle S$. With this argument, we can conclude that stability in a given material can only be achieved in the presence of vacancies [43]. Moreover, the presence of vacancies in a given structure can amplify electron transport. We also propose that the presence of vacancies in a material is of paramount importance as far as the controlling of diffusion is concerned.

There are some key concepts which one has to consider when characterizing point defects in two-dimensional materials. Among other fundamental concepts, we have: the point defect formation energy, charge transition levels, the U-parameter and the binding energy of defect complexes. We briefly discuss the determination of these critical concepts in the sections that follow. We use the hydrogen vacancy (V_H), the carbon vacancy (V_C) and the hydrogen-carbon vacancy (V_{CH}) to show how these concepts are calculated.

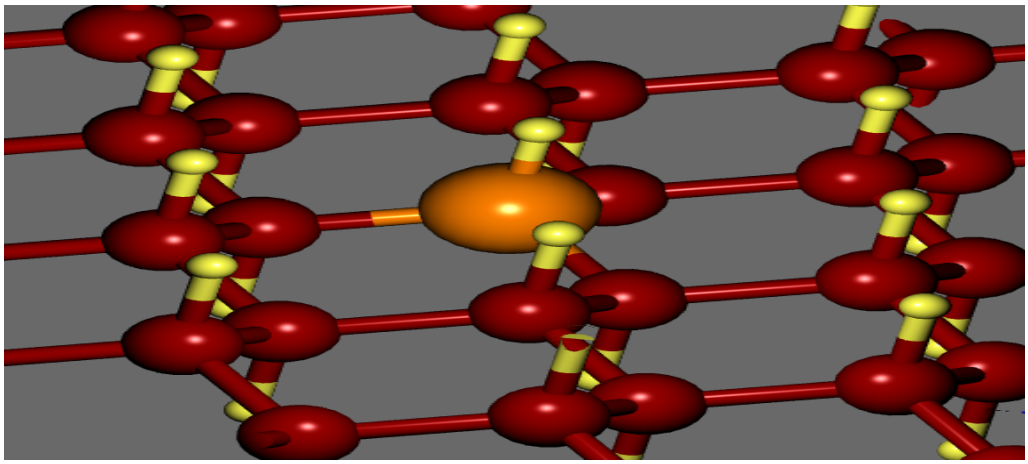

Figure 2.6: Point defect complex which is formed by a combination of two or more point defects. The two point defects are the substitutional sulphur atom (shown by the orange sphere) which is adjacent to a hydrogen vacancy. The hydrogen atoms are represented by the yellow spheres while the carbon atoms are represented by the red spheres.

2.3.2 Formation energy

The derivation of formation energies is a very important step in the characterization of point defects. The formation energy gives information on defect concentration, the expected defect positions in the crystal lattice and some other factors that have to be considered when incorporating the defect into the crystal lattice. The point defect formation energy depends on the total energy of the pristine crystal structure and the total energy of the structure in which a defect has been embedded. The charge state of the defect and the chemical potential energies of the atomic species that have either been added to or removed from the crystal structure when the defect was formed are also crucial concepts that have to be considered when calculating the formation energy.

2.3.2.1 Hydrogen vacancy (V_H)

For a hydrogen vacancy, V_H^q, having a charge state q (0, -1 or 1), we derived the formation energy, $E^f(V_H^q)$, using the equation

$$E^f(V_H^q) = E_T(V_H^q) - E_T(pristine) + \mu H + qE_F + E_{corr} \tag{2.6}$$

where $E_T(V_H^q)$ is the total energy of a graphane supercell that has the hydrogen vacancy embedded in it,

$E_T(pristine)$ represents the total energy of the pristine supercell,

μH is the chemical potential of the hydrogen atom,

E_F represents the Fermi energy of the electron, either added or removed to form, V_H^{-1} or V_H^{+1} and

E_{corr} denotes the correction term to take account of errors that arise because of the use of the supercell approach.

2.3.2.2 Carbon vacancy (V_C)

Similarly, we derived the formation energy for the carbon vacancy, $E^f(V_C^q)$, using equation 2.7

$$E^f(V_C^q) = E_T(V_C^q) - E_T(pristine) + \mu C + qE_F + E_{corr} \tag{2.7}$$

where q represents the singly positive, singly negative and the neutral charge state respectively (+1,-1, 0),

$E_T(V_C^q)$ is the total energy of a graphane supercell that contains the carbon vacancy point defect in charge state q,

$E_T(pristine)$ denotes the total energy of the pristine supercell,

μC is the chemical potential energy of the carbon atom,

E_F and E_{corr} represent the Fermi level and the correction term respectively.

2.3.2.3 Carbon-hydrogen vacancy (V_{CH})

We deduced the formation energy [46] of a carbon-hydrogen double vacancy using the equation 2.8.

$$E^f(V_{CH}^q) = E_T(V_{CH}^q) - E_T(pristine) + \mu H + \mu C + qE_F + E_{corr} \tag{2.8}$$

where q denotes the singly positive, singly negative and the neutral charge state

respectively (+1,-1, 0),

$E_T(V_{CH}^q)$ represents the total energy of a graphane supercell that has the carbon-hydrogen vacancy of charge state q, embedded in it,

$E_T(pristine)$ denotes the pristine supercell's total energy,

μH and μC respectively represents the chemical potential energies of the hydrogen and carbon atoms,

E_F and E_{corr} denotes the Fermi level and the correction term taken in that order.

2.3.3 U-parameter

We determine the U-parameters using the formation energies of the point defect in the three charge states under our consideration (positive, negative and neutral). For a given point defect, we deduce this fundamental parameter using equation 2.9

$$U = E_f^{q+1} + E_f^{q-1} - 2E_f^q \tag{2.9}$$

where U represents the U-parameter value when the Fermi-level is fixed at 0 eV;

$E_f^{q+1}$is the formation energy of the point defect in the positive charge state;

E_f^{q-1} denotes the formation energy of the point defect in the negative charge state;

E_f^q represents the formation energy of the defect in the neutral charge state.

We derived the U-parameter for the hydrogen vacancy (V_H) and the carbon vacancy (V_C) using the equation 2.10 and 2.11 respectively.

$$U[V_H] = E^f[V_H^{+1}] + E^f[V_H^{-1}] - 2E^f[V_H^0] \tag{2.10}$$

$$U[V_C] = E^f[V_C^{+1}] + E^f[V_C^{-1}] - 2E^f[V_C^0] \tag{2.11}$$

For our third vacancy configuration, V_{CH}, we derived the U-parameter value by

utilizing equation 2.12

$$U[V_{CH}] = E^f[V_{CH}^{+1}] + E^f[V_{CH}^{-1}] - 2E^f[V_{CH}^{0}] \tag{2.12}$$

2.3.4 Charge transition levels

Charge transition levels are of extreme importance because they have a bearing on the electrical and optical properties of a material. The charge transition levels show the energy level at which a point defect is likely to change its charge state. At these energy levels, the point defect can either emits or capture an electron. The transition energy levels are calculated relative to the valence band maximum ($E_F = 0$ eV). The derivation of the charge transition levels, $\varepsilon(q_1 \mid q_2)$ is based on equation 2.13 as illustrated below.

$$\varepsilon(q_1 \mid q_2) = \frac{E^f(D^{q_1}; E_F = 0) - E^f(D^{q_2}; E_F = 0)}{q_2 - q_1} \tag{2.13}$$

where $\varepsilon(q_1 \mid q_2)$ represents a transition from an initial charge state q_1 (+1,0) to a final charge state q_2 (0,-1);

$E^f(D^{q_1}; E_F = 0)$ is the formation energy of a point defect, D, whose initrial charge state is q_1 (+1,0) when the Fermi-level, E_F, is equal to 0 eV;

$E^f(D^{q_2}; E_F = 0)$ represents the formation energy of a point defect, D, whose final charge state is q_2 (0,-1) when the Fermi-level, E_F, is equal to 0 eV.

We determined the charge transition levels for V_H, $\varepsilon(+1 \mid 0)$ and $\varepsilon(0 \mid -1)$ using equations 2.14 and 2.15 respectively. The two point defect states (+1/0 and 0/-1) are equal in energy when we deduce the transition energy levels.

$$\varepsilon(+1 \mid 0) = \frac{E^f(V_H^{+1}; E_F = 0) - E^f(V_H^{0}; E_F = 0)}{0 - 1} \tag{2.14}$$

$$\varepsilon(0 \mid -1) = \frac{E^f(V_H^{0}; E_F = 0) - E^f(V_H^{-1}; E_F = 0)}{-1 - 0} \tag{2.15}$$

The determination of the charge transition levels for the carbon vacancy, V_C, was

done using the respective equations 2.16 and 2.17

$$\varepsilon(+1 \mid 0) = \frac{E^f(V_C^{+1}; E_F = 0) - E^f(V_C^0; E_F = 0)}{0 - 1} \tag{2.16}$$

$$\varepsilon(0 \mid -1) = \frac{E^f(V_C^0; E_F = 0) - E^f(V_C^{-1}; E_F = 0)}{-1 - 0} \tag{2.17}$$

We derived charge transition levels for, V_{CH}, using the equations 2.18 and 2.19 taken in that order.

$$\varepsilon(+1 \mid 0) = \frac{E^f(V_{CH}^{+1}; E_F = 0) - E^f(V_{CH}^0; E_F = 0)}{0 - 1} \tag{2.18}$$

$$\varepsilon(0 \mid -1) = \frac{E^f(V_{CH}^0; E_F = 0) - E^f(V_{CH}^{-1}; E_F = 0)}{-1 - 0} \tag{2.19}$$

2.3.5 Binding energy

The concept of binding energy is important in the characterization of point defects in two-dimensional materials. The binding energy is the difference in energy between the total formation energy of a point defect complex and the sum of the formation energies of the isolated point defect constituents.The magnitude of the binding energy gives the idea of the strength of the point defect interaction that results in the formation of a complex. Binding energy represents the amount of energy that is required in order to infinitely separate the point defects from each other. This parameter therefore provides valuable information of the stability of the defect complex.

2.3.6 Literature Review on: vacancy point defects, substitutional point defects and point defect complexes in graphane

Yang [2] employed DFT calculations to study the effect of substituting hydrogen atoms in the graphane chair configuration with transition-atoms impurity. They initially calculated fundamental information of pristine graphane using first principles under DFT

framework. The Projector Augmented Wave (PAW) method was used in line with the VASP code [39]. The method of Perdew et al [32][31] was implemented to deal with the exchange-corrrelaton functionals. In this work, they found out that missing hydrogen atoms produce defect levels within the band gap and these defect states are spin-polarized. The induced defects produce magnetic moments and if the vacancies are filled with a transition metal atom impurity, magnetism in line with Hund's rules is realised. The resulting structure is stable and has potential applications in spintronics and nanotechnology [2].

In their contribution of 2015, Mapasha et al [27] investigated electronic as well as magnetic properties of the hydrogen vacancy induced graphane. They focused on the most stable chair conformer whose pristine structure was altered by the creation of hydrogen vacancies on the hexagonal carbon ring. In this work, the DFT calculations were carried out under the Vienna Ab Initio Simulation Package (VASP) code. The fundamental exchange and correlation functionals were derived with the utilisation of Perdew, Burke and Ernzerhof's (PBE) generalised gradient approximation [31]. Among other findings, Mapasha et al [27] found out that hydrogen vacancies have positive formation energies and the vacancies give rise to metallic and semi-metallic magnetic moments. This raises the possibility of spintronics applications for defect-modified graphane. Another notable outcome of this study is that both positive and negative charge doping of the hydrogen vacancy configurations can considerably reduce the magnetic moments.

Lebegue et al [47] calculated the electronic structure properties of the chair and boat conformers of graphane, for both the ground states and excited states. They used the VASP code which was implemented under the projector augumented wave (PAW) approach to derive the ground and excited states properties of the two conformers. For the purpose of comparison, they determined the electronic structure properties of the two structures using the GW approximation together with the projector augumented wave method. They reported a direct band gap located at the BZ centre for both the chair and boat conformers. In this contribution, the effect of introducing a hydrogen

vacancy or a hydroxyl group was also studied for the chair conformer. Defect states that can be useful for nano-electronic applications were noted close to the Fermi level, just above the valence band maximum.

In their contribution, Deak et al [48][49] used standard DFT methods as well as screened non-local hybrid density functional supercell plane wave method (HSE06) [48][49] under the generalized Kohn-Sham theory to determine formation energies, excitation energies, charge transition levels, migration barrier energies and reaction energies for seven related defects in bulk diamond. The defects studied are: single vacancy (V), divacancy (V_2), substitutional nitrogen (N_S), pair of substitutional nitrogen (N_2), nitrogen-vacancy center (NV), pair of substitutional nitrogen and vacancy complex (N_2V). From this class of defects, the prominent one is the NV center. The nitrogen-vacancy center can be used as quantum bit and in nano-sensors. The NV formation processes of irradiation and annealing can give rise to other defect complexes whose properties also have to be comprehended.

In their work Cherati et al [18] characterized the electronic, magnetic and optical properties of substitutional oxygen defect as well as the oxygen complexes formed with vacancies and in diamond host material. They found out that the oxygen-vacancy complexes give rise to multiple defect levels within the diamond band gap. Thiering and Gali [50] also carried out an indepth research on substitutional oxygen defects and oxygen-hydrogen complexes formed in diamond. The work was motivated by the desire to find oxygen defects that can be used in diamond as quantum bits. One objective of their contribution was also to find out if there are oxygen defects and complexes that are related to the NV center and that can be utilised for quantum memory as well as applications in metrology [50]. The methodology that was used is density functional theory first principles calculations within the plane-wave supercell framework approach. The defects studied are: interstitial oxygen, substitutional oxygen , oxygen-vacancy complex (OV) and complexes formed by substitutional oxygen with oxygen-vacancy and hydrogen defects [50]. Among other results, Thiering and Gali found out that

oxygen defects in diamond are electrically active and they give rise to orbitals that are highly correlated. The neutral oxygen-vacancy defect shows a non-radiative decay path which is vey fast and is not similar to the NV defect. The Jahn-Teller distortion was exhibited by some defects such as oxygen-vacancy center in the positive charge state [50].

Capelli et al [51] reported an efficient process that is used for the formation of NV defect centres in diamond crystal called annealing *in situ*. Their proposed method involves the two processes of irradiation and annealing done simultaneously during the formation of NV centre defects. This method was compared to the standard phenomenon that starts with high particle irradiation which is then separately followed by annealing. The formation of NV centre defects is optimized by irradiating the diamond sample with high energy electrons when the temperature and pressure are considerably higher than those normally used in the standard procedure. In their contribution, they reported that annealing in situ significantly increases the conversion of nitrogen substitutional defects to NV centre defects by 117%. The high temperature facilitates the migration of the vacancies in the crystal and they are captured by the nitrogen substitutional defects as they diffuse through the diamond crystal. Ensemble of NV centre defects is important for optical sensing devices, biolabelling techniques and in lasers as well as biomedical applications [51].

In their article of 2008, Larsson and Delaney [52] used first principles DFT to study the electronic structure of the NV center in hydrogen-terminated diamond nano-clusters of two different sizes. The nano-clusters which they referred to as small and large are $C_{165}H_{100}$ and $C_{286}H_{144}$ respectively. The NV center in diamond comprises a substitutional nitrogen atom which is in an adjacent position to a carbon vacancy resulting in the formation of a defect complex [53]. The defect can exist in the neutral state, NV^0 and the negative charge state, NV^{-1}. The NV^0 state comprises five electrons-three from the carbon atoms and two from the nitrogen [52]. The NV^0 can accept one electron to form NV^{-1}-which thus has a total of six electrons. According to Lenef and

Rand [14], there are four sp^3 hybridized orbitals directed towards the vacancy. Linear combination of these orbitals form three ground state energy levels u, v and e. The five sp^3 hybridized electrons form ground state electron arrangement of $u^2v^2e^1$ for NV^0. When the NV^0 takes an additional electron to form NV^{-1}, the ground state electron arrangement changes to $u^2v^2e^2$. The two carbon atoms that are replaced by a vacancy and the substitutional nitrogen atom lie on a C_3 axis resulting in the defect having C_{3v} symmetry [52]. The ground state of the defect, $^3A_2$, has three energy levels which can be modeled by a single Slater determinant [54][55]. Similarly, the excited state, ^3E, is also three-fold degenerate and this state requires modeling by two or more Slater determinants.

Weber et al [7] present the criteria that can be used to search for potential host materials and deep center defects that are similar to the nitrogen-vacancy center in diamond. This was motivated by the fact that the NV-center's quantum states can be reproduced, controlled, measured and exploited as quantum bits (qubits). Qubits forms the building blocks for the operation of quantum computers. The search for innovative hosts and deep centers is also influenced by the apparent difficulties that engineers face in growing and fabricating diamond devices. In order to clearly illustrate their perspective, Weber et al [7] compared the nitrogen-vacancy center's electronic structure in diamond with that of a number of deep centers in 4H silicon carbide. For the diamond crystal, first principles calculations were done with the utilization of supercells containing 64 carbon atoms while the SiC supercells contained 96 atoms. The DFT calculations were done using the Projector Augmented Wave method [56] within the VASP code. Defect energy calculations were carried out using constrained DFT.

The given host criteria discussed in this work primarily exist in order to eliminate decoherence in the deep centre defect. Among others, a suitable host material must satisfy the criteria listed below.

- It must have a bandgap which is wide enough to accommodate the defect's multiple sub-states;

- the spin-orbit coupling must be small so that undesirable spin flips are eliminated within the bound states of the defect;
- the host can be a bulk crystal or single thin-film crystals that are of high quality so that unwanted defects and paramagnetic flaws are not present as they negatively affect the spin states of the deep centre;
- isotopes of elements whose nuclear spin is zero so that undesirable spin bath effects can be removed from the host using isotopic engineering techniques. A possible deep centre defect must meet the following expectations as derived from the NV-1in diamond
- a bound state that can be utilized as a qubit, that is, it must be considerably lasting and paramagnetic (have at least one unpaired electron). Moreover,there must be at least two defect states that have appropriate energy levels splittings to form spin sublevels;
- the defect's optical transitions must not bring about unwanted interference from energy states of the of the host material. The magnitude of the energy used to probe the qubit must be lower than the ionisation energy of the host;
- the energy difference between the bound states must be relatively high to eliminate thermal excitations which obliterate vital spin information;
- polarizability of the qubit state through a suitable optical pumping cycle- this must encompass transition from the lowest energy state to an excited state before a non-radiative spin-selective decay evolution;
- the qubit state luminescence must show any change in the qubit sublevels evolution. The transition from one sublevel to another must be measurable, spin-conserving and shown by a clear variation in any of the wave properties such as wavelength, amplitude or intensity.

Chapter 3

Material Property Derivation

We employ electronic structure methods to comprehend the properties of materials. In this section we commence from the wave function theory (WFT) as proposed by Erwin Schrödinger in 1925[1]. We then delve into the early approximations that were developed in an attempt to simplify and solve the many-body Schrödinger equation. The first approximation we consider is the Born-Oppenheimer (BO), which is then followed by Hartree's independent electron approximation. The Hartree-Fock formalism will then be dealt with as an extension of the later. The last section of this chapter deals with Density Functional Theory (DFT) which is now widely used by many computational material researchers to derive apt properties of many-body systems.

3.1 Wave Function Theory

Materials are made up of many nuclei and electrons that are constantly interacting with one another [40]. The properties of any given material depends on these interactions. In an attempt to derive the properties of many-body systems[2], Erwin Schrödinger proposed that all the observables of a given system are contained in the wavefunction, Ψ [57].

[1] Erwin Schrödinger was awarded the Physics Nobel prize in 1933 for the wave function theory which he proposed in 1925

[2] We refer to the many nuclei and electrons in a given material and how they interact as a many-body system.

Schrödinger initiated the idea that the solution to his equation, as given by equation 3.1, unlocks the key to the derivation of many properties of a given system.

$$\hat{H}\Psi = E\Psi \tag{3.1}$$

Where

$\hat{H}$ represents the Hamiltonian or total energy operator of the many-body system,

Ψ is the wave function of the many electrons-nuclei system,

E is the energy eigenvalue or the total energy of the system under consideration.

We can derive many properties of a given system by solving the equation $\hat{H}\Psi = E\Psi$ with the objective of deducing the total energy of the system- in particular the ground state energy [41]. The expectation value of the Hamiltonian operator over any wave function from a given basis set will always yield an energy eigenvalue which is equal to or greater than the true ground state energy of a given system [58][59]. This is true according to the variational principle which is discussed in the next section.

Once the total ground state energy of a non-degenerate system is obtained, properties such as: charge density, bond energy and length, barrier heights and potential energy surface can be derived for the system. The physical properties of a given system are therefore linked to the ground state energy or the total energy or alternatively the differences that exist between the total energies [60]. Thus, the derivation of the total ground state energy for a given system is the fundamental initial stage required in order to come up with the properties of the system. The determination of the total ground state energy by way of minimizing the total energy of the system can be used to predict the geometric and electronic properties of the system under consideration. The variational method is a powerful tool useful for the determination of the lowest energy state.

3.1.1 Variational Principle

In order to determine the total ground state energy, E_{GS}, we commence by constraining the wave function to be a member of a set of functions that satisfies orthonomality. We approximate the ground state energy by way of minimizing the expectation value of the Hamiltonian over a given wave function from the set [61]. The expectation value of the Hamiltonian, $\hat{H}$, over any arbitrary choice of a wave function from the set of basis wave functions, will always yield an energy value which is equal to or bigger than the true ground state energy [62][58].

In order to get an expression for the ground state energy, we multiply both sides of equation 3.1 by Ψ^* and put integral signs so that we have the following equation

$$\int \Psi^* \hat{H} \Psi dr = \int E_{GS} \Psi \Psi^* dr \tag{3.2}$$

Thus the ground state energy is given by

$$E_{GS} = \frac{\int \Psi^* \hat{H} \Psi dr}{\int \Psi \Psi^* dr} \tag{3.3}$$

Once, we have the ground state energy, other fundamental properties of a many-body system can be deduced.

3.1.2 The Many-Body System Hamiltonian

For a many-body system, the Hamiltonian can be split into two components, that is the sum of the total kinetic energy operator, $\hat{T}$, and total potential energy operator, $\hat{V}$, of the system [63], i.e

$$\hat{H} = \hat{T} + \hat{V} \tag{3.4}$$

For this system, the total energy Hamiltonian operator can further be expanded to five terms as shown by equation 3.5

$$\hat{H} = \hat{T}_e + \hat{T}_n + \hat{V_{n-e}} + \hat{V_{e-e}} + \hat{V_{n-n}} \tag{3.5}$$

Where

$\hat{T}_e$ is the total kinetic energy of all the electrons, N_e, in the system under consideration, given by equation 3.6

$$\hat{T}_e = -\frac{\hbar^2}{2m_e}\sum_{i=1}^{N_e}\nabla_i^2 \tag{3.6}$$

$\hat{T}_n$ represents the total kinetic energy of all the system nuclei, N_n, and it is given by equation 3.7

$$\hat{T}_n = -\frac{\hbar^2}{2M_n}\sum_{I=1}^{N_n}\nabla_I^2 \tag{3.7}$$

$\hat{V_{n-e}}$ is the Coulomb attraction between the nuclei and the electrons. It is given by equation 3.8

$$\hat{V_{n-e}} = -\sum_{i=1}^{N_e}\sum_{I=1}^{N_n}\frac{Z_I e^2}{\left|\vec{r_i} - \vec{R_I}\right|} \tag{3.8}$$

$\hat{V_{e-e}}$ is the Coulomb electron-electron repulsion term between the i^{th} and j^{th} electrons. The expression to determine $\hat{V_{e-e}}$ is depicted by equation 3.9

$$\hat{V_{e-e}} = \frac{1}{2}\sum_{i=1}^{N_e}\sum_{j,j\neq i}^{N_e}\frac{e^2}{|\vec{r_i} - \vec{r_j}|} \tag{3.9}$$

$\hat{V_{n-n}}$ denotes the Coulomb repulsion between the $I^{th}$and J^{th} nuclei and it is given by equation 3.10

$$\hat{V_{n-n}} = \frac{1}{2}\sum_{I=1}^{N_n}\sum_{J,J\neq I}^{N_n}\frac{Z_I Z_J e^2}{\left|\vec{R_I} - \vec{R_J}\right|} \tag{3.10}$$

$\vec{r_i}$ and $\vec{R_I}$ shows the positions of the i^{th} electron and the I^{th} nucleus respectively.

In order to get a clear insight into the many aspects that are encompassed by

equation 3.5 we need to state the complete many nuclei-electron Hamiltonian, that is

$$\hat{H} = -\frac{\hbar^2}{2m_e}\sum_{i=1}^{N_e}\nabla_i^2 - \frac{\hbar^2}{2M_I}\sum_{I=1}^{N_n}\nabla_I^2 - \sum_{i=1}^{N_e}\sum_{I=1}^{N_n}\frac{Z_I e^2}{\left|\vec{r_i} - \vec{R_I}\right|} + \frac{1}{2}\sum_{i=1}^{N_e}\sum_{j,j\neq i}^{N_e}\frac{e^2}{|\vec{r_i} - \vec{r_j}|}$$

$$+ \frac{1}{2}\sum_{I=1}^{N_n}\sum_{J,J\neq I}^{N_n}\frac{Z_I Z_J e^2}{\left|\vec{R_I} - \vec{R_J}\right|} \tag{3.11}$$

The expanded Schrödinger equation for the many-body system is as shown by equation 3.12.

$$(-\frac{\hbar^2}{2m_e}\sum_{i=1}^{N_e}\nabla_i^2 - \frac{\hbar^2}{2M_I}\sum_{I=1}^{N_n}\nabla_I^2 - \sum_{i=1}^{N_e}\sum_{I=1}^{N_n}\frac{Z_I e^2}{\left|\vec{r_i} - \vec{R_I}\right|} + \frac{1}{2}\sum_{i=1}^{N_e}\sum_{j,j\neq i}^{N_e}\frac{e^2}{|\vec{r_i} - \vec{r_j}|}$$

$$+ \frac{1}{2}\sum_{I=1}^{N_n}\sum_{J,J\neq I}^{N_n}\frac{Z_I Z_J e^2}{\left|\vec{R_I} - \vec{R_J}\right|})\Psi = E\Psi \tag{3.12}$$

However, solving this complicated equation is a tall order since the motion of the ions is coupled with the motion of the electrons [42]. Consequently, there is need to come up with some approximations designed to simplify the Schrödinger equation. In the next section, we consider our first approximation as proposed by Born and Oppenheimer in 1927 [64].

3.2 Born-Oppenheimer Approximation

In 1927, Born and Oppenheimer came up with a fundamental approximation that enables the motion of the nuclei to be separated from the electronic motion [64]. One of the main ideas of this approximation is that the mass of an ion is considerably bigger than that of an electron , $M_I \gg m_e$- hence the motion of an electron is extremely fast as compared to the motion of an ion. The ions can thus be considered to be essentially static. The kinetic energy term for the ions can therefore be approximated to be zero,

that is,

$$\hat{T_n} = -\frac{\hbar^2}{2M_I}\sum_{I=1}^{N_n}\nabla_I^2 \approx 0 \tag{3.13}$$

The ions in the many-body system cannot follow the motion of the electrons and the position that each ion occupy in a material is assumed to be constant. From this point of view we can consider the nuclei-nuclei interaction, $\hat{V_{n-n}}$, to be a constant, C, as depicted by equation 3.14

$$\hat{V_{n-n}} = \frac{1}{2}\sum_{I=1}^{N_n}\sum_{J,J\neq I}^{N_n}\frac{Z_I Z_J e^2}{\left|\vec{R_I} - \vec{R_J}\right|} \approx C \tag{3.14}$$

This adiabatic approximation has considerably simplified equation 3.12 by way of decoupling the electronic Hamiltonian from ionic Hamiltonian. This has reduced the complexity of the task at hand as we can now focus on finding the solutions of the simpler equation 3.15, given as

$$(\hat{T_e} + \hat{V_{n-e}} + \hat{V_{e-e}})\Psi_e = E_e\Psi_e \tag{3.15}$$

which can be expanded to equation 3.16

$$(-\frac{\hbar^2}{2m_e}\sum_{i=1}^{N_e}\nabla_i^2 - \sum_{i=1}^{N_e}\sum_{I=1}^{N_n}\frac{Z_I e^2}{\left|\vec{r_i} - \vec{R_I}\right|} + \frac{1}{2}\sum_{i=1}^{N_e}\sum_{j,j\neq i}^{N_e}\frac{e^2}{|\vec{r_i} - \vec{r_j}|})\Psi_e = E_e\Psi_e \tag{3.16}$$

where Ψ_e is the wave function of the many-electron system,

E_e is the energy eigenvalue of the many-electron system.

Using atomic mass units we can further simplify equation 3.16 by making the approximation that $\hbar^2 \approx m_e \approx e^2 \approx 1$, that is

$$(-\frac{1}{2}\sum\nabla_i^2 - \sum_{i=1}^{N_e}\sum_{I=1}^{N_n}\frac{Z_I}{\left|\vec{r_i} - \vec{R_I}\right|} + \frac{1}{2}\sum_{i=1}^{N_e}\sum_{j,j\neq i}^{N_e}\frac{1}{|\vec{r_i} - \vec{r_j}|})\Psi_e = E_e\Psi_e \tag{3.17}$$

Finding solutions of equation 3.17 is still problematic because of the challenges posed by electron-electron interactions. In a fine attempt to deal with this obstacle, Hartree

proposed the independent electron approximation in 1928 [65].

3.3 Hartree's Independent Electron Approximation

The main idea that Hartree proposed in 1928 was the simplification of the many electron wave function, Ψ_e, by way of expressing it as a product of one electron wave functions [65], thus we have

$$\Psi_e(\vec{r_1},\vec{r_2},\vec{r_3}.....\vec{r_{N_e}}) = \Psi_1(\vec{r_1})\Psi_2(\vec{r_2})\Psi_3(\vec{r_3}).....\Psi_{N_e}(\vec{r_{N_e}}) \tag{3.18}$$

By initiating the independent electron picture Hartree circumvented the problems brought about by electron-electron interaction by simplifying the many electron equation 3.15 to a set of one electron Schrödinger equations:

$$(\hat{T_e} + \hat{V_{n-e}} + \hat{V_H})\Psi_i = \varepsilon_i\Psi_i \tag{3.19}$$

which can also be stated as

$$(\hat{T_e} + \hat{V_{eff}})\Psi_i = \varepsilon_i\Psi_i \tag{3.20}$$

where

$$\hat{V_{eff}} = \hat{V_{n-e}} + \hat{V_H} \tag{3.21}$$

The symbols: Ψ_i represents the wave function of the i^{th} independent electron,

ε_i stands for the energy eigenvalue of the independent i^{th} electron,

$\hat{V_H}$ represents the Hartree potential,

$\hat{V_{eff}}$ is the net or effective potential which is given by equation 3.21 above,

$\hat{T_e}$ represents one electron kinetic energy,

$\hat{V_{n-e}}$ denotes the Coulomb attraction between a single electron and the average value of the ionic potentials.

The Hartree potential, $\hat{V_H}$, is the mean potential that the i^{th} electron experiences as a consequence of being in the net field created by all the other electrons, that is $N_e - i^{th}$ electrons. Expanding the one electron Schrödinger equation 3.19, we get the formula:

$$(-\frac{1}{2}\sum\nabla_i^2 - \sum_{i=1}^{N_e}\sum_{I=1}^{N_n}\frac{Z_I}{\left|\vec{r_i} - \vec{R_I}\right|} + \frac{1}{2}\sum_{i=1}^{N_e}\sum_{j,j\neq i}^{N_e}\frac{1}{|\vec{r_i} - \vec{r_j}|})\Psi_i = \varepsilon_i\Psi_i \tag{3.22}$$

3.4 Hartree-Fock Approximation

The Hartree formalism has a number of shortcomings that necessitated a further development of a new theory- the so called Hartree-Fock approximation [66]. Before we delve into the Hartree-Fock formalism, we hereby state some of the deficiencies of the Hartree theory.

3.4.1 Short-comings of the Hartree theory

The theory treated electrons as distinguishable, yet electrons are indistinguishable. Furthermore, the theory does not take account of the anti-symmetric nature of the wave function used to represent the motion of electrons. Electrons are fermions, hence the wave function used to represent them must be anti-symmetric. If we interchange two electrons, the sign of the wave function has to change.

The Pauli exclusion principle which states that no two electrons can have the same set of quantum numbers is also not considered in the Hartree theory. The movement of an electron is fully explained by a set of four quantum numbers, namely n, l , m_l and m_s

where n represents the principal quantum number which denotes the radius of the

position of an electron from the nucleus of an atom;

l gives the shape of the electron orbital;

m_l is the quantum number which shows the orientation of the electron orbit;

m_s is the magnetic spin quantum number which is used to denote the rotation of each electron. In simple terms it shows the electron spin-up $(+\frac{1}{2})$ or spin-down $(-\frac{1}{2})$.

Electron spin is a vital and integral property of an electron. This concept of electron spin is of great importance because it is related to the generation of a magnetic field among other things. The Hartree theory does not include this fundamental electron characteristic and this is a yawning gap in this formalism. Furthermore the Hartree approximation does not include the electron exchange and correlation aspects which are of fundamental importance in the derivation of the properties of a many-electron system. These deficiencies in this theory showed that there was need to extend Hartree's independent electron picture. Vladimir Fock is credited with the extension of the Hartree theory and his work culminated in the development of the so called Hartree-Fock theory [66] [67]. At the core of the Hartree-Fock formalism is the use of a set of matrix elements called the Slater determinant to represent the many electron wave function [54][55].

3.4.2 The Slater Determinant

The Slater determinant was introduced in 1929 by John C Slater [54]. In simple terms a Slater determinant is a matrix expression which is utilized to represent the concepts entwined in a multi-electron wave function. The determinant is built from independent electron wave functions or electron spin-orbitals. It satisfies the anti-symmetric nature of a many-electron wave function as well as the requirements of the Pauli exclusion principle [55]. The usefulness of the Slater determinant in the representation of a multi-electron wave function can be demonstrated by using the smallest many-electron system which is composed of only two electrons, e_1 and e_2 located at positions, r_1 and r_2. The two-electron wave function, Ψ_m, can be constructed as a matrix by using two spin-

orbitals $\Psi_1(r_1)$ and $\Psi_2(r_2)$ as shown below

$$\Psi_m(r_1, r_2) = \frac{1}{\sqrt{2}} \begin{bmatrix} \Psi_1(r_1) & \Psi_2(r_1) \\ \Psi_1(r_2) & \Psi_2(r_2) \end{bmatrix} \tag{3.23}$$

The rows in the Slater determinant represents the single electron particle states. In the many electron wave function, these states are denoted by a complete set of the four quantum numbers for each electron. The columns represent the electron coordinates comprising three space variables and one spin component. The antisymmetric nature of the electron wave function is entwined in the Slater determinant because if two rows or two columns are interchanged, the sign of the determinant is flipped. Pauli's exclusion principle is also accomodated in the Slater determinant because if any two rows or two columns are identical the determinant vanishes.

Equation 3.23 can be modified to the expression given by equation 3.24, that is

$$\Psi_m(r_1, r_2) = \frac{1}{\sqrt{2}} \left[\Psi_1(r_1)\Psi_2(r_2) - \Psi_1(r_2)\Psi_2(r_1)\right] \tag{3.24}$$

The square root of two represents the normalisation constant for the two electron system. The Slater determinant can be generalised for a multi-electron system comprising N_e electrons as shown by equation 3.25

$$\Psi_m = \frac{1}{\sqrt{N_e!}} \begin{bmatrix} \Psi_1(r_1) & \Psi_2(r_1) & \Psi_3(r_1) & .. & .. & .. & .. & .. & .. & \Psi_{N_e}(r_1) \\ \Psi_1(r_2) & \Psi_2(r_2) & ... & .. & .. & .. & .. & .. & .. & ... \\ \Psi_1(r_3) & \Psi_2(r_3) & ... & .. & .. & .. & .. & .. & .. & ... \\ ... & ... & ... & .. & .. & .. & .. & .. & .. & ... \\ ... & ... & ... & .. & .. & .. & .. & .. & .. & ... \\ ... & ... & ... & .. & .. & .. & .. & .. & .. & ... \\ ... & ... & ... & .. & .. & .. & .. & .. & .. & ... \\ ... & ... & ... & .. & .. & .. & .. & .. & .. & ... \\ \Psi_1(r_{N-1}) & ... & ... & .. & .. & .. & .. & .. & .. & ... \\ \Psi_1(r_{N_e}) & \Psi_2(r_{N_e}) & ... & .. & .. & .. & .. & .. & .. & \Psi_{N_e}(r_{N_e}) \end{bmatrix} \tag{3.25}$$

3.5 *ab initio* Density Functional Theory

If we have a many-electron system that has N electrons, in order to derive possible properties of this system, we need three spatial variables x, y and z as well as electron spin, ζ, for each electron. We therefore need four variables or four coordinates to describe the motion of each electron. For N electrons, we must have $4N$ Schrödinger equations to describe our system. For instance, given a system that has only 10 electrons, we must have 40 Schrödinger equations to understand this system. Therefore, the larger the system becomes, the more complicated it is to solve all the equations under consideration.

The difficulty above prompted researchers to think along the lines of using electron density[3] to get properties of many-electron systems. The use of electron density as an apt variable decreases the $4N$ spatial coordinates to only 4 spatial coordinates comprising 3 spatial coordinates and 1 electron spin component. The genesis of *ab initio* DFT[4] was first initiated by Thomas and Fermi who showed the existence of a one to

[3] Electron density is the number of electrons of a given system per unit volume.
[4] *ab initio* means from the beginning and there are no empirical parameters entwined in DFT.

one correspondence between the charge density and many-particle wave function [68].

3.5.1 Thomas-Fermi model

Thomas and Fermi in 1927 showed the existence of an implicit connection between the electron density and the external potential [69], that is

$$n(r) = \gamma \{\mu - V_{eff}(r)\}^{\frac{3}{2}} \tag{3.26}$$

where $n(r)$ is the electron density of a non-interacting uniform electron gas,

μ is the chemical potential of the system,

V_{eff} is the effective potential given by the sum of the external and the Hartree potential, i.e

$$V_{eff} = V(r) + V_H \tag{3.27}$$

γ is a constant given by equation 3.28

$$\gamma = \frac{1}{3\pi^2}\left(\frac{2m}{\hbar^2}\right)^{\frac{3}{2}} \tag{3.28}$$

The Thomas and Fermi model was a paramount initial step towards comprehending the many-body system as is shown in the section that follows.

3.5.2 Hohenberg- Kohn Theorems (HK I and HK II)

The firm foundation of Density Functional Theory (DFT) is found in Pierre Hohenberg and Walter Kohn's two theorems (HK I and HK II) that were proposed in 1964 [70]. Hohenberg and Kohn came up with two fundamental theorems that opened a new ground for computational modelling methods. The first theorem proved that it is possible to use the ground state electron density to determine the external potential, the ground state energy, the Hamiltonian and other properties of a non-degenerate many-electron

system [63]. HK I is generally referred to as an existence theorem since it doesn't show much more than the existence and the possible use of the electron density to derive other properties. HK II initiated the search for the electron density and heralded the advent of DFT.

3.5.2.1 Hohenberg and Kohn's First Theorem and Proof

Hohenberg and Kohn's first theorem (HK I) was considered for the lowest energy state of a system of interacting electrons moving under the influence of the system's external potential, $V(r)$, as well as the electron-electron Coulomb repulsion forces [61]. The theorem applies to a ground state which is non-degenerate[5] and on which there is no external influence such as magnetic field. HK I states that:

For a non-degenerate ground state of a many-electron system, the external potential is a unique functional[6] *of the electron density.*

From this principle Hohenberg and Kohn came up with a fundamental expression in which the electron density was used as a variable,

that is:

$$E[n(r)] \equiv \int V(r)n(r)dr + F[n(r)] \tag{3.29}$$

where

$E[n(r]$ is the energy of the system for a given electron density $n(r)$ at some position r;

$\int V(r)n(r)dr$ is the nuclei-electron attraction intergrated over all space- i.e it is the external potential which is interacting with the electron density;

$F[n(r)]$ is a universal functional given in terms of the density.

The external potential depends on the system under consideration but the universal functional is the same for any given system. Comparing equation 3.29 with the equation

[5] A non-degenerate ground state has only one energy value that corresponds to the system.
[6] A functional is a type of function whose argument is also a function of some other variable.

3.30, it is apparent that the universal functional, $F[n(r)]$, contains the kinetic energy term, $\hat{T}_e$, and the Coulomb electron-electron repulsion term - $\hat{V}_{e-e}$, that is

$$\hat{H} = \hat{E} = \hat{V}_{n-e} + \hat{T}_e + \hat{V}_{e-e} \tag{3.30}$$

All the other quantum mechanical effects that exist because of the electron-electron interaction are embedded in the universal functional term [71]. In order to use HK I, there is need to prove the uniqueness of the theorem, that is there is a one to one correspondence between a given external potential and a given ground state electron density. This is proved via *reductio ad absurdum* [72]. We make an assumption and then test its validity or correctness. If the assumption leads to a valid outcome then it is correct but if it leads to an impossible result, then we can conclude that the assumption is false [72]. *Reductio ad absurdum* therefore has three main steps, that is

- we make an assumption,
- we test the validity of the assumption,
- if the assumption leads to a valid result, then it is correct. Conversely, an impossible result shows that the assumption is false

Our point of departure is the assumption that it is possible to obtain two different external potentials, V_b and V_c, from similar non-degenerate ground state density, n_0. The external potentials, V_b and V_c, corresponds to the Hamiltonians, H_b and H_c [61]. They also yield the ground state wave functions, Ψ_{b_0} and Ψ_{c_0}, as well as ground state energy, E_{b_0} and E_{c_0} respectively. The ground state energy at b and c are given by

$$E_{b_0} = \langle \Psi_{b_0} \mid H_b \mid \Psi_{b_0} \rangle \tag{3.31}$$

and

$$E_{c_0} = \langle \Psi_{c_0} \mid H_c \mid \Psi_{c_0} \rangle \tag{3.32}$$

Applying, the Rayleigh Ritz variational principle [62], the ground state energy at b must be less than[7] the expectation value of H_b applied over any other wave function that we try from a given basis set, Ψ_{c_0},

that is

$$E_{b_0} \prec \langle \Psi_{c_0} \mid H_b \mid \Psi_{c_0} \rangle \tag{3.33}$$

subtracting and adding H_c to H_b we have

$$E_{b_0} \prec \langle \Psi_{c_0} \mid H_b - H_c + H_c \mid \Psi_{c_0} \rangle \tag{3.34}$$

and this can be written as

$$E_{b_0} \prec \langle \Psi_{c_0} \mid H_b - H_c \mid \Psi_{c_0} \rangle + \langle \Psi_{c_0} \mid H_c \mid \Psi_{c_0} \rangle \tag{3.35}$$

which gives

$$E_{b_0} \prec \langle \Psi_{c_0} \mid H_b - H_c \mid \Psi_{c_0} \rangle + E_{c_0} \tag{3.36}$$

The Hamiltonian at b is given by

$$\hat{H}_b = \hat{T} + \hat{V_{e-e}} + \hat{V}_b \tag{3.37}$$

whereas the Hamiltonian at c is given by

$$\hat{H}_c = \hat{T} + \hat{V_{e-e}} + \hat{V}_c \tag{3.38}$$

Since the kinetic energy and the electron-electron repulsion terms are universal, they are identical in equations 3.38 and 3.37, thus we have

$$\hat{H}_b - \hat{H}_c = \hat{V}_b - \hat{V}_c \tag{3.39}$$

[7]The inequality holds if the system has a non-degenerate ground state energy

The difference between the two Hamiltonians, $\hat{H}_b$ and $\hat{H}_c$ is determined only by the difference between the external potentials which is system dependent. Therefore equation 3.36 can be written as

$$E_{b_0} \prec \langle \Psi_{c_0} \mid V_b - V_c \mid \Psi_{c_0} \rangle + E_{c_0} \tag{3.40}$$

The product $\Psi_{c_0}.\Psi_{c_0}$ integrated over all space yields the ground state electron density, n_0, thus we can transform equation 3.40 to become

$$E_{b_0} \prec \int \left[v_b(r) - v_c(r) \right] n_0(r) dr + E_{c_0} \tag{3.41}$$

If we interchange b and c and we follow the same procedure commencing from equation 3.33, we yield the result

$$E_{c_0} \prec \int \left[v_c(r) - v_b(r) \right] n_0(r) dr + E_{b_0} \tag{3.42}$$

Adding equation 3.41 to equation 3.42 we get the output

$$E_{b_0} + E_{c_0} \prec E_{c_0} + E_{b_0} \tag{3.43}$$

This is a contradiction since a given energy cannot be less than itself. We have thus proved that the ground state density of a non-degenerate system uniquely determines the external potential. If we have the external potential, we can deduce the Hamiltonian and then derive the wavefunction to use.

3.5.2.2 Hohenberg and Kohn's Second Theorem and Proof

Hohenberg and Kohn's second theorem states that there is an existence of a universal energy functional, $E[n(r)]$, for a given external potential, $V(r)$, and the ground state energy is the global minimum for the functional [70]. The electron density that minimizes the universal functional is the precise ground state density [61]. HK II, just like HK I, is applicable to ground state electron densities only- excited states electron

densities are excluded. This set of electron densities applicable to only the ground state of a given system that has a certain value of the external potential is referred to as V *representable*. The proof for HK II is simple and straight-forward. We commence from a particular system that has external potential $V(r)$ and ground state density $n_0(r)$. The ground state energy, E_{a_0} at an arbitrary position is derived from the expectation value of the hamiltonian H_{a_0} over the wave function, Ψ_{a_0}, that is

$$E_{a_0} = \langle \Psi_{a_0} \mid H_{a_0} \mid \Psi_{a_0} \rangle \tag{3.44}$$

Since this is the lowest energy that the system under consideration can have, it follows therefore that any different electron density which is connected to another wave function, Ψ_b, will yield an energy value which is greater than the ground state energy , that is $\langle \Psi_b \mid H_{a_0} \mid \Psi_b \rangle$ is greater than $\langle \Psi_{a_0} \mid H_{a_0} \mid \Psi_{a_0} \rangle$.

3.5.3 Kohn-Sham Equations

The Hohenberg-Kohn theorems played a pivotal role in the development of density functional theory as a quantum mechanical method. The energy functional for a system of interacting electrons as given by equation 3.45 became a fundamental step towards the practical implementation of DFT to derive material properties. This energy functional can be given as

$$E_i[n(r)] = \int V(r)n(r)dr + F_i[n(r)] \tag{3.45}$$

which can can be expanded to

$$E_i[n(r)] = \int V(r)n(r)dr + \hat{T}_i[n(r)] + V_{i_{e-e}}\hat{[}n(r)] \tag{3.46}$$

and thus we have

$$F_i[n(r)] = \hat{T}_i[n(r)] + V_{i_{e-e}}\hat{[}n(r)] \tag{3.47}$$

where $F_i[n(r)]$ is the universal functional for a system of interacting electrons,

$\hat{T}_i[n(r)]$ is the kinetic energy functional for the interacting electrons,

$V_{i_{e-e}}\hat{[}n(r)]$ is the electron-electron repulsion term,

i denotes that the energy functionals are for a system of interacting electrons.

However, the stumbling block is the determination of the universal functional, $F_i[n(r)]$ which encompass the electron-electron interaction term, $V_{i_{e-e}}\hat{[}n(r)]$. In order to overcome this problem, Kohn and Sham [73] proposed to consider a fictitious system of non-interacting electrons that has a charge density which is equivalent to that of a real system. The transition from an interacting to a non-interacting electron system represents a simplification of the problem at hand since we now have, $V_{e-e}\hat{[}n(r)] = 0$. The universal functional no longer contains the one on one electron-electron repulsion term which is difficult to deal with. The Hohenberg-Kohn energy functional for a system of interacting electrons is transformed to the Kohn-Sham energy functional as depicted by equation 3.48

$$E_{KS}[n(r)] = \int V(r)n(r)dr + F_{KS}[n(r)] \tag{3.48}$$

which can be written as

$$E_{KS}[n(r)] = \int V(r)n(r)dr + \hat{T_{KS}}[n(r)] + \hat{E_{HXC}}[n(r) \tag{3.49}$$

where $\int V(r)n(r)dr$ is the external potential term, which is the same for given system whether the electrons are interacting or not,

$E_{KS}[n(r)]$ is the Kohn-Sham energy functional,

$F_{KS}[n(r)]$ is the Kohn-Sham universal functional,

$\hat{T_{KS}}[n(r)]$ is Kohn-Sham total kinetic energy,

$\hat{E_{HXC}}[n(r)$ is the correction term, which encompass the Hartree energy, E_H, and the exchange and correlation energy, E_{XC}.

The transition from an interacting system to a non-interacting one transforms the

Schrödinger equation $(\hat{T_e} + \hat{V_{n-e}} + \hat{V_H})\Psi_i = \varepsilon_i \Psi_i$ to the Kohn-Sham version [5], that is

$$(\hat{T_{KS}} + \hat{V_{KS}})\Phi_{KS} = \varepsilon_{ni}\Phi_{KS} \tag{3.50}$$

where Φ_{KS} is the Kohn-Sham wave function that is assumed to be Slater determinant,

ε_{ni} is the non-interacting energy eigenvalue,

$\hat{V_{KS}}$ is the Kohn-Sham potential.

The derivation of the Kohn-Sham potential is of paramount importance in order to be able to solve equation 3.50. In order to do this we commence from the Euler equation [74]

$$\frac{\delta F}{\delta n(r)} + V(r) = 0 \tag{3.51}$$

which implies that

$$\frac{\delta F}{\delta n(r)} = -V(r) \tag{3.52}$$

Likewise for the Kohn-Sham terms we have

$$\frac{\delta \hat{T_{KS}}}{\delta n(r)} + V_{KS}(r) = 0 \tag{3.53}$$

which also implies that

$$\frac{\delta \hat{T_{KS}}}{\delta n(r)} = -V_{KS}(r) \tag{3.54}$$

From equation 3.49, the Kohn-Sham universal functional is given by equation 3.55 [74]

$$F_{KS}[n(r)] = \hat{T_{KS}}[n(r)] + \hat{E_{HXC}}[n(r) \tag{3.55}$$

which can be expanded to

$$F_{KS}[n(r)] = \hat{T_{KS}}[n(r)] + E_H\hat{[}n(r) + E_{XC}\hat{[}n(r)] \tag{3.56}$$

The functional derivative with respective to density of each term in this expression is

[74]

$$\frac{\delta F}{\delta n(r)} = \frac{\delta \hat{T_{KS}}}{\delta n(r)} + \frac{\delta \hat{E_H}}{\delta n(r)} + \frac{\delta \hat{E_{XC}}}{\delta n(r)} \tag{3.57}$$

Substituting equations 3.52 and 3.54 in equation 3.57 we have

$$-V(r) = -V_{KS}(r) + \frac{\delta \hat{E_H}}{\delta n(r)} + \frac{\delta \hat{E_{XC}}}{\delta n(r)} \tag{3.58}$$

The Hartree potential is given by [74],

$$V_H = \frac{\delta \hat{E_H}}{\delta n(r)} \tag{3.59}$$

and likewise the exchange and correlation potential is given by,

$$V_{XC} = \frac{\delta \hat{E_{XC}}}{\delta n(r)} \tag{3.60}$$

Inserting V_H and V_{XC} in equation 3.58 yields the Kohn-Sham potential [74] which is made up of three components as depicted by equation 3.61

$$V_{KS}(r) = V(r) + V_H + V_{XC} \tag{3.61}$$

A set of Kohn-Sham equations has to be solved in a self-consistent manner as outlined in the section that follows.

3.6 Solving Kohn-Sham Equations Self-consistently

The initial step when solving Kohn-Sham equations is the guessing of the electron density as shown by table 3.1 [74]. The second step is the systematic derivation of the Kohn-Sham potential which comprises the system's external potential, the Hartree potential and the exchange-correlation potential. After this, the solving of the Kohn-Sham equations is the next fundamental stage which enables the calculation of the electron density in step 4. If there is convergence, one can then determine critical

Table 3.1: Recordings of the fundamental steps for solving the Kohn-Sham equations in a self-consistent manner.

Step 1	*Initial electron density guess*	$n\uparrow(r)n\downarrow(r)$
Step 2	*Derivation of* $Kohn-Sham$ *potential*	$V_{KS}(r)=V(r)+V_H[n(r)]+V_{XC}[n\uparrow(r)n\downarrow(r)]$
Step 3	*Solving of* $Kohn-Sham$ *equations*	$(\hat{T_{KS}}+\hat{V_{KS}})\Phi_{KS}=\varepsilon_{ni}\Phi_{KS}$
Step 4	*Calculation of electron density*	$n(r)=\sum_i f_i \mid \Phi_{KS}(r) \mid^2$
Step 5	*Determination of* $self-consistency$	If self-consistent go to step 6 If not, start again from step 2
Step 6	*Material properties output*	Ground state energy, forces, stresses, strain, energy gaps, bond lengths etc

material properties such as ground state total energy. Other crucial material properties can then be derived from the total energies or differences in the total energies of the system at play [75]. The solutions to the Kohn-Sham equations involve a number of paramount concepts such as symmetry considerations which is basically used to determine a basis set.

3.6.1 Symmetry transformation and Brillouin zone

The comprehension of the properties of a given material is simplified by the application of symmetry principles. A symmetry operation is a transformation on a crystal structure that leaves the crystal structure invariant- the crystal remains the same in every respect after the transformation [76][57]. Important symmetry operations include:

- identity symmetry operation- E;

- crystal rotation about a given axis-C_n;
- parallel displacement or translation of an infinite crystal lattice-t;
- inversion symmetry operation-i and
- reflection in a vertical or horizontal plane- σ_v and σ_h respectively.

All the likely symmetry operations of a crystal are contained in the space group of the crystal. The space group of a given crystal lattice under consideration gives all the possible symmetry operations for that group. A given space group is made up of an invariant sub-group of primitive translations of the form

$$\left\{\varepsilon \mid \overrightarrow{R_n}\right\}$$

where

$$\overrightarrow{R_n} = n_1\vec{t_1} + n_2\vec{t_2} + n_3\vec{t_3} \tag{3.62}$$

n_1,n_2 and n_3 denotes integers whereas n refers to the set of the three integers under consideration;

$\vec{t_1}$, $\vec{t_2}$ and $\vec{t_3}$ represents three basic primitive translations for the direct lattice and they are linearly independent;

A set of the entire points that are spanned by the vectors $\overrightarrow{R_n}$ is referred to as the Bravais lattice [8]. All the primitive translations are given by equation 3.62

$$\left\{\varepsilon \mid \overrightarrow{R_n}\right\} = e^{\left(i\vec{k}.\overrightarrow{R_n}\right)} \tag{3.63}$$

and

$$\vec{k} = k_1\vec{b_1} + k_2\vec{b_2} + k_3\vec{b_3} \tag{3.64}$$

$\vec{k}$ represents a wave vector that is used to derive all the irreducible representations of a pure translations group under consideration.

[8] Bravais lattice is defined as a set of vectors that is closed under the operations of vector addition and subtraction [40]

$\vec{b}_1$, $\vec{b}_2$ and $\vec{b}_3$ denotes the primitive vectors of the reciprocal lattice.

The reciprocal space[9] of the direct Bravais lattice is the fundamental space that is spanned by the three vectors $\vec{b_1}$, $\vec{b_2}$ and $\vec{b_3}$.

For a real space that has a unit cell of volume, v, we derive the reciprocal lattice from the primitive vectors as shown by equation 3.65 [40]

$$\left\{ \begin{array}{lcl} \vec{b_1} & = & \frac{2\pi}{v}(\vec{t_2} \times \vec{t_3} \\ \vec{b_2} & = & \frac{2\pi}{v}(\vec{t_1} \times \vec{t_3} \\ \vec{b_3} & = & \frac{2\pi}{v}(\vec{t_1} \times \vec{t_2} \end{array} \right\} \tag{3.65}$$

The fundamental space that is spanned by the three vectors $\vec{b_1}$, $\vec{b_2}$ and $\vec{b_3}$ is referred to as the reciprocal space [10] of the direct Bravais lattice.

Symmetry operations are of fundamental importance as they reduce the understanding of the properties of the entire crystal structure to just the comprehension of a tiny portion of the crystal- unit or primitive cell . The whole crystal structure is formed by apt transformations of this unit cell. In reciprocal lattice the primitive cell is referred to as the Brillouin zone (BZ) [41]. The BZ in reciprocal lattice forms the smallest possible periodic unit of the crystal. At the heart of understanding the properties of a given crystal structure is the comprehension of everything that happens in the BZ. Any physical observable that is true in the BZ is also true for the whole crystal structure under consideration.

Understanding the fundamental properties of a crystal structure hinges on understanding the processes that happens in the reciprocal lattice. The reason why the reciprocal space is of crucial importance is that wave vectors can only be aptly described in reciprocal space. Inversion symmetry consideration can further simplify the problem at hand since we now need to only consider half of the first BZ. Rotation considerations also reduces the problem to just one eighth of the BZ which is the irreducible part of the BZ [77]. Symmetry considerations simplify the problem at hand and so does Bloch's

[9]Reciprocal space is a set of wave vector $\vec{k}$ that produces plane waves that have the periodicity of the Bravais lattice under consideration [40]

theorem which is discussed in the section that follows.

3.6.2 Bloch's Theorem

The fundamental idea that was proposed by Bloch is that the wave function of an electron moving in a periodic lattice can be given as a plane wave function which is multiplied by a term that denotes the periodicity of the crystal lattice [78]. The point of departure for Bloch's theorem is the use of a plane wave function to describe the motion of electrons under the influence of a periodic potential generated by the static nuclei . The electronic wave function given as a plane wave, $e^{i\vec{k}.\vec{r}}$, is modulated by the periodicity of the Bravais lattice, $u_{n\vec{k}}(\vec{r})$. Thus for a given band index, n, we have

$$\Psi_{n\vec{k}}(\vec{r}) = e^{i\vec{k}.\vec{r}} u_{n\vec{k}}(\vec{r}) \tag{3.66}$$

The periodicity of the crystal as given by equation 3.66 is entwined in the square of the electronic wave function [40][79].

$$\Psi_{n\vec{k}}(\vec{r}) = \Psi_{n\vec{k}}(\vec{r} + \vec{R}) \tag{3.67}$$

Bloch's theorem can alternatively be given as

$$e^{i\vec{k}.\vec{R}} \Psi(\vec{r}) = \Psi(\vec{r} + \vec{R}) \tag{3.68}$$

The periodicity which is embedded in Bloch's theorem is used to simplify the problem at hand since the Kohn-Sham potential is periodic for a given Bravais lattice [73], that is

$$V_{KS}(\vec{R}) = V_{KS}(\vec{r} + \vec{R}) \tag{3.69}$$

Bloch's theorem entwine the important concept of kinetic energy cut-off as described in the section that follows.

3.6.3 Kinetic energy cut-off

Using Bloch's theorem the wave function of the electrons, $\Psi_{\vec{k}}(\vec{r})$, in a periodic crystal is given as a product of two terms- the plane wave $e^{i\vec{k}.\vec{r}}$ and the function $u_{\vec{k}}(\vec{r})$ [45]. The motion of the electrons as represented by the plane wave multiplied by the function that represents the periodicity of the crystal yields the equation

$$\Psi_{\vec{k}}(\vec{r}) = e^{i\vec{k}.\vec{r}} u_{\vec{k}}(\vec{r}) \tag{3.70}$$

The function $u_{\vec{k}}(\vec{r})$ can be expanded as a Fourier series of plane waves basis set of the reciprocal lattice, i.e

$$u_{\vec{k}}(\vec{r}) = \sum_{G} cG, e^{iG.\vec{r}} \tag{3.71}$$

where G represents the reciprocal lattice vectors.

Combining equations 3.70 and 3.71 gives us the expression for the electronic wave function in a periodic crystal structure, i.e

$$\Psi_{\vec{k}}(\vec{r}) = \sum_{G} cG, e^{iG.\vec{r}} e^{i\vec{k}.\vec{r}} \tag{3.72}$$

thus

$$\Psi_{\vec{k}}(\vec{r}) = \sum_{G,k} c, G + k e^{i(G+k).\vec{r}} \tag{3.73}$$

whereby c and $G + k$ are coefficients.

As outlined above, equation 3.73 confirms that the electronic wave function in a periodic lattice structure is a Fourier series. The substitution of equation 3.73 in the one electron Kohn-Sham equation gives equation 3.74 which is aptly applicable in reciprocal space, that is

$$\sum_{G'} \left[\frac{1}{2} \mid k + G \mid^2 \delta_{GG'} + V_{KS}^{\sigma}(G - G') \right] C_{i,k+G'} = \varepsilon_i C_{i,k+G'} \tag{3.74}$$

where $\frac{1}{2} \mid k+G \mid^2 \delta_{GG'}$ and $V_{KS}^{\sigma}(G-G')$ denotes the Fourier expansion of the kinetic energy and Kohn-Sham potential respectively.

We can further make the equation above explicitly clear by substituting the V_{KS} by its three components, $V_{ext} + V_H + V_{XC}$ so that we yield the following Fourier series expansion [60][27].

$$\sum_{G'} \left[\frac{1}{2} \mid k+G \mid^2 \delta_{GG'} + V_{ext}(G-G') + V_H(G-G') + V_{XC}(G-G') \right] C_{i,k+G'} = \varepsilon_i C_{i,k+G'} \tag{3.75}$$

This Fourier series expansion is infinite, therefore in order to solve the Kohn-Sham equations, an upper limit of the kinetic energy term has to be set up. This is known as the kinetic energy cut-off and it depends on the maximum value taken by G- that is $G_{cut-off}$. The cut-off kinetic energy is given by the expression below

$$E_{cut-off} = \frac{1}{2} \mid k + G_{cut-off} \mid^2$$

The utilization of the threshold kinetic energy has its own constraints to the overall calculations. The accuracy of the DFT computational calculations is negatively affected by imposing the cut-off kinetic energy but the results can be significantly improved by using a large enough upper value of the kinetic energy [61]. This value is determined by way of performing kinetic energy convergence testing.

3.6.4 Convergence testing

Convergence testing is of paramount importance in first principles calculations because it gives invaluable information about the apt peak kinetic energy, the K-points and the lattice constants of the plane wave basis set. High values of the kinetic energy cut-off, K-points as well as the lattice constants improve the accuracy of the first principles calculations, but this is done at the expense of increasing the computational cost. It is thus extremely important to have an acceptable balance between the values of these

parameters and the computational cost. These suitable values are deduced by way of convergence testing as illustrated by figures 3.1, (a), (b) and (c). This procedure is done by way of varying the threshold values of kinetic energy, K-points as well as the lattice constant and checking for the convergence of fundamental concepts such as the total energy. Incorrect values of these pertinent parameters can lead to unreliable or inaccurate results. The general procedure for convergence testing is as follows:

- select an apt range of the parameter (kinetic energy, K-points or lattice constant) whose cut-off value we desire;
- carry out density functional theory first principles calculations, commencing with the a chosen minimum value of the parameter at play;
- systematically increase, the values of the parameter under consideration as do the same calculations;
- check for the convergence of crucial material properties such as *total energy* as the values of the parameter at play are increased;
- the suitable value(s) of the parameter (kinetic energy, K-points or lattice constant) under investigation is reached if there is a minimal change of the property at play (*total energy* in this case) as the parameter is increased.

A correct and optimal cut-off value(s) is reached if there is a good balance between the computational cost and the accuracy or preciseness of the material properties that are being predicted.

Another approximation, that is of critical importance when solving the Kohn-Sham equations is the Pseudo-potential approximation.

3.6.5 Pseudo-potential approximation

The main idea of this approximation is the use of an effective ionic potential referred to as $pseudo-potential$ to substitute the actual Coulomb potential of the nucleus and the

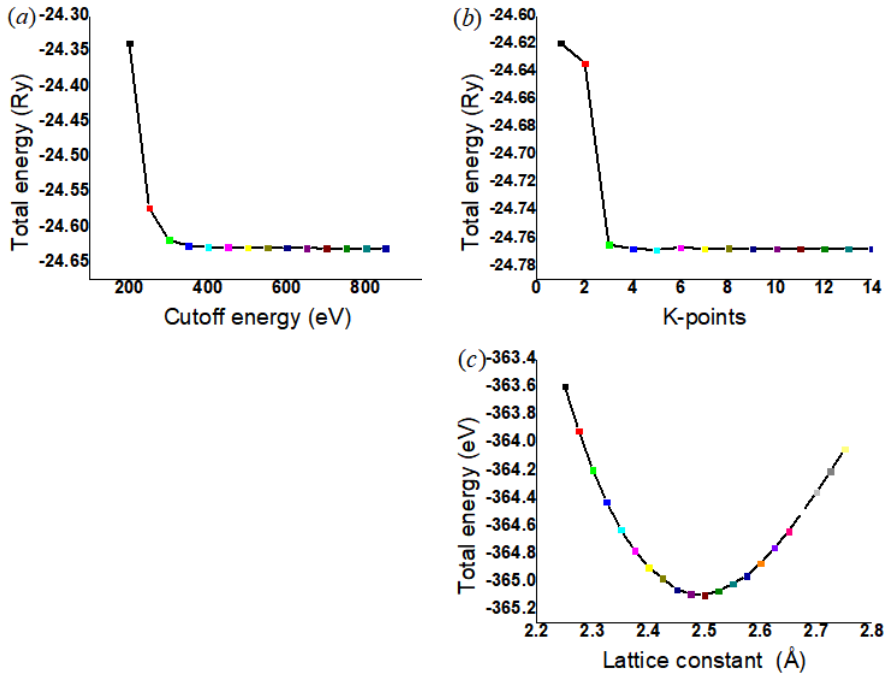

Figure 3.1: Convergence testing: (a) total energy versus cut-off kinetic energy (b) total energy versus K-points (c) total energy versus lattice constant

core-electrons. The pseudo-potential is the effective ionic potential regarded as having an influence on the valence electrons only. This approximation is sometimes referred to as the $frozen - core$ approximation because the potential between the nucleus and the inner electrons is not considered. We have different forms of pseudo-potentials to use depending on the calculations and the DFT codes at play [75][61]. For instance, $PKA\ pseudo - potential$, the $norm - conserving$ and $ultrasoft$ pseudo-potentials. The last two are very popular and frequently used by many computational material physics researchers. In the section that follows we briefly explore these pseudo-potential approximations.

3.6.5.1 PKA Pseudo-potential

This so called PKA pseudo-potential approximation stems from the contribution done by Phillips, Kleinman and Antonicik [80][81]. This pseudo-potential approximation divides the potential into two categories- the highly localized part which is not easy to

reproduce using wave functions and the smooth component which can be represented by plane wave functions [61]. Using this approximation we can have eigen-functions of the form

$$\hat{H}\Psi_i^v(r) = \left[-\frac{1}{2}\nabla^2 + V(r)\right]\Psi_i^v(r) \tag{3.76}$$

This can also be given as

$$\left[-\frac{1}{2}\nabla^2 + V(r)\right]\Psi_i^v(r) = \varepsilon_i^v\Psi_i^v(r) \tag{3.77}$$

where the effective potential is represented by $V(r)$.

$\Psi_i^v(r)$ can represent different forms of pseudo-potential functions.

Different pseudo-potential equations can be obtained by way of substituting $\Psi_i^v(r)$ with an apt smooth function. For example, consider the pseudo-potential equation generated by Phillips, Kleinman and Antoncik [81][80], which is shown by equation 3.78.

$$\left[H^{\hat{P}KA}\widetilde{\Psi}_i^v(r) = -\frac{1}{2}\nabla^2 + \widetilde{V}^{PKA}(r)\right]\Psi_i^v(r) = \varepsilon_i^v\Psi_i^v(r) \tag{3.78}$$

This is an eigenvalue problem where $\widetilde{\Psi}_i^v(r)$ replaced $\Psi_i^v(r)$ in equation 3.76 and this term denotes the smooth pseudo-function. Therefore the pseudo-potential construction of the PKA method formulated equations based on the smooth component of the valence electrons function which also encompassed another function as part of the overall function. This method differs from the norm-conserving pseudo-potential as outlined below.

3.6.5.2 Norm-conserving Pseudo-potential

The pseudo-potential functions for this method are derived from apt atomic information. Norm-conserving pseudo-potentials are *ab initio* pseudo-potentials because they do not depend on any empirical parameteres. Pseudo-potential functions based on

norm-conservation are normalised and they are constructed in such a way as to depict the valence electron properties of a given system. The valence electrons pseudo-potential functions must hold as far as conditions of orthonormality are concerned, i.e

$$\langle \Psi_i^{\sigma,PS} \mid \Psi_J^{\sigma^{'},PS} \rangle = \delta_{i,j}\delta_{\sigma,\sigma'} \tag{3.79}$$

$\Psi_i^{\sigma,PS}(r)$ represents the pseudo-potential functions that adhere to norm-conservation. This construct give rise to Kohn-Sham equations of the form

$$(H_{KS}^{\sigma,PS} - \varepsilon_i^{\sigma})\Psi_i^{\sigma,PS}(r) = 0 \tag{3.80}$$

The norm-conserving pseudo-potential functions have a number of conditions that have to be satisfied to improve the *ab initio* pseudo-potential values [61]. Some of the conditions are

- the total electron eigenvalues of the system and pseudo-potential eigenvalues must have a consensus for a given configuration of the atoms,
- the total electron wave functions of a system under considerations must agree with the pseudo-potential wave functions for values greater than a given core radius, r_c,
- the logarithmic derivatives of the total electron wave functions and the pseudo-potential wave functions logarithmic derivatives must have an agreement at the core radius, r_c,
- norm-conservation must hold for values less than the core radius, i.e there must be an agreement of the integrated charge for each given wave function for values less than the core radius and
- the initial derivative of the energy (that falls under the logarithmic derivatives) of the pseudo-potential wave functions must have a consensus with the total electron

wave function's initial energy derivative at r_c, as well as for all values greater than r_c.

It is imperative to also state that, the pseudo-potentials for the core-electrons are for the values less than r_C(cut-off radius) while the pseudo-potentials values for the valence electrons correspond to values greater than r_C as shown by figure 3.2 [82][83][84].

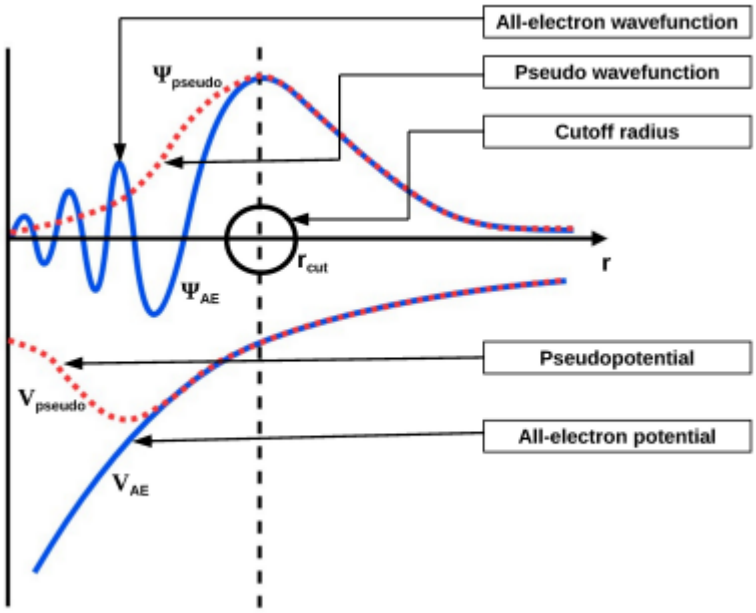

Figure 3.2: Schematic representation of the Pseudo-potential approximation.

When solving, the Kohn-Sham equations, we need further first principles estimations such as local density approximation and generalized gradient approximation to deal with the exchange and correlation aspects.

3.7 Local Density Approximation

The term that is difficult to deal with that requires further approximation is the exchange and correlation energy, E_{XC}, from which we can derive the exchange and correlation potential, V_{XC}. Therefore in this section we first discuss the two fundamental terms- exchange and correlation. We then delve into the simplest approximation de-

veloped in order to determine expressions for exchange and correlation- that is the spin-free local density approximation (LDA). Our next focus will be the local spin density approximation (LSDA) which was proposed as an apt improvement to LDA since it encompasses spin polarization.

3.7.1 Exchange and Correlation

Electrons are fermions, therefore the wave function used to describe their properties has to be antisymmetric. We have two scenarios to consider- the first one is when two electrons have the same spin. The antisymmetric property of the wave function gives rise to a spatial separation between the electrons. As a result of this, there is an apparent reduction in the Coulomb energy of the electronic system under consideration. We define the energy reduction of the same spin two-electron system because of the antisymmetry of the wave function as the exchange energy of the system [60]. As depicted under the Hartree-Fock approximation [66], the determination of the total energy of a many electron system must encompass the exchange energy if the approximation is to produce reliable output.

Our second scenario is for electrons that have opposite spin. For this situation, the electronic system Coulomb energy can further be reduced to a value which is relatively below the Hartree-Fock value. This is possible because once again the antisymmetric nature of the wave function produces a spatial separation between the electrons. The difference between the Coulomb energy of electrons that have opposite spin and the Coulomb energy of same spin electrons is called correlation energy [60]. The determination of correlation energy is extremely difficult- some researchers are using the Quantum Monte Carlo (QMC) simulations to derive a value for correlation energy [85]. There are a number of fundamental concepts that are entwined in the exchange and correlation term, E_{XC} . The correction to the electron-electron coulomb repulsion, the self-interaction error correction (SIC) and all the other quantum mechanical effects are all bundled up in the exchange and correlation term. This fundamental term also con-

tains the kinetic energy difference between a real system and a fictitious non-interacting system [75].

The exchange and correlation energy term, E_{XC}, is given by the difference between the true energy functional, $E[n(r)]$ and a combination of the Kohn-Sham kinetic energy, $\hat{T_{KS}}[n(r)]$ and the Hartree potential, V_H. In this section we briefly derive the expression for the exchange and correlation energy term. We commence by giving the expression for the true energy functional which is

$$E[n(r)] = \hat{T}[n(r)] + \hat{V_{ext}}[n(r)] + \hat{V_{e-e}}[n(r)] \tag{3.81}$$

The Kohn-Sham energy functional is given by combining the Kohn-Sham kinetic energy with the Kohn-Sham potential, that is

$$E_{KS}[n(r)] = \hat{T_{KS}}[n(r)] + \hat{V_{KS}}[n(r)] \tag{3.82}$$

and this expression can be expanded to

$$E_{KS}[n(r)] = \hat{T_{KS}}[n(r)] + \hat{V_{ext}}[n(r)] + V_H[n(r)] + \hat{V_{XC}}[n(r)] \tag{3.83}$$

For the same system, the external potential, $\hat{V_{ext}}[n(r)]$, is constant, therefore the exchange and correlation energy is given by

$$E_{XC}[n(r)] = \hat{T}[n(r)] + \hat{V_{ext}}[n(r)] + \hat{V_{e-e}}[n(r)] - \{\hat{T_{KS}}[n(r)] + \hat{V_{ext}}[n(r)] + V_H[\hat{n}(r)]\} \tag{3.84}$$

thus

$$E_{XC}[n(r)] = \hat{T}[n(r)] + \hat{V_{e-e}}[n(r)] - \{\hat{T_{KS}}[n(r)] + V_H[\hat{n}(r)]\} \tag{3.85}$$

The simplest approximation developed in order to deal with electron exchange and correlation is the spin-free local density approximation (LDA).

3.7.2 Spin-free Local Density Approximation

For spin-free LDA the derivation of the E_{XC} functionals depends on the density at the local position under consideration [61]. To pave the way for the utilisation of LDA, we make a fundamental assumption that the electron density is uniform at each position in the given space. This is referred to as the uniform electron gas (UEG) model [86]. One point of departure in LDA is the splitting of E_{XC} functional into two parts, that is the exchange and correlation components as depicted by equation 3.86 [75].

$$E_{XC}[n(r)] = E_X[n(r)] + E_C[n(r)] \tag{3.86}$$

where $E_X[n(r)]$ is the exchange energy functional for the many-electron system,

$E_C[n(r)]$ is the correlation energy functional for the system.

The exchange energy functional is explicitly derived in LDA and it is given by equation 3.87. The value of α can be either 1 or $\frac{2}{3}$ depending on whether one is considering Slater or Dirac exchange energy respectively [75].

$$E_X^{LDA}[n(r)] = -\frac{9\alpha}{8}(\frac{3}{\pi})^{\frac{1}{3}} \int n^{\frac{4}{3}}(r)dr \tag{3.87}$$

For a system of many electrons, we can further split the exchange and correlation functional into a form that shows the energy per electron [75],

that is

$$E_{XC}^{LDA}[n(r)] = \int \epsilon_x[n(r)]n(r)dr + \int \epsilon_c[n(r)]n(r)dr \tag{3.88}$$

or

$$E_{XC}^{LDA}[n(r)] = \int \epsilon_{xc}[n(r)]n(r)dr \tag{3.89}$$

which can be simplified to

$$E_{XC}^{LDA}[n(r)] = N\epsilon_{xc}[n(r)] \tag{3.90}$$

whereby $\epsilon_x[n(r)]$ represents the exchange energy functional per given particle within our system,

$\epsilon_c[n(r)]$ denotes the correlation energy per electron,

$\epsilon_{xc}[n(r)]$ is the exchange and correlation energy per electron,

N is the number of electrons in the system given by $N = \int n(r)dr$.

The exchange energy per system particle is given by equation 3.91, that is

$$\epsilon_x^{LDA}[n(r)] = -\frac{9\alpha}{8}(\frac{3}{\pi})^{\frac{1}{3}} \int n^{\frac{1}{3}}(r)dr \tag{3.91}$$

It is important to state that so far we have a gap because we have not given an explicit term for the correlation energy, $E_C[n(r)]$ and $\epsilon_c[n(r)]$. In 1980, Ceperley and Alder utilised the Quantum Monte Carlo (QMC) simulations to try and plug the gap [36]. After this Vosko, Wilk and Nusair derived different expressions for the correlation term using apt data obtained from Ceperley and Alder research efforts [87][36].

Until now, we have considered expressions for the exchange and correlation that are spin free. If electron spin comes into play, LDA is slightly modified to give spin polarised local density approximation which is explained in the next section.

3.7.3 Local Spin Density Approximation

The local spin density approximation (LSDA) encompasses the main idea of using the density entwined with spin polarisation at a given point in space[10]. Therefore the variable function, $[n(r)]$, is resolved into two components, that have opposite spins [88],

that is

$$n(r) = n\uparrow(r) + n\downarrow(r) \tag{3.92}$$

Equation 3.88 is thus transformed to

[10]The electron spin property may entail the inclusion of a magnetic field.

$$E_{XC}^{LSDA}[n\uparrow(r)n\downarrow(r)] = \int \epsilon_x^{UEG}[n\uparrow(r)n\downarrow(r)]n(r)dr + \int \epsilon_c^{UEG}[n\uparrow(r)n\downarrow(r)]n(r)dr \tag{3.93}$$

The determination of exchange and correlation energy together produces more accurate results as compared to deriving them separately, thus we can have

$$E_{XC}^{LSDA}[n\uparrow(r)n\downarrow(r)] = \int \epsilon_{xc}^{UEG}[n\uparrow(r)n\downarrow(r)]n(r)dr \tag{3.94}$$

However, LDA and LSDA have a number of constraints that we discuss in the section that follows.

3.7.4 Limitations of LDA/LSDA

LDA is an apt approximation for systems whose density is uniform from one point to another in space. However, the electron densities of real systems vary. Therefore LDA/LSDA has a number of limitations, which among others include underestimation of lattice parameters, correlation energy, bond lengths, band gaps, orbital moments as well as magnetic moments [75]. LDA/LSDA also overestimates the exchange energy. Density functionals beyond LDA/LSDA give more accurate results because they have more input information and the variation of the electron density is also considered. The next section of this contribution deals with generalised gradient approximation (GGA) which was developed in an attempt to reduce the limitations above.

3.8 Generalised Gradient approximation

The generalised gradient approximation (GGA) derives the exchange and correlation expressions based on the local density as well as the gradient of the electron density [31]. This does close some of the shortcomings brought about by considering the many-electron system as being homogeneous. The density of real many electron system varies

from one point to another in space. The non-uniformity of the electron density is accounted for in the inclusion of the gradient in the exchange and correlation calculations [75]. GGA can be regarded as a semi-local approximation since the gradient of the electron density takes care of the inhomogeneity of the system away from the point in space under consideration. Langreth and Mehl [89] gave the GGA expression as

$$E_{XC}^{GGA}[n(r)] = \int \epsilon_{xc}^{GGA}\{n(r), \nabla n(r)\}dr \tag{3.95}$$

The inclusion of spin polarization modifies equation 3.95 to

$$E_{XC}^{GGA}[n\uparrow(r)n\downarrow(r)] = \int \epsilon_{xc}\{n\uparrow(r), n\downarrow(r), \nabla n\uparrow,(r)\nabla n\downarrow(r)\}n(r)dr \tag{3.96}$$

which can be written as

$$E_{XC}^{GGA}[n\uparrow(r)n\downarrow(r)] = \int \epsilon_{xc}[n(r)]n(r)f_{xc}[n\uparrow(r), n\downarrow(r), \nabla n\uparrow,(r)\nabla n\downarrow(r)]n(r)dr \tag{3.97}$$

or

$$E_{XC}^{GGA}[n\uparrow(r)n\downarrow(r)] = \int \epsilon_{xc}^{LDA}\{n(r)\}f_{xc}\{n\uparrow(r), n\downarrow(r), \nabla n\uparrow,(r)\nabla n\downarrow(r)\}n(r)dr \tag{3.98}$$

where ∇n is the gradient of the electron density at a given position.

Generalised gradient approximation functionals are not very accurate in the derivation of material properties. We have more accurate DFT functionals that extract certain values of exchange and correlation from different schemes such as LDA, GGA and Hartree-Fock [90][63][91] and these are entwined together to form the so called hybrid functionals.

3.9 Hybrid functionals

We have a number of hybrid functionals that are being widely used in accordance with the different material research areas [92]. For instance, Becke [75] came up with an expression that extracted various components of the exchange and correlation functionals from the Hartree-Fock formalism, local density approximation [93] as well as the generalized gradient approximation to give the hybrid functional given by equation 3.99

$$E_{xc}^{B3} = E_{xc}^{LSD} + a(E_{xc}^{\lambda=0} - E_{x}^{LSD}) + bE_{x}^{B} + cE_{c}^{PW91} \tag{3.99}$$

The exact amount of the exchange in a functional of this nature is extracted through the constant a. The purpose of a, b and c is to introduce corrections to the exchange and correlation of the local density approximation. The precise amounts of the exchange and correlation is thus controlled by the values taken by these constants [75]. One of the most widely used functional in the area of material science research is B3LYP [94] which is given by equation 3.100

$$E_{xc}^{B3LYP} = (1-a)E_{x}^{LSD} + aE_{xc}^{\lambda=0} + bE_{x}^{B88} + cE_{c}^{LYP} + (1-c)E_{c}^{LSD} \tag{3.100}$$

In 1996, Becke [75][92] decreased the parameters at play to the few shown by equation 3.101

$$E_{xc}^{B1} = E_{xc}^{DFT} + a(E_{x}^{\lambda=0} - E_{xc}^{DFT}) \tag{3.101}$$

where a was given an exact value of 0.28.

Subsequently, Becke [75] initiated a completely novel exchange and correlation functional type which involves a detailed fitting procedure, i.e.

$$E_{xc}^{B97} = E_{x}^{\alpha\alpha} + E_{x}^{\beta\beta} + E_{c}^{\alpha\alpha} + E_{c}^{\beta\beta} + E_{c}^{\alpha\beta} + c_{x}^{HF}E_{x}^{HF} \tag{3.102}$$

In the expression given by equation 3.102, every component besides the Hartree-

Fock exchange involves a power series (second order terminated) in which the electron density as well as the reduced density gradient are entwined. A number of material science researchers are still coming up with different forms of hybrid functionals that are applicable to a wide variety of materials. Comparing the different forms of functionals that have been proposed, one can put it forward that , the more information we extract from the electron density, the more accurate are the derived material properties. However, this is done at the expense of increasing the computational costs.

Chapter 4

Results and Discussion:

Published paper 1

In this Chapter we report a published paper entitled ***"Thermodynamic stability and formation energies of hydrogen and carbon vacancy centres in hydrogenated graphene."*** This contribution was published as H. Mapingire and R. E. Mapasha by the South African Institute of Physics, Proceedings of SAIP 2023 with the ISBN: 978-0-7961-3774-6. In this article, we computed formation energies, U-parameters, thermodynamic energy transition levels as well as density of states for three types of monovacancies in graphane. The considered vacancies are: a hydrogen vacancy (V_H), a carbon vacancy (V_C) and a carbon vacancy adjacent to a hydrogen vacancy (V_{CH}). The computed physical quantities are of fundamental importance in terms of the characterization of vacancy point defects in graphane. The results of this work is pertinent in terms of comprehending nitrogen-vacancy complexes in graphane as well as the point defects' potential applications in nano-technology.

Thermodynamic stability and formation energies of hydrogen and carbon vacancy centres in hydrogenated graphene

H Mapingire and R E Mapasha
Department of Physics, University of Pretoria, Pretoria, 0002, South Africa
E-mail: edwin.mapasha@up.ac.za

Abstract. We utilise Quantum espresso simulations to compute formation energies, thermodynamic transition levels and effective U-parameters for the mono-vacancies V_H, V_C and V_{CH} in hydrogenated graphene. Our first-principles calculations show that the formation processes of all the three vacancy point defects are endothermic, hence they need activation energy to form. The point defects give rise to defect states that exhibit spin-polarisation and are possible candidates for novel nano-technology applications. The derived U-parameters are all positive showing the stability of the point defects in the positive and negative charged states.

---

1. Introduction

The comprehension of the properties of point defects such as lattice vacancies is of fundamental importance because of their various applications in nano-technology. Defects have a bearing on the life-time perfomance and efficiency of technological devices. A defect may make a material useful for various technological innovations or conversely may make a material to be unusable [1]. Considerable research on the properties of point defects in two-dimensional materials is crucial for gaining a comprehensive understanding of these defects, with the goal of utilising them in nano-scale technological devices

In this contribution, we focus on hydrogen and carbon vacancies in hydrogenated graphene because they generally induce defect states within the bandgap of some two-dimensional materials and may be possible colour centers [2]. Graphene is a two-dimensional material that is composed of carbon atoms that are covalently bonded to each other in such a way as to form a structure that is hexagonal in nature [3]. If hydrogen atoms are chemisorbed to the carbon atoms, we form hydrogenated graphene- a two-dimensional material that has generated intense interest because of the tunable bandgap which is formed at the gamma point [4]. Hydrogenated graphene is a saturated

hydro-carbon that is sp^3-hybridized[5]. During the growth or formation processes of hydrogenated graphene [6], atomically confined point defects can form. A lattice structure can have an ion or an atom missing from a particular lattice site, giving rise to a lattice vacancy. Lattice vacancies can be formed as a result of less than perfect packing of atoms during the phenomenon of crystallization. The comprehension of the properties of point defects such as impurity atoms, Frenkel defects, Scholtky as well as lattice vacancies is of fundamental importance because of their various applications in nano-technology. Defects have a bearing on the life-time perfomance and efficiency of technological devices. Moreover, the presence of vacancies in a given structure can amplify electron transport. We also propose that the presence of vacancies in a material is of paramount importance as far as the controlling of diffusion is concerned.

In our current contribution, we examine the thermodynamic stability (formation energy), charge transition level and electronic properties of the mono-vacancies V_H, V_C and V_{CH} in hydrogenated graphene for different charge states. Furthermore, we derive the U-parameters which have a bearing on the stability of these vacancies. To correctly identify the positions of transition levels and defect states, we used hybrid functionals.

2. Characterization methods

The initial and fundamental stage in the characterization of point defects is the determination of the defect formation energy. Utilizing Quantum Espresso [7] first principles computations guided by the Kohn-Sham density functional theory [8], we computed the formation energy of all the vacancy configurations housed in a $6 \times 6 \times 1$ supercell of the chair conformer. The hydrogenated graphene supercell layer comprised a total of 143 carbon and hydrogen atoms for the V_H and V_C configurations while the V_{CH} configuration had a total of 142 atoms. With the aid of convergence testing, we used wave function and charge density threshold values of 3.30×10^1 Ry and 3.30×10^2 Ry respectively. In all our entire calculations we included spin component and a force convergence threshold value of 1.0×10^{-6} Å / eV. We allowed our calculations to run for a maximum of 200 electron steps. The initial calculations for all the defect config-

urations was geometric optimization which is crucial as it allows the relaxation of all the atomic species. We utilized the ultra-soft pseudopotentials to simulate the interaction between the nuclei and the electrons. For the Brillouin zone sampling, we used a $3 \times 3 \times 1$ Monkhorst –Pack [13]. For better computational accuracy and improved property characterization we used HSE hybrid functionals [9] to run our entire calculations. For the purpose of removing spurious contributions that are there as a result of the interaction that exists between the point defects and their periodic images, we utilized the CoFFEE correction scheme [21].

We deduced the formation energy using equation 1 [10], where $E_T[V_i^q]$ denotes the supercell total energy in which a vacancy, V, of atomic type i and that has a charge state q is entwined. $E_T[pure]$ represents the pristine supercell total energy of the crystalline structure at play. The integer n_i stands for the atomic species of i type that have been removed from their lattice sites within the supercell during the vacancy creation phenomenon. The chemical potential of atomic species that have been removed from their lattice positions is represented by μ_i. The terms E_F and E_C represents the Fermi energy and the correction energy respectively.

$$E^f[V_i^q] = E_T[V_i^q] - E_T[pure] - \sum_i n_i\mu_i + qE_F + E_c \quad \text{.....(1)}$$

Fundamental characterization information is embedded in defect level diagrams. These diagrams are graphs of formation energy versus Fermi level positions. Transition levels are Fermi level positions whereby the formation energy of two consecutive charge states are equivalent. Thermodynamic transition levels can be deduced from the defect level diagrams. The difference in energy between successive thermodynamic transition levels yields the U-parameters [11].

3. Results

In the sub-sections that follow, we present our findings which give invaluable insights into the stability and electronic structure of the hydrogen vacancy, carbon vacancy and the carbon-hydrogen vacancy in hydrogenated graphene.

3.1. Hydrogen vacancy (V_H)

This point defect is created in hydrogenated graphene by removing a single hydrogen atom that is attached to a carbon atom giving rise to a dangling bond on the parent carbon atom as depicted by figure 1(a). The removal of a hydrogen atom causes a slight distortion of the system's atomic geometry. We derived formation energy of 2.64 eV for this hydrogen mono-vacancy as shown by table 1. This value is in close agreement with the formation energy derived by Mapasha *et al* [12]. The positive formation energy shows the defect formation process is endothermic and non-spontaneous[13][14].

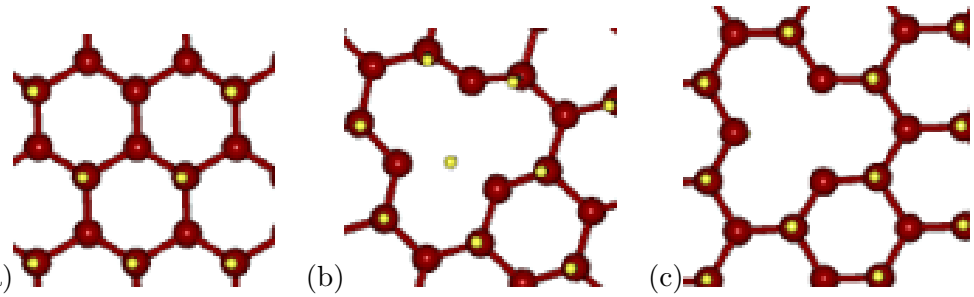

Figure 1. Vacancy point defects in hydrogenated graphene: (a) V_H (b) V_C and (c) V_{CH}. The red spheres represent carbon atoms while the yellow spheres represent hydrogen atoms.

Table1. Formation energies and Fermi-level position for vacancy point defects in graphane.

$Defect$	$Charge\ state$	$Formation\ energy\ (eV)$	$Fermi-level\ position\ (eV)$	$Formation\ energy\ (eV)[E_F = 0eV]$
V_H	0	2.64	-0.38	2.64
	$-$	4.49	$+1.35$	3.14
	$+$	1.59	-2.39	3.98
V_C	0	12.57	.....	12.57
	$-$	12.36	$+1.40$	13.76
	$+$	13.98	-1.42	13.98
V_{CH}	0	13.75	$+0.60$	13.75
	$-$	13.41	$+1.37$	14.78
	$+$	11.53	-2.33	13.86

Charging the defect negatively increased the formation energy significantly to 4.49 eV as illustrated by table 1. The V_H defect in the neutral charge state has one unpaired

electron. The addition of an extra electron may give rise to coulombic repulsive forces between the electrons inducing the noted increase in the formation energy. The formation energy of the singly positive charge state of the hydrogen mono-vacancy is 1.59 eV which is considerably low albeit positive. V_H^0 exhibits C_S(m) symmetry group transformations while both V_H^{-1} and V_H^{+1} depicts C_{3v}(3m) symmetry transformations. The V_H defect is thus subject to the Jahn-Teller distortion [15][16] since there is a lowering of symmetry when the defect forms. The C_{3v}(3m) symmetry group is subject to possible intrinsic splittings, hence there is a likelihood of utilising V_H defect for spintronics applications [17]. Analysis of the density of states (DOS) plots as depicted by figure 2 shows that the hydrogen monovacancy induces defect electronic states within the graphane band gap. The defect states are asymmetrical in contrast to the bulk states that are clearly aligned. We anticipate this defect to show traits of magnetism because of the presence of unpaired electrons. We predict that this defect slightly widens the graphane bandgap. A closer examination of the DOS plots shows that the V_H^0 and V_H^{+1} defect states may be coupled with the bulk states, hence are not clearly distinct as compared to the V_H^{-1} states. The DOS plots for V_H^{-1} show spin-polarised defect states which we predict to be shallow donor levels close to the conduction band.

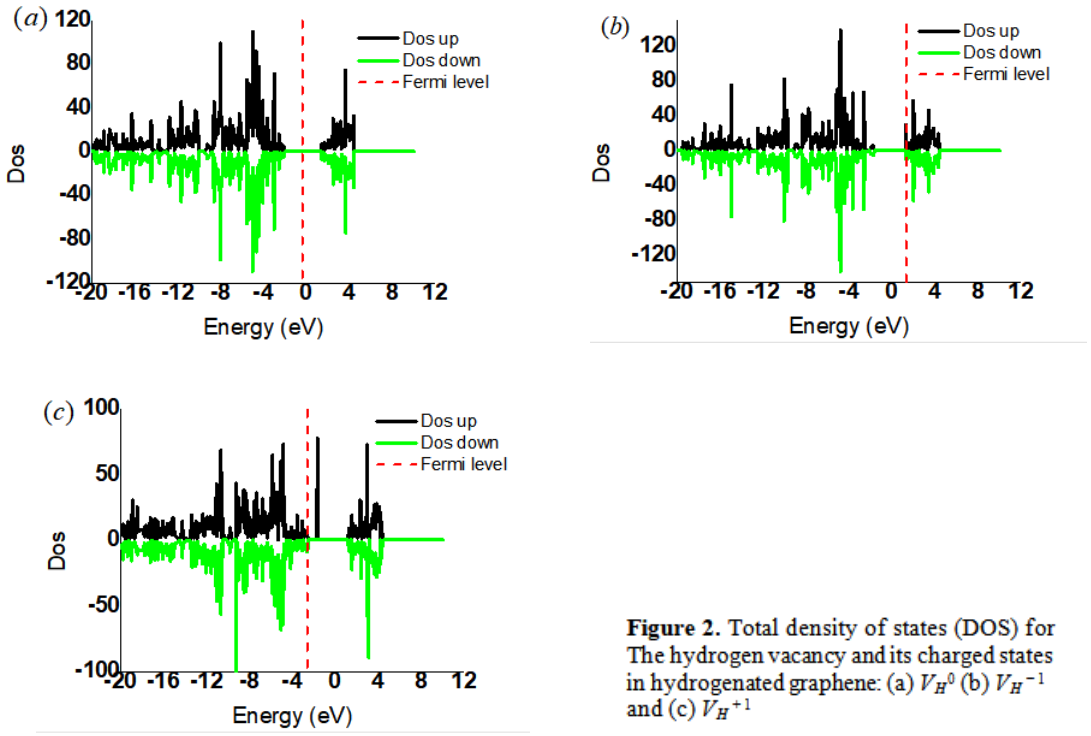

Figure 2. Total density of states (DOS) for The hydrogen vacancy and its charged states in hydrogenated graphene: (a) $V_H{}^0$ (b) $V_H{}^{-1}$ and (c) $V_H{}^{+1}$

The presence of these states close to the conduction band edge raises the possibility of utilising this point defect for nano-electronics and optical applications [18]. The calculated value of the U-parameter for this vacancy point defect is +1.84 eV. The positive U-parameter value for this point defect shows that this defect permits the formation of the singly positive and singly negative charge states without notable traits of instability. The calculated charge transition levels, $(+1/0)$ and $(0/-1)$ for this defect, are respectively -1.34 eV and 0.5 eV. This is in good agreement with the transition levels depicted by the defect level diagram of figure 3.

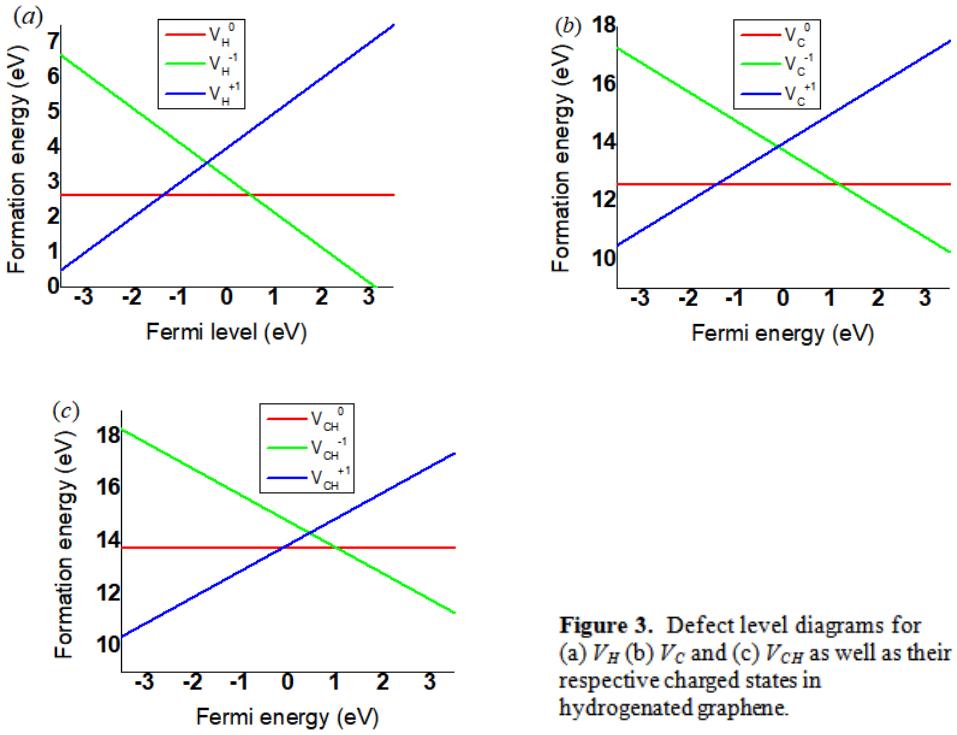

Figure 3. Defect level diagrams for (a) V_H (b) V_C and (c) V_{CH} as well as their respective charged states in hydrogenated graphene.

3.2. Carbon vacancy (V_C)

A carbon monovacancy point defect is formed when a single carbon atom is removed from its site on a hydrogenated graphene monolayer as shown by the image of figure 1 (b). The removal of a carbon atom forms four dangling bonds - three from the nearest three adjacent carbon atoms and one from the hydrogen atom that still exist in the vicinity of the created vacancy. The carbon vacancy in its neutral state, V_C^0, has four unbonded electrons. We propose that the existence of these four unpaired electrons induce notable electronic repulsive coulombic forces. As a result of this we put it forward that the formation energy of this defect is very high and positive at a value of 12.57 eV as depicted in table 1. Charging the defect negatively to form V_C^{-1} lowered the formation energy slightly to 12.36 eV. We noted that the presence of this defect induce heavy lattice distortion of the atoms in the vicinity of the defect. V_C^0 and V_C^{-1} exhibited the C_s(m) symmerty constraints, hence there is lowering of symmetry from the high symmetry point group of the pristine structure -C_{3m}(m). We thus have noted that the carbon monovacancy formation in the graphane monolayer is subject

to the pseudo Jahn-Teller static distortions. The V_C defect induces deep and shallow level defect states within the graphane bandgap. A close examination of DOS plots as shown by figure 4 depicts multiple defect states within the bandgap of graphane. The asymmetric nature of these defect states clearly shows the magnetic traits as shown by figure 4. The bulk states are also asymmetrical showing that this defect can be exploited for various magnetic applications such as magnetic nano-sensors. Charging this defect to form V_C^{-1} gave rise to a distinct spin-up state just above the Fermi level. This spin polarised defect state is also deep and considerably isolated from the band edges. Just like the V_C^0, the DOS plot for V_C^{-1} is also non-aligned. The derived thermodynamic transition level values, $(+1\ /\ 0)$ and $(0\ /\ -1)$ are respectively -1.41 eV and 1.19 eV. These values correlate with the values shown by the defect level diagram shown by figure 3(b). V_C yielded a positive value of the U-parameter +2.60 eV showing stability for charged states formation.

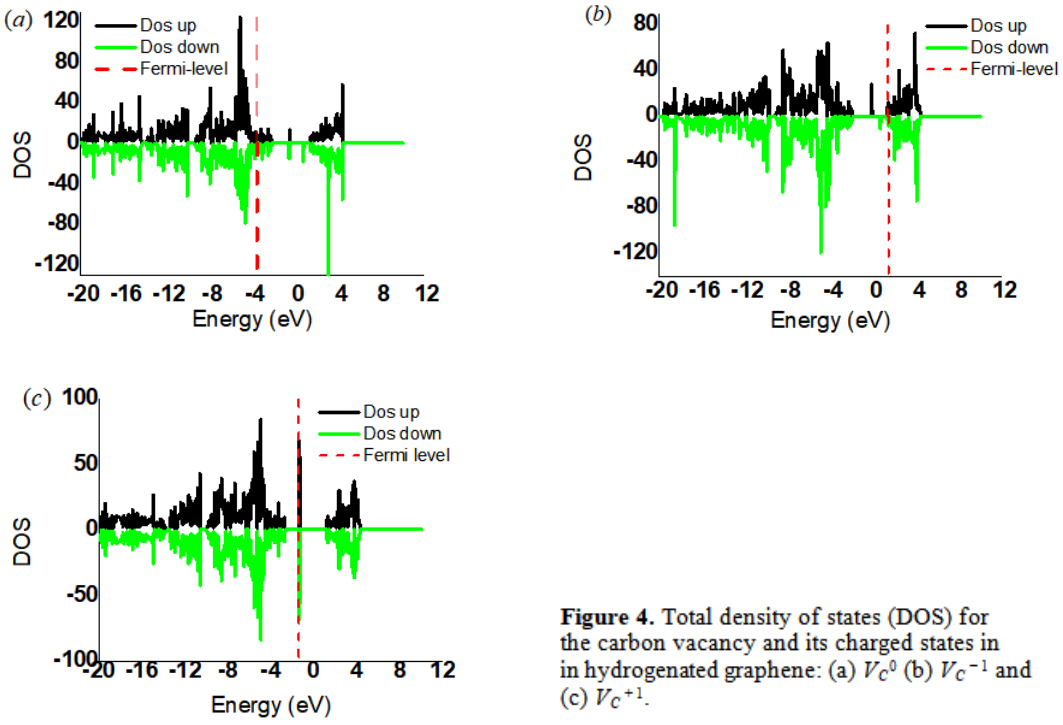

Figure 4. Total density of states (DOS) for the carbon vacancy and its charged states in in hydrogenated graphene: (a) V_C^0 (b) V_C^{-1} and (c) V_C^{+1}.

3.3. Carbon-hydrogen vacancy (V_{CH})

A carbon-hydrogen vacancy is formed on hydrogenated graphene when both a carbon

atom and the hydrogen atom attached to the very same carbon atom are simultaneously removed from their sites as illustrated by figure 1(c). It is energetically costly to form this defect. The calculated formation energy is 13.75 eV for V_{CH}^{0}as shown in table 1. Charging the defect reduces the formation energy to 13.41 eV for V_{CH}^{-1} and to 11.53 eV for V_{CH}^{+1}. The defect symmetry for the neutral and charged states is C_s(m) . This symmetry is preserved for all the configurations we considered. We can thus propose that the defect transition from one thermodynamic charge state to another is not subject to Jahn-Teller distortions. V_{CH} point defect in the neutral charge state induces spin-polarised states in the bandgap of graphane. The defect induces magnetism since the both the defect states and the bulk states are asymmetrical as shown by figure 5. Careful analysis of the total DOS plots shows multiple defect states close to the band edges for V_{CH}^{0}. The defect states clearly induces magnetism, hence there is a real possibility of manipulating the V_{CH} point defect for various magnetic applications. The negatively charged state of this defect , V_{CH}^{-1}, also induces spin-polarised defect states within the hydrogenated graphene bandgap. The calculated charge transition levels ($+$ / 0) and $(0/-1)$ are respectively -0.11 eV and 1.03 eV and these values align with those depicted by the defect level diagram of figure 3(c). V_{CH}^{-1} is also magnetic and brings about both donor and acceptor states close to the band edges. The transition from V_{CH}^{0} to V_{CH}^{-1} seems to quench the magnetism. We also noted that the transition of the defect from the neutral state to the singly positive charged state seems to completely eliminate the magnetic traits of the defect. However, this transition give rise to spin-up states and spin-down states that are non-spin polarised. The spin-up states in the middle of the bandgap are symmetric to the spin-down states, hence we propose that V_{CH}^{+1} is non-magnetic. V_{CH} yielded a positive value of the U-parameter which is 1.14 eV.

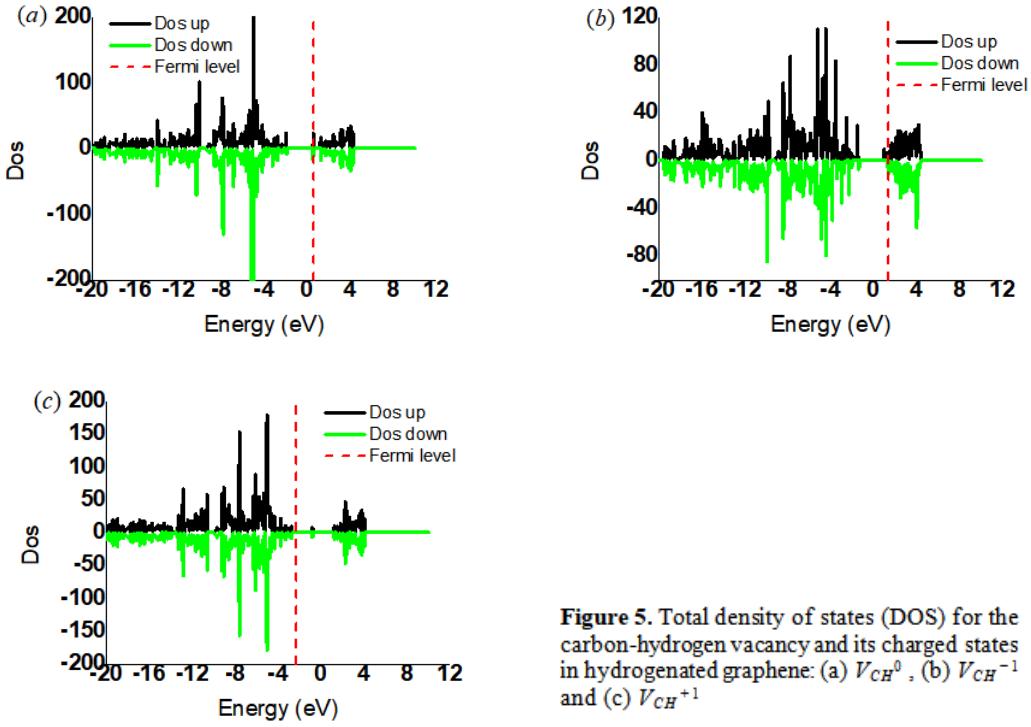

Figure 5. Total density of states (DOS) for the carbon-hydrogen vacancy and its charged states in hydrogenated graphene: (a) $V_{CH}{}^{0}$, (b) $V_{CH}{}^{-1}$ and (c) $V_{CH}{}^{+1}$

4. Summary and conclusion

With the aid of first-principles computations we studied the effects of the presence of vacancy point defects in hydrogenated graphene. We characterised hydrogen and carbon monovacancies of the type V_H, V_C and V_{CH}. These vacancy point defects yielded relatively high positive formation energies. The implication of this finding is that these point defects require an activation energy for them to form. Moreover, the concentration of vacancy point defects in two-dimensional materials may be very low making it difficult to observe and analyse them except with the use of very sophisticated instruments which are not readily available to all and sundry. V_H has lower formation energies as compared to V_C and V_{CH}. We can therefore propose that, of the three types of point defects considered, V_H is likely to form as compared to the other two. We also noted that vacancies in hydrogenated graphene modify the electronic structure of this material because of the creation of partially occupied defect states between the band gap. A possible positive implication of this is the utilization of these point defects for band gap engineering in hydrogenated graphene [19]. We also found out that these vacancy

point defects alter the chemical and optical properties of this two-dimensional material, raising the possibility of utilising them as for novel nano-technology applications. These point defects are also generally subject to the pseudo Jahn-Teller distortion [20] which encompass a decrease in the lattice system's energy by way of eliminating the lattice structure's degeneracy. One critical finding of this contribution is that all the considered point defects yielded positive effective U-parameters showing that they permit the formation of singly positive and singly negative charged states without giving rise to any form of instability. The acceptor levels $(0\,/\,-)$ of the vacancy point defects have higher energies as compared to the donor levels $(+\ /\,0)$ and hence the arrangement of the thermodynamic transition states is not inverted showing that these defects are stable in their respective charged states. Among other challenges, a comprehensive analysis of vacancy point defects is affected by factors such as temperature, characterization techniques as well as their inevitable interaction with some other defects. As an ongoing study, it is imperative to investigate the nitrogen-vacancy complexes in hydrogenated graphene in order to determine if it is possible to reduce the high activation energy.

Acknowledgements

We would like to express our heart-felt gratitude to the University of Pretoria postgraduate funding for providing the sponsorship for this project. We also would like to thank the Centre for High Perfomance Computing (CHPC) for availing first principle simulation resources. REM also thanks NiTheCS for financial support.

References

[1] Ashcroft N W, Mermin N D and Wei D 2016 Solid State Physics (L. S. Han, ed.) Cengage Learning

[2] Yu P Y, Cardona M 1996 Fundamentals of Semiconductors: Physics and Materials Properties

[3] Novoselov K S, Geim A K, Morozov S V, Jiang D, Zhang Y, Dubonos S V, Grigorieva I V and Firsov A 2004 Science 306666-69

[4] Lebegue, S.; Klintenberg, M.; Eriksson, O.; Katsnelson, M. I. 2009 Phys. Rev. B: Condens. Matter Mater. Phys.**79** (24), 245117

[5] Podlivaev A I and Openov L A 2017 Condensed Matter106110-15

[6] Whitener K E 2018 J. Vac. Sci. Technol. A **36**, 05G401, 1-15

[7] Giannozzi P et al 2009 Condens. Matter 21395502

[8] Kohn W and Sham L J 1965Phys. Rev., **140**, A1133

[9] Heyd J, Scuseria G E and Ernzerhorf M 2003 Journal of Chemical Physics **118** 8207-8215.

[10] Zhang S B and Northrup J E 1991Phys. Rev. Lett. **67** 2339

[11] Dreyer C E, Alkauskas A, Lyons J L, Janotti A and Van de Walle C G 2018 Annu. Rev. Mater. Res. **48** 2.1-2.26

[12] Mapasha R E, Molepo M P and Chetty N 2016 Physica E**79** 52-58

[13] Kittel C 2005 Introduction to Solid State Physics (Stuart Johnson, ed.). John Wiley and Sons, Inc.

[14] Patterson J and Bailey B 2010 Solid-State Physics (J. D Patterson and B. C. Bailey, ed.). Springer, 2010.

[15] Gehring G A and Gehring K A 1975 Rep. Prog. Phys.381-89

[16] Bersuker I B 2001Chem. Rev.**101**, 4 1067-1114

[17] Gali A 2019Nanophotonics 8 (11)

[18] Freysoldt C, Grabowski B, Hickel T, Neugebauer J, Kresse G, Janotti A and Van de Walle C G, 2014 Rev. Mod. Phys.**86**. 253

[19] Lebegue S, Klintenberg M, Eriksson O, and Katsnelson M I 2009Phy. Rev. B**79** 245117

[20] O'Brien M C M and Chancey C C, 1993 Am. J. Phys.61688-697

[21] Naik M.H, Jain M.: CoFFEE: Corrections For Formation Energy and Eigenvalues for charged defect simulations, Elsivier 226, pp. 114-126 (2018)

Chapter 5

Results and Discussion:

Published paper 2

This chapter gives a complete account of the paper "**First principles characterization of nitrogen substitutional point defects in graphane (CH)".** The article was published as H. Mapingire and R. E Mapasha by SA Institute of Physics, Proceedings of SAIP 2023 and was assigned the ISBN: 978-0-7961-3774-6. In this chapter we present first principles characterization of three types of nitrogen substitutional point defects in the two-dimensional material- graphane. We do a comprehensive investigation of the formation energies, charge transition levels, U-parameters and density of states for: a nitrogen atom substituting a hydrogen atom (N_H) , a nitrogen atom substituting a carbon atom (N_C) and a nitrogen atom substituting both a carbon and a hydrogen atom (N_{CH}) in the graphane chair conformer. Understanding of the key aspects of nitrogen substitutional point defects in graphane is a pre-requisite in the intensive exploration of nitrogen-vacancy complexes in hydrogenated graphene.

First principles characterization of nitrogen substitutional point defects in graphane (CH)

H Mapingire and R E Mapasha
Department of Physics, University of Pretoria, Pretoria, 0002 South Africa
Email: edwinmapasha@up.ac.za

Abstract. We present ab initio characterization of nitrogen substitutional point defects and their different charge states in the two-dimensional material graphane. Our present first principles calculations were carried out within the framework of density functional theory implemented in the quantum espresso code. We derived the formation energies and thermodynamic charge transition levels for the nitrogen substitutional point defects of the form N_H, N_C and N_{CH}. We also determined the U-parameters for these point defects as it is crucial as far as defect mobility is concerned. The defect formation phenomena are all endothermic, hence the point defects are energetically expensive to form. N_C and N_{CH} yielded a positive effective U-parameter showing their stability should single negative and single positive charge states form. The point defects in this contribution induced spin-polarised defect states within the graphane bandgap and they can thus be exploited for various nano-magnetic and nanoelectronics applications.

1. Introduction

The isolation and characterization of the two-dimensional material (2-D) graphene in 2004 at the University of Manchester by Novoselev and Geim [1] opened floodgates of interest in different kinds of 2-D materials [2][3][4]. Graphene is an sp2 hybridized material composed of a network of carbon atoms that are covalently bonded to each other to form a stable chicken-wire like hexagonal structure [5]. The isolation of a graphene monolayer was done using the now well known micro-mechanical cleavage or the skotch-tape method [6]. Graphene has a number of interesting properties that have attracted research interest far and wide. However, the absence of a band-gap in graphene has limited its direct application in nano-electronics [7]. A number of material researchers

are seeking apt ways of creating a band-gap in graphene in order to open new ground of application for graphene derived 2-D materials [8]. In their work, Sahin et al proposed dimensionality reduction and the use of functionalization [9]. Alternatively, one can adsorb atoms or molecules or functional groups onto a graphene layer. These two methods can give rise to charge doping and the opening up of an electronic band-gap. Two-dimensional materials that are synthesised from graphene in more or less similar ways as discussed above are referred to as graphene derivative materials [8]. Among others, we have graphane which is hydrogenated graphene [10], fluorographene which is fluorinated graphene as well as chlorographene or chlorinated graphene. In 2007 Sofo *et al* [11] used first-principles derivation of total energy to predict the existence and stability of graphane (CH) as a semi-conductor hydrocarbon which is completely saturated. Graphene hydrogenation give rise to the formation of a direct bandgap at the Brillouin zone centre of graphane. The different properties of graphane come into play because of the different ways in which hydrogen atoms can be intertwined with the carbon atoms on a graphene monolayer. The structures of the six main allotropes of graphane- chair, stirrup, boat-1, boat-2, tricycle and twist-boat- depends on the ways in which the hydrogen atoms are attached to the carbon atoms in each hexagonal carbon ring [12]. The chair conformer is the most stable with the periodic up and down hydrogenation pattern. The other graphane stereo isomers that have been proposed in research articles includes: the armchair; the twist-boat; the twistboat-chair and the tricycle which comes from the chair and stirrup combination [13]. Whitener [14] discussed a number of methods that can be used to synthesise graphane. The prominent ones are: the exposure of graphene to hydrogen plasma and plasma-assisted chemical vapour deposition (CVD). Our current study of the 2-D graphane is motivated by its various apt applications that have been reported in literature. These include piezoelectricity, thermoelectricity, nanoelectronics, transistors, nano-composites and electron-phonon superconductors [12]. In our current contribution, we do a comprehensive study of nitrogen substitutional point defects in graphane. We do an indepth study of nitrogen substitutional point defects

of the form N_C, N_H and N_{CH} in the graphane chair conformer, as shown by figure 1. The N_C substitutional point defect is formed when a nitrogen atom substitutes a carbon atom from its lattice site on a graphane monolayer as shown by figure 1(a). The substituted carbon atom has four valence electrons that enables it to covalently bond to other three nearest neighbour carbon atoms as well as to a hydrogen atom giving rise to sp3 orbital hybridization. The N_H substitutional point defect is formed by inserting a nitrogen atom on a hydrogen atom lattice site as depicted by figure 1(b). The nitrogen atom's five valence electrons will cause the N_H defect in the neutral charge state to have four unpaired electrons since one of the five electrons will be involved in the single covalent bond between the nitrogen atom and the nearest carbon atom. The simultaneous substitution of a carbon atom together with its covalently bonded hydrogen atom by a nitrogen atom forms an N_{CH} point defect on a graphane monolayer as illustrated by figure 1(c). This defect has two unpaired electrons in the neutral charge state, N_{CH}^{0}, while N_{CH}^{-1} and N_{CH}^{+1} have three and one unpaired electrons respectively. Our current study is motivated by a number of factors, which among others include the fact that the knowledge of point defects in graphane is still not yet complete.

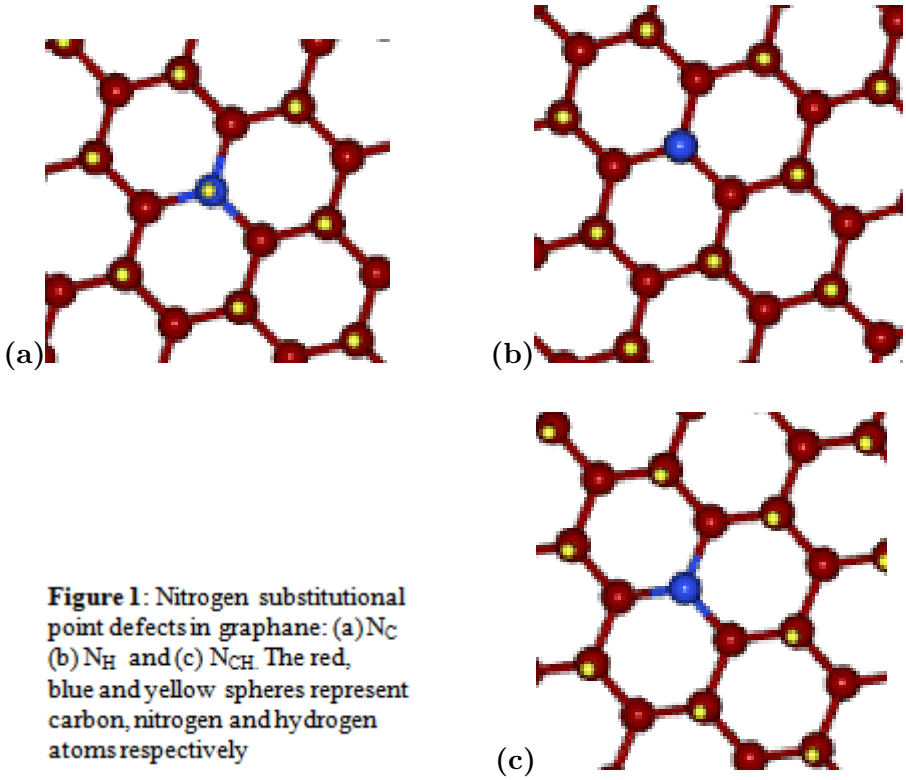

Figure 1: Nitrogen substitutional point defects in graphane: (a) N_C (b) N_H and (c) N_{CH}. The red, blue and yellow spheres represent carbon, nitrogen and hydrogen atoms respectively

2. Method

Our first principles calculations were perfomed within the confines of density functional theory (DFT) using the Kohn-Sham methodology [15]. We employed the Quantum Espresso code (QE) [16] to run our calculations. Using QE plane wave basis set, we derived fundamental properties of the unit cell of graphane which comprises two carbon and two hydrogen atoms. In deriving these properties, we utilised the Heyd, Scuseria and Ernzerhof (HSE) Hybrid functional [17]. We used the ultra-soft pseudopotentials to model the interaction between the ions and the electrons [18]. We employed the supercell approach to run our entire calculations. The utilisation of the supercell method was motivated by the realisation that this approach facilitates the use of mathematical concepts that exploit the periodicity of the system under considerations [19]. Furthermore, this method can describe the band structure of the crystal system reasonably well and the results yielded by this approach are relatively easy to interpret as compared to other approaches that may present challenges in these aspects [20]. After the derivation of

the requisite properties of the unit cell of graphane, we expanded this cell to a $6 \times 6 \times 1$ supercell comprising 144 atoms - 72 carbon atoms and 72 hydrogen atoms. We created a separation of 15 Å in order to eliminate spurious interlayer interactions which can be a source of unwanted errors for this method. Convergence testing convinced us to use 450 eV and 4500 eV as the cut-off energy values of the wave function and charge density respectively. We used a $3 \times 3 \times 1$ Monkhorst –Pack [21] k-point sampling for the Brillouin zones and for corrections, we used the CoFFEE correction scheme. To ensure reliable results, the threshold value of the force convergence was set at 1.0×10^{-6} eV / Å. To understand the properties of any given material, the point of departure is the derivation of the formation energy. As outlined by Van de Walle as well as Zhang and Northrup [22][23] , we derived the defect formation energy, Ef[Dq], using the equation 1

$$E^f[D^q] = E_T[D^q] - E_T[pure] - \sum_i n_i \mu_i + qE_F + E_{corr} \qquad (1)$$

where $E_T[D^q]$ represents the total energy of a supercell in which the defect , D, of charge state q is embeded. $E_T[pure]$ is the total energy of the pristine supercell of the material under consideration and n_i is an integer that represents the number of $i - type$ atoms that have been added to (for $n_i \succ 0$) or removed from (for $n_i \prec 0$) the supercell in order to create the defect. The term μ_i represents the chemical potentials of the type of atomic species at play while E_F denotes the Fermi energy of the electrons calculated relative to the valence band edge. E_{corr} represents the correction term that takes care of errors that may be introduced by the utilisation of the supercell approach. We define thermodynamic level of transition for charge states q_a and q_b as the position of the Fermi-level whereby the formation energy of the two charge states are the same [24][25][20]. We determined the charge transition levels using equation 2, whereby $E^f(D^q; E_F = 0)$ represents the value of the formation energy for defect D which is in the q charge state when $E_F = 0$, i.e the Fermi level is located precisely at the valence band maximum.

$$\varepsilon(q_a \mid q_b) = \frac{E^f(D^{q_a}; E_F = 0) - E^f(D^{q_b}; E_F = 0)}{q_b - q_a} \qquad (2)$$

The thermodynamic transition levels are of extreme importance because it has been shown experimentally that charge state q_a is stable for the Fermi level positions that are below $\varepsilon(q_a \mid q_b)$ and q_b is stable for the Fermi level positions above $\varepsilon(q_a \mid q_b)$ [25][20][24]. One other paramount concept we considered in this contribution is the U-parameter which is the energy difference between two consecutive thermodynamic energy transition levels [20]. We determined the U-parameter using the equation 3. The physical quantities E_f^{q+1}, E_f^{q-1} and E_f^q denote the respective formation energies of the defect in charge states $q+1$, $q-1$ and q taken in that order.

$$U = E_f^{q+1} + E_f^{q-1} - 2E_f^q \qquad (3)$$

3. Results

Table 1 shows an overview of our first principles results for the three point defect configurations. In the next sub-section we systematically analyse our findings in this contribution.

3.1 Nitrogen substituting a carbon atom [N_C]

The dopant nitrogen atom has five valence electrons in its outermost shell. The adsorbed nitrogen atom is expected to also form sp^3 hybridization with three nearby carbon atom and one hydrogen atom. The additional electron brought by the nitrogen impurity is anticipated to substantially increase the electrical conductivity of the graphane material. The N_C point defect is an n-type point defect because of the presence of this one unpaired electron on the dangling bond. We expect nitrogen-doped graphane to depict paramagnetism or ferro-magnetism because of the presence of this unpaired electron. Our first principles calculations show that N_C defect formation process is non-spontaneous and endothermic with a high positive formation energy of 8.91 eV as shown by table 1. It is energetically expensive to form this defect. We tried to alter the formation energy by populating N_C^0 with an additional electron to form N_C^{-1}.

Table 1: Formation energies for nitrogen substitutional point defects in graphane.

$Defect$	$Charge$ $State$	$Formation$ $Energy(eV)$	$U-parameter$ (eV)	$Fermi-level$ $Position(eV)$	$Electron$ $Difference$ $With$ $Pristine$	$Defect$ $Type$
N_C	0	8.91	0.14	+1.10	−1	$n-type$
	−	8.64		+1.45	−2	$n-type$
	+	5.66		−2.21	0	−
N_H	0	2.74	−	−1.15	−4	$n-type$
	−	−		−	−	−
	+	2.37		−2.67	−3	$n-type$
N_{CH}	0	7.23	3.72	−1.93	0	−
	−	7.20		+1.39	−1	$n-type$
	+	6.88		−2.71	+1	$p-type$

The formation energy slightly decreased to 8.64 eV. Charging the defect by a single positive charge significantly lowers the formation energy albeit positive to 5.66 eV. We deduced that N_C point defect transforms according to the C_s(m) symmetry constraints while both N_C^{-1} and N_C^{+1} are subject to C_{3v}(3m) symmetry group transformations. Since C_{3v}(3m) point group is subject to the presence of spinor states, we suggest that this defect can be exploited for spintronics applications. We also noted that the formation of N_C^0 may be subject to the Jahn-Teller effect [26] because of the lowering of the symmetry from C_{3v}(3m) for pristine graphane to C_s(m) which is depicted in the neutral state of this point defect. Analysis of the DOS plots shows that N_C^0 and N_C^{-1} induces non-spin polarised defect states considerably away from the Fermi level. We noted spin-up states and spin-down states close to the conduction band minimum as shown by figure 2. The DOS graph shows that the majority spin states are symmetric to the minority spin states. We predict that N_C^0 and N_C^{+1} finetune the bandgap in such a way as to widen it while N_C^{-1} seemingly has no effect on the size of the bandgap. We again have observed that both N_C^0 and N_C^{+1} induces shallow donor levels as depicted by figure 2. We also noted that for N_C^0 and N_C^{-1} the Fermi level is pushed to a position very close to the conduction band edge while for N_C^{+1} it is positioned close to the valence band edge. As shown by table 1, N_C yielded a positive U-parameter value of 0.14 eV showing the stability of this defect in terms of allowing the formation of the negative and positive charged states.

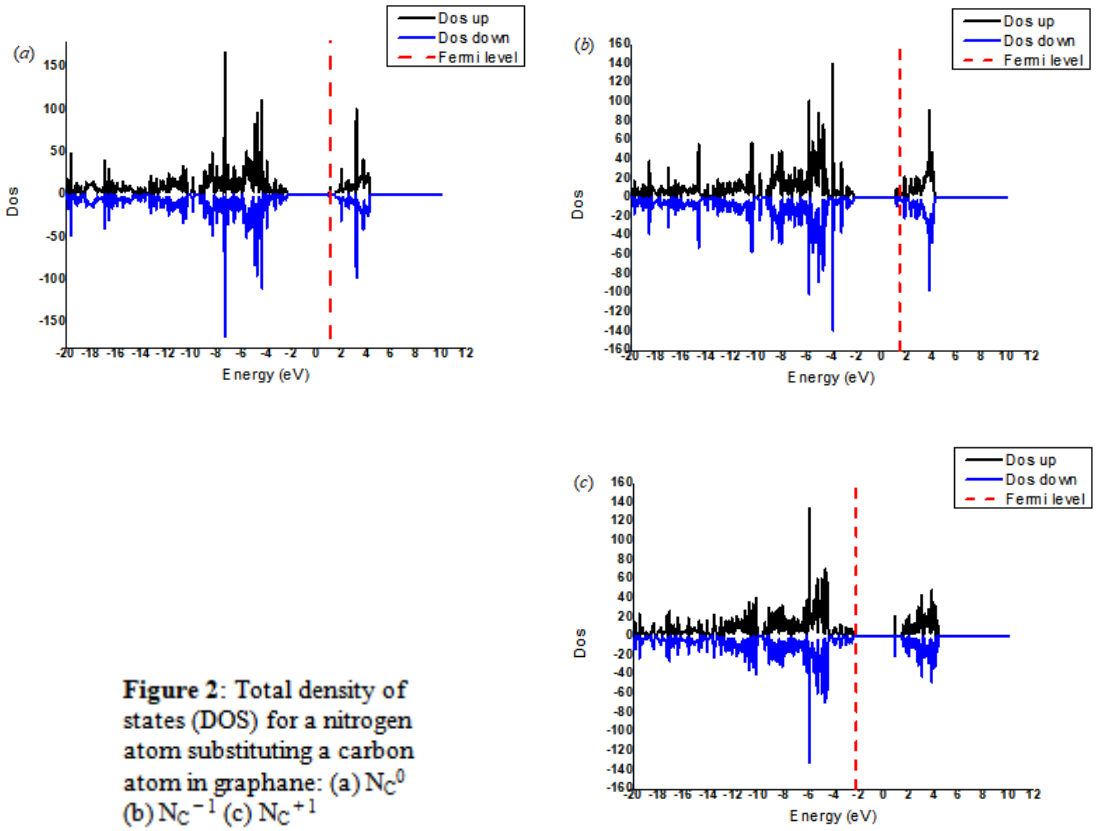

Figure 2: Total density of states (DOS) for a nitrogen atom substituting a carbon atom in graphane: (a) N_C^0 (b) N_C^{-1} (c) N_C^{+1}

3.2 Nitrogen substituting a hydrogen atom $[N_H]$

The N_H^0 and N_H^{+1} are expected to be n-type defects because of the presence of four and three unpaired electrons respectively. The formation energy of the N_H^0 defect is relatively low at a value of 2.74 eV hence the defect formation phenomenon is non-spontaneous. The withdrawal of a single electron to form N_H^{+1} decreased the formation energy slightly to 2.37 eV as depicted by table 1. In our calculations, the N_H point defect exhibited two charge states and hence has a single thermodynamic charge transition level. There is a lowering of symmetry from the C_{3s}(3m) to the C_s(m) symmetry group for the N_H point defect modified graphane. This seems to show the manifestation of the Jahn-Teller distortion [27]. The C_s(m) symmetry transformations are preserved for the neutral and positive charge states. However, the absorption of an atom on a hydrogen site causes a heavy geometric distortion of the lattice structure around the vicinity of the point defect. The N_H^{+1} defect is electrically active since there are clear

spin-polarised defect states between the bandgap. If there are any defect states for N_H^0 and N_H^{-1}, we propose that these states are intertwined with bulk states close to the bandgap edges, hence they are not clearly distinct. The DOS plots shown by figure 3 shows that there is a possibility of this defect widening the bandgap. N_H^{-1} pushes the Fermi-level to the conduction band edge while both N_H^0 and N_H^{+1} moves the Fermi-level to positions close to the valence band edge.

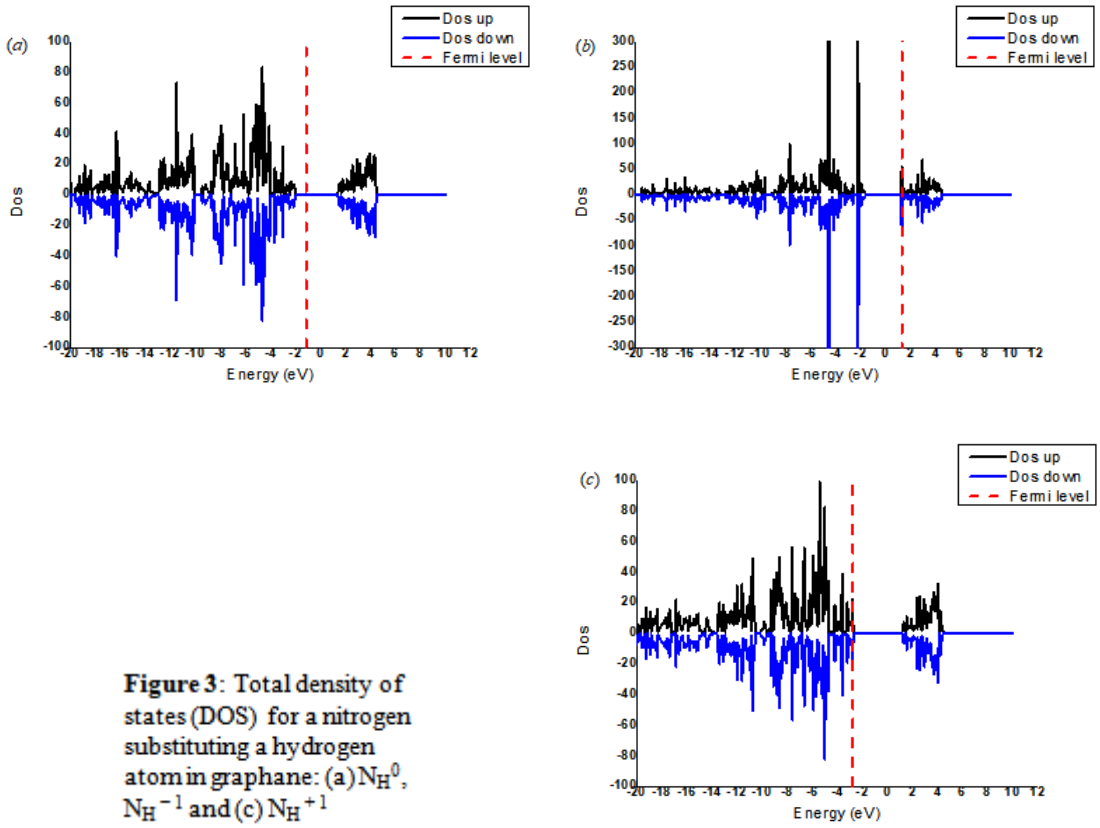

Figure 3: Total density of states (DOS) for a nitrogen substituting a hydrogen atom in graphane: (a) N_H^0, N_H^{-1} and (c) N_H^{+1}

3.3 Nitrogen substituting both a carbon and hydrogen atom [N_{CH}]

The N_{CH} defect formation process is endothermic and non-spontaneous. This defect is energetically expensive to form with a high positive formation energy of 7.23 eV. Charging the defect negatively and positively slightly reduces the formation energies to 7.20 eV and 6.88 eV respectively as recorded in table 1. The presence of this defect lowers the symmetry of the graphane monolayer from the high symmetry point group C_{3v}(3m) to the point group C_s(m) that has lower symmetry transformations. This

change in symmetry may be due to the Jahn-Teller effects [26]. The withdrawal or the addition of a single electron restores the symmetry to $C_{3v}(3\mathrm{m})$. Spinor functions are inherent to the $C_{3v}(3\mathrm{m})$ point group, hence there is a likelihood of utilising this defect for spintronics applications. A careful analysis of the DOS plots for N^0_{CH} shows that the majority spin states are symmetric to the minority spin states proving that the material is non-magnetic.

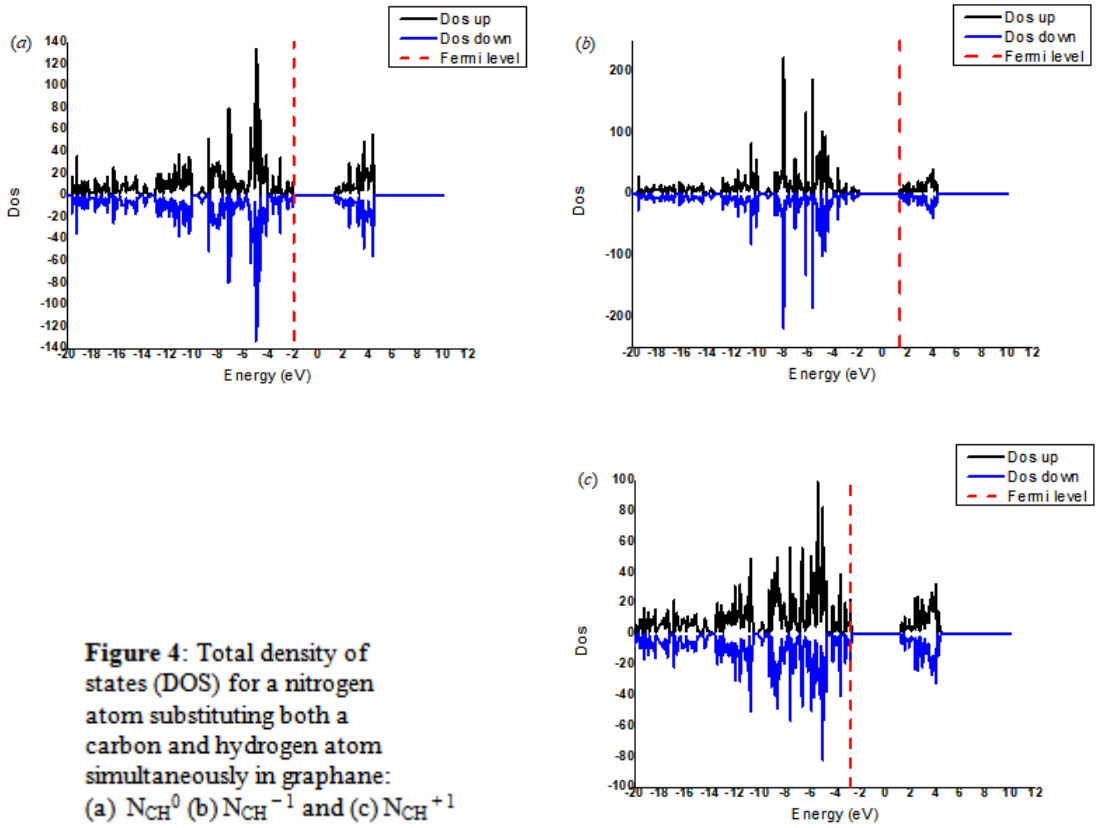

Figure 4: Total density of states (DOS) for a nitrogen atom substituting both a carbon and hydrogen atom simultaneously in graphane: (a) $N_{CH}{}^{0}$ (b) $N_{CH}{}^{-1}$ and (c) $N_{CH}{}^{+1}$

We have two dangling bonds from the dopant nitrogen atom and we propose that the two electrons on these broken bonds are likely to form a pair. Our DOS results as shown by figure 4 seem to show that this point defect doesn't induce states in the middle of the bandgap. If there are any states introduced by this defect in the bandgap, they are coupled with the bulk states and are therefore not well separated from the band edges. This finding seems not to be in line with Pujari and Kanhere's [28] finding that this type of defect in graphane induces spin-polarised states in the middle of the bandgap. The use of the tetrahedra method to deduce the DOS plots may have caused

this uncertainty as far as our current contribution is concerned. However, we do not hasten to add that the presence of N_{CH} defect in a graphane monolayer modifies the bulk states close to the band edges and the N_{CH}^{-1} seem to show some magnetic traits since some states are asymmetric. N_{CH} defect is more stable in the neutral state than the singly positive charge state. The positive U-parameter value of 3.72 eV for N_{CH} shows that this defect does not show instability if positive and negative charged states form. However, the transition from one charge state to another requires a relatively greater amount of energy as compared to N_C point defect.

Conclusion

In this contribution we systematically investigated the thermodynamic stability as well as the electronic properties of point defect modified graphane monolayer. We characterised point defects in the form of nitrogen substitutional dopants. We found out that all the point defects considered in this report have relatively high positive formation energies. We also found out that charging the defects increases the formation energy when the Fermi level is fixed at 0 eV. If the Fermi level is not fixed, charging the defects generally decreases the formation energy. All the defects need activation energy to form. We also noted that these point defects are generally subject to the Jahn-Teller effect which lowers the energy of a given system by removing degeneracy. One of our findings is that the n-type point defects do not induce magnetism or defect states in the middle of the bandgap. The findings by Wang et. al. [29] was that the n-type defects generally do not induce magnetism in graphane. Our results are considerably consistent with this report. N_C fine-tuned the graphane bandgap and induced localised spin-polarised defect energy states. Therefore these defects can be exploited for tailored applications such as magneto-optical sensing, quantum metrology and nano-electronic uses. N_C and N_{CH} gave rise to positive effective values of the U-parameter. These defects thus exhibit stability should single negative and single positive states form. The arrangement of the thermodynamic transition states are not inverted and this explains the stability of the defect. To the best of our knowledge, this has not yet been reported.

Moreover, our current contribution has armed us with the critical knowledge that we required for us to be on a good platform to intensively study the resultant complex formations of these point defects in our next contribution in future. This is worth investigating in order to determine whether a combination of the native defects and the substitutional extrinsic defects can lower the activation energy.

Acknowledgements

The authors are greatly indebted to the university of Pretoria post graduate funding and the Centre for High Perfomance Computing (CHPC) for providing the simulation resources for this project. REM thanks NRF and NiTheCS for supporting the project financially.

References

[1] Novoselov K S, Geim A K, Morozov S V, Jiang D, Zhang Y, Dubonos S V, Grigorieva I V and Firsov A 2004 Science **306** 666-69

[2] Araujo P T, Terrones M and Dresselhaus M S 2012: Materials today **15** 98-109

[3] Zhang Y G, Cheng G D, Peng W and Tang Z 2014 Comp. Mat. Sci. **95** 316-19

[4] Dreyer C E, Alkauskas A, Lyons J L, Janotti A and Van de Walle C G 2018 Annu. Rev. of Mater. Res. **48**, 2.1-2.26

[5] Podlivaev A I and Openov L A 2017 Condensed Matter **106** 110-15

[6] Geim A K N and Novoselov K S 2007 Nature Materials **6** 183-91

[7] Mapasha R E, Molepo M P and Chetty N 2016 Physica E **79** 52-58

[8] S. Haldar S and Sanyal B 2016 Defects in Graphene and its Derivatives(IntechOpen:Nayak P K)

[9] Sahin H, Leenaerts O, Singh S K and Peeters F M 2015 Cond-mat. mtrl-sci. 1-14,

[10] Samarakoon D K and Wang X Q 2011 Structural and Electronic Properties of Hydrogenated Graphene, Physics and Applications of Graphene - Theory (InTech)

[11] Sofo J O, Chaudhari A S and Barber G D 2007 Phys. Rev. B **75**, 153401

[12] Zhou C, Chen S, Lou J, Wang J, Yang Q, Liu C and Huang D 2014 Nanoscale Research Letters **9** 26

[13] Reshak A H and Auluck S 2014 4(70) 37411-18 The Royal Society of Chemistry

[14] Whitener K E 2018 J. Vac. Sci. Technol. A **36**, 05G401, 1-15

[15] Kohn W and Sham L J 1965 Phys. Rev., **140**, A1133

[16] Giannozzi P et al 2009 Condens. Matter **21** 395502

[17] Heyd J, Scuseria G E and Ernzerhorf M 2003 Journal of Chemical Physics **118** 8207-8215.

[18] Vanderbilt D 1990 Phys. Rev. B, **41**, 7892-7895

[19] Koch W and Holthausen M C 2001 A Chemist's Guide to Density Functional Theory (Wiley-Vch)

[20] Freysoldt C, Grabowski B, Hickel T, Neugebauer J, Kresse G, Janotti A and Van de Walle C G 2014 Rev. Mod. Phys. **86**. 253-305

[21] Monkhorst H J and Pack J D 1976 Phys. Rev. B **13** 5188-5192

[22] Van de Walle C G, Laks D B, Neumark G F and Pantelides S T 1993 Phys. Rev. B. **47** 9425

[23] Zhang S B and Northrup J E 1991 Phys. Rev. Lett.**67** 2339

[24] Gali A 2019 Nanophotonics **8** (11)

[25] Thiering G and Gali A 2016 Phys. Rev. B **94** 125202

[26] Bersuker I B 2001Chem. Rev.101, **4** 1067-1114

[27] Gehring G A and Gehring K A 1975 Rep. Prog. Phys.**38** 1-89

[28] Pujari B S and Kanhere D G 2009 J. Phys. Chem. **113**(50). 21063-21067

[29] Wang Y, Ding Y, Shi S and Tang W 2011 Appl. Phys. Lett, **98**. 163104

Chapter 6

Results and Discussion:

Published paper 3

This chapter is a published paper which is entitled **"First principles exploration of N-V point defect complexes in graphane: analysis of energetic stabilities and electronic properties"**. This contribution was published as H. Mapingire, C. Fwalo and R. E. Mapasha in the International Journal of Theoretical Physics, Volume 64, article number 43 (2025). In the article, we employed first principles computations within the framework of density functional theory to investigate fundamental electronic properties and energy concepts of four types of substitutional nitrogen dopant-vacancy complexes in the graphane two-dimensional material. The point defect complexes we explored are: a substitutional nitrogen impurity that is adjacent to hydrogen vacancy ($N_C V_H$), a dopant nitrogen atom which is adjacent to a carbon-hydrogen vacancy ($N_C V_{CH}$), a nitrogen atom substituting both a carbon and hydrogen atom contiguous with a hydrogen vacancy ($N_{CH} V_H$) and a nitrogen dopant atom substituting both carbon and hydrogen atoms from their lattice sites, adjacent to a carbon-hydrogen vacancy ($N_{CH} V_{CH}$).

First principles exploration of N-V point defect complexes in graphane: analysis of energetic stabilities and electronic properties

H. Mapingire
Department of Physics, University of Pretoria, Pretoria 0002, Republic of South Africa.
Corresponding email: pingaton74@gmail.com
C. Fwalo
Department of Physics, University of Pretoria, Pretoria, Republic of South Africa
R. E. Mapasha
Department of Physics, University of Pretoria, Pretoria, Republic of South Africa

Abstract: In this study, we employ first principles calculations within the framework of density functional theory to comprehensively investigate the energetic stabilities and electronic properties of various nitrogen dopant-vacancy complexes: N_CV_H, N_CV_{CH}, $N_{CH}V_H$ and $N_{CH}V_{CH}$ in the graphane two-dimensional material. The creation of N_CV_H and $N_{CH}V_H$ complexes require less energy than that of N_CV_{CH} and $N_{CH}V_{CH}$, according to the formation energy analysis. The binding energies analysis reveals that all the considered N-vacancy complexes are stable when compared to their isolated counterparts. Based on U-parameter values derivation, it is easier for $N_{CH}V_H$ complex (1.09 eV) to undergo transition from one charge state to another as compared to N_CV_{CH} (2.52 eV). The N-vacancy complexes induce acceptor and donor states within the graphane band gap, which alters during transition states (0 to -1 or 0 to +1). This comparative study has provided fundamental insights into the possibilities of utilizing nitrogen-vacancy centers in graphane for band gap engineering and nano-technology tailored applications.

Keywords: graphane; defect complex; density functional theory; formation energy; binding energy; density of states.

---

1. INTRODUCTION

A deep center is a point defect whose energy states are bound or confined to a particular region in a given system [1]. As far as deep center point defects are concerned, we have three fundamental things to consider - that is, the characteristics of the deep center defects, the specifications of host materials in which the defects are embedded and the possible applications. Weber et al [1] discussed at length a number of crucial factors that have to be considered for possible deep center defects and host materials.

For technological applications, the quantum states of the defects must be measurable, controllable, reproducible and isolated from the host atom states. Host materials for deep center defects have to be thin-film or bulk crystals of high quality. Moreover, these materials must have spin-orbit coupling that is small and a band gap that is considerably wide [2].

The prominent deep centre point defect in bulk materials is the nitrogen vacancy center (NV) in diamond [3-6]. This point defect complex can be put into two classes namely the neutral (NV^0) and the negatively charged nitrogen vacancy centre (NV^{-1}) [7-8]. The NV^{-1} in diamond has a number of important applications such as its utilization in highly secure communication, metrology, quantum computing and spintronics applications [9-10]. Material science researchers are actively seeking new and suitable deep center defects as well as apt host materials. This work is therefore motivated by the desire to unravel novel point defect complexes that may be similar or different to the NV center in terms of their functionalities [11]. Since time immemorial, engineers and technologists have been moving from bulk electronic devices to extremely tiny devices which are made up of only a few atoms. As a result, two dimensional materials such as graphene have come into the picture for nano-technology applications.

Graphene has unique properties such as excellent heat conductivity, high electrical conductivity and good mechanical stability [12-16]. These and other properties can be exploited for various electronic and nanotechnology uses [17-20]. However, the non-existence of a band gap in graphene has limited its technological applications. This short-coming in graphene can be overcome by chemical functionalization [21]. The unique structure of graphene emanates from a network of carbon atoms that are covalently bonded to each other forming hexagonal rings [22]. Attaching hydrogen atoms to each of these carbon atoms give rise to hydrogenated graphene or graphane [23]. It is one of the objectives of this contribution to analyze graphane [24] as a likely host material for point defect complexes. Graphane has a lower dimension as compared to diamond (in which the nitrogen vacancy center is housed) which is a three dimensional

material [25]. The world over there is a move from bulk electronic devices to very tiny devices made up of only a few atoms [26].

Zhou et al [27] reported various structures of graphane configurations that have been theoretically derived. The primary allotropes of graphane are: the chair, the stirrup, the boat and the tricycle [28][23][29-34]. The names given to these structures depend on the many ways in which the hydrogen atoms are chemisorbed to the carbon atoms in each carbon ring. The chair conformer has been reported in literature as the most stable [35][24][36][37]. In this contribution, we limit our investigation to the point defects that can form in the chair conformer since it is the most stable [38][23][39].

The exploration of the possibility of using the two-dimensional material graphane as an apt host for deep center point defects that falls under impurity-vacancy complex is an attractive area of research. The unique properties of graphane and the experimental realisation of this material makes it a possible good candidate host material for the miniaturization of electronics, optoelectronic applications and for the fabrication of superconductivity devices [40][41][35][42][43][16][44][17][45]. The broad aim of this contribution is to derive the formation energies of nitrogen impurity-vacancy complexes in graphane with the objective of utilizing this group of point defects in nano-technology applications. This contribution is driven by the benefits that technologists will get by searching and finding new host materials for NV center and other similar deep center defects. Besides this, exploration and characterization of other deep center defects may open new ground of technological innovation as well as introduce new devices and new functionalities.

2. THEORETICAL METHODS

We carried theoretical calculations based on the Quantum Espresso simulation method [46]. In our calculations, we utilized a $6 \times 6 \times 1$ supercell comprising 144 atoms for pristine graphane. Our structure was made up of 72 hydrogen atoms attached to 72 carbon atoms in an alternating and uniform manner. The exchange and correlation functionals [47] were initially derived using the well-known method of Perdew, Burke and Ernzern-

hof under the generalized gradient approximation(GGA) [48]. For comparison purposes we also carried out our calculations using the Heyd-Scuseria-Ernzerhof (HSE) exchange and correlation functional [49]. Convergence testing convinced us to use 450 eV and 4500 eV as the cut-off plane wave function and threshold charge density respectively [50]. We performed our calculations using $3 \times 3 \times 1$ k-point Brillouin zone sampling [51]. For "occupations" we used "smearing" under the "methfessel-paxton" scheme [52-53]. The starting potential and starting wave functions were both set as "atomic". We ran our simulations based on non-polarized wave functions and we set the convergence threshold to a value of 1×10^{-8} Ry. The electronic steps were set to a maximum value of 200.

2.1 DEFECT FORMATION ENERGIES

The determination of formation energies is a crucial step in the characterization of any defect [54][6][55]. Among other fundamental things, the formation energy gives information on defect concentration, the anticipated defect positions in the crystal lattice as well as information on important factors that have to be considered when incorporating the defect into the lattice [56][26]. The defect formation energy largely depends on the total energy of the pristine structure, the total energy of the structure in which a defect has been embedded, the charge state of the defect and the chemical potential energies [57][25][58] of the atomic species that have either been removed or added to the crystal structure when the defect was formed. The formation of a positive or negative defect charge state hinges on the electrons removed or added to the supercell under consideration. This aspect is therefore also of vital importance in the derivation of the formation energy. The general equation used to determine the formation energy, $E_f[D^q]$, for a defect D which is having a charge state q is [59][58][26]

$$E_f[D^q] = E_T[D^q] - E_T[bulk] - \sum_i n_i\mu_i + qE_F + E_{corr} \quad \text{.....(1)}$$

The terms $E_T[D^q]$ and $E_T[bulk]$ respectively represent the total energies of the supercell that has a defect and the one for a pristine or defect-free supercell. The

quantity n_i denotes the atomic species that were either removed from or added to the supercell under consideration in order to form the defect. The value for n_i is positive if atomic species are added to the supercell and negative when atomic species are removed from the pristine supercell. The term μ_i takes account of the chemical potential energies of the atomic species that were either removed from or added to the pristine supercell. E_F stands for the Fermi level or the chemical potential for the electron whose value is given conventionally with respect to the valence band maximum [26].

In this contribution, we derived formation energies for three positions of the Fermi-level (-3.5 eV, 0 eV and 3.5 eV) because this facilitated an in-depth analysis of the defect configurations when the Fermi level is positioned close to the valence band, in the band gap as well as close to the conduction band. This is of crucial importance because of the aspect of defect migration. The Fermi level value depends on the value taken by q. When electrons are added to the supercell, q takes a negative value in contrast to a positive value which it takes when electrons are removed. E_{corr} is a correction term that is there to account for different effects such as electrostatic interactions, elastic interactions as well as effects brought about by methods used to construct the supercell [60]. In order to eliminate unwanted contributions that exist because of the interaction between the point defects and their periodic images, we used the CoFFEE correction scheme since it is apt for simulation system that uses periodic boundary conditions [61].

2.2 BINDING ENERGY AND U-PARAMETER

The concept of binding energy is of fundamental importance in the study of point defects in two-dimensional materials because it gives the idea of the strength of the point defect interaction that results in the complex formation. Binding energy is defined as the total amount of energy that is needed in order to infinitely separate the point defects from each other. Binding energy therefore provides valuable information of how stable a defect complex is [62]. Freysoldt et al [54], derived the binding energy expression, E_b, as the difference in energy between the total formation energy of a point defect complex and the sum of the formation energies of the isolated point defect constituents. If we

have two isolated point defects denoted by D^1 and D^2, their binding energy can be determined from equation 2

$$E_b = E^f[D^1] + E^f[D^2] - E^f[D^1D^2] \text{.....(2)}$$

The physical quantities $E^f[D^1]$ and $E^f[D^2]$ are representing the formation energies of the two isolated point defects respectively. $E^f[D^1D^2]$ denotes the total formation energy of the resultant complex formed by the two point defects, D^1 and D^2.

The U-parameter is an important concept that represents the difference in energy between two successive thermodynamic energy transition levels [54]. This fundamental parameter gives invaluable information about the value of the activation energy that is required if a defect has to undergo transition from one charge state to another. The U-parameter can be derived from the defect formation energies of the different charge states by using equation 3 [54][60], i.e.

$$U = E_f^{q+1} + E_f^{q-1} - 2E_f^q \text{.....(3)}$$

The terms E_f^q, E_f^{q+1} and E_f^{q-1} represents the formation energies of the defect in the neutral, positive and negative charge states respectively.

3. RESULTS

In this section we commence by exploring the point defect configurations for the relaxed structures: N_CV_H, N_CV_{CH}, $N_{CH}V_H$ and $N_{CH}V_{CH}$. We will then systematically analyze our results starting with the bond lengths and charge distribution. We will also discuss the derived formation energies, binding energies and U-parameter values at length. In the last part of our results section, will briefly discuss the defect level diagrams before we coherently explore the total density of states of the four defect configurations as well as their charged states.

3.1 Defect Configurations

The N_CV_H point defect comprises a substitutional nitrogen impurity and an adjacent

hydrogen vacancy as shown by figure 1 (a). The nitrogen atom has five valence electrons of which four are involved in covalent bonding. Three carbon atoms are covalently bonded to the nitrogen impurity. A hydrogen atom is also attached to the foreign nitrogen atom. The remaining one electron from the substitutional nitrogen impurity is free and subject to interesting transition from one state to another.

The $N_C V_{CH}$ point defect is formed by substituting a carbon atom with a nitrogen impurity which is adjacent to a carbon-hydrogen vacancy as depicted by figure 1 (b). The substitutional nitrogen atom is covalently bonded to two nearest neighbour carbon atoms as well as a hydrogen atom. Of the five nitrogen electrons in the outermost energy level a pair of unbonded electrons remains. The substituted carbon-hydrogen double vacancy also leaves two dangling bonds. We therefore have four free electrons in this defect.

The third defect configuration that we considered is $N_{CH} V_H$. This point defect complex comprises a nitrogen atom substituting both a carbon and hydrogen atom contiguous with a hydrogen vacancy. In this case, the substitutional nitrogen atom is covalently bonded to three nearest neighbour carbon atoms leaving a lone pair of unbonded electrons. The hydrogen vacancy gives rise to a single dangling bond. We thus have three free electrons in this defect configuration which is depicted by figure 1 (c).

The $N_{CH} V_{CH}$ defect configuration is formed by removing both carbon and hydrogen atoms from their lattice sites and replacing this pair of atoms with a single nitrogen atom as illustrated by figure 1 (d). The substitutional nitrogen atom lies next to a carbon-hydrogen vacancy. This substitutional nitrogen impurity is covalently bonded to two neighbouring carbon atoms. Of the five nitrogen valence electrons, three are not involved in bonding. The carbon-hydrogen vacancy give rise to two dangling bonds and thus two electrons from the two nearest neighbour carbon atoms are unbonded. This defect configuration, therefore has five free electrons. These identified defect configurations are relaxed and characterized using density functional theory. In the sections that

follow, we explore the structural and energetic stability aspects. Among other aspects, we analyze bond lengths, formation energy, binding energy, U-parameters, defect level diagrams as well as density of states.

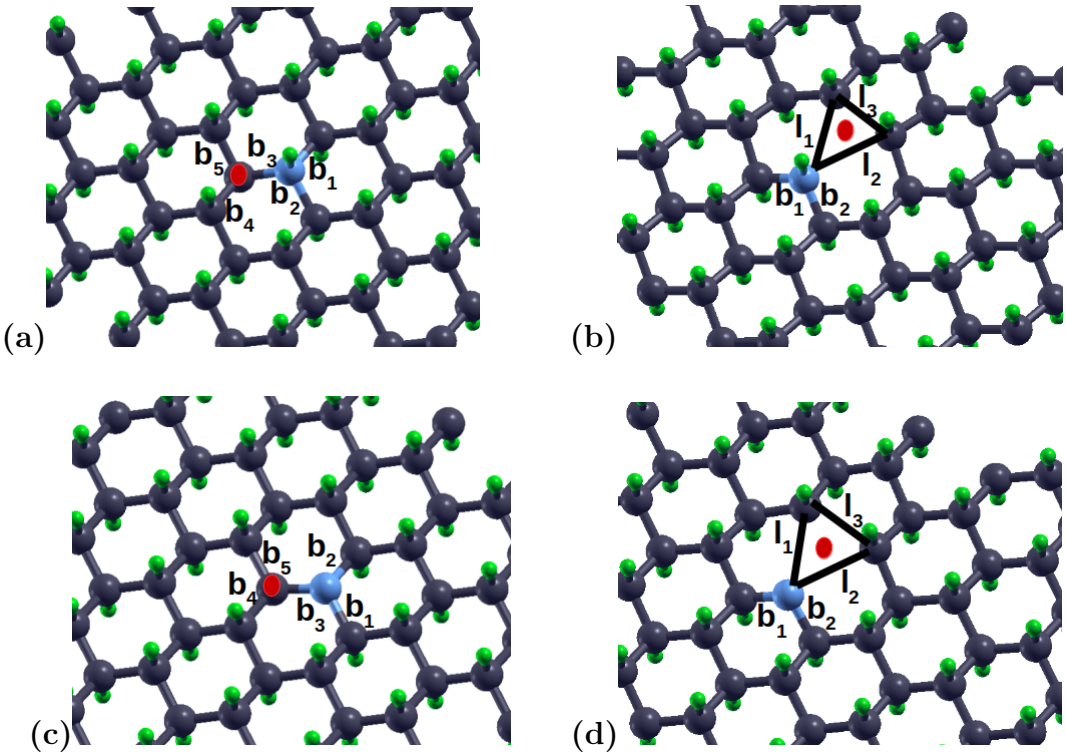

Fig 1: Structure of nitrogen-vacancy point defect complexes created in graphane: (a) N_CV_H (b) N_CV_{CH} (c) $N_{CH}V_H$ and (d) $N_{CH}V_{CH}$. The grey, light blue and green spheres respectively represent carbon, nitrogen and hydrogen atoms. The red sphere represents a vacancy (V_H or V_{CH}) that has been created at that site.

3.2 Bond Lengths and Charge Distribution

Bond lengths (the distance between nuclei that are involved in bonding) are influenced by a number of factors such as molecular structure, atomic sizes, nature of the bonding orbitals, bond order, electronegativity differences and atomic hybridization. In this contribution, our focus is on atomic hybridization of the point defect complexes N_CV_H, N_CV_{CH}, $N_{CH}V_H$ and $N_{CH}V_{CH}$ as shown in figure 1. When a foreign atom occupies the lattice site of a native atom or when a vacancy is created in a lattice structure to form point defect complexes, there is an inevitable reorganization of the valence electrons. This results in the formation of hybrid orbitals that may have partially or

completely different orientations and shapes as compared to the initial atomic orbitals. The new atomic hybridization can give rise to notable changes in bond lengths as shown by the new bond lengths of N_CV_H, N_CV_{CH}, $N_{CH}V_H$ and $N_{CH}V_{CH}$ in table 1. One inevitable outcome of the new atomic hybridization is the electron density redistribution within or around the point defect complex as depicted by figure 2.

For N_CV_H, addition of a single electron decreases the bond lengths b_1 and b_2 slightly from 1.516 Å to 1.515 Å while b_3, b_4 and b_5 slightly increased from 1.497 Å to 1.498 Å. The removal of a single electron to form $N_CV_H^{+1}$ increased the bond lengths b_1 and b_2 to a value of 1.537 Å while the values of b_3, b_4 and b_5 decreased as shown in table 1. $N_{CH}V_H^{-1}$ yielded an increase of the bond lengths b_1 , b_4 and b_5 as opposed to both b_2 and b_3 that decreased in values. We noted that the removal of a single electron from $N_{CH}V_H$ to form $N_{CH}V_H^{+}$, increased all the bond lengths except b_3 that decreased in value when compared to its value for the neutral configuration. N_CV_{CH} in both the negative and positive charge states gave rise to an increase of b_1, b_2, l_1, l_2 and l_3 as depicted in the recordings of table 1. $N_{CH}V_{CH}^{-1}$ yielded decreased values of b_1, b_2, l_1, l_2 and l_3 when compared with the neutral configuration.

The withdrawal of an electron from $N_{CH}V_{CH}$ resulted in the decrease of the bond lengths b_1 and b_2 while l_1, l_2 and l_3 increased in values. Generally, we noted that for all our configurations, b_1 is equivalent to b_2 while b_4 has the same magnitude as b_5. Moreover, we also noted that l_1 and l_2 have equal magnitudes for all the point defect configurations at play. Our observations as noted above emanate from the outcome of adding (removing) an electron to (from) a point defect complex. The influence of an extra electron (or an electron deficiency) can alter the electron density at the vicinity of the carbon, nitrogen and hydrogen atoms that are involved in bonding. This can in turn considerably distort the strength of the electron-electron repulsive forces due to the difference in polarity. In response to this, bonding atoms may shift away from each other or towards each other, giving rise to the non-uniform variation of the bond lengths shown in table 1.

Table 1: Bond lengths of nitrogen dopant-vacancy defect complexes in graphane: (a) N_CV_H , (b) N_CV_{CH} , (c) $N_{CH}V_H$ and (d) $N_{CH}V_{CH}$.

Defect	*Charge state*	*Bond lengths* (Å)								
		b_1	b_2		b_3	b_4	b_5			
(a) N_CV_H	0	1.516	1.516	$b_1 = b_2$	1.495	1.497	1.497	$b_4 = b_5$		
	−1	1.515	1.515	$b_1 = b_2$	1.497	1.498	1.498	$b_4 = b_5$		
	+1	1.537	1.537	$b_1 = b_2$	1.475	1.470	1.470	$b_4 = b_5$		
		b_1	b_2		l_1	l_2	l_3			
(b) N_CV_{CH}	0	1.431	1.431	$b_1 = b_2$	2.643	2.643	2.019	$l_1 = l_2$		
	−1	1.452	1.452	$b_1 = b_2$	2.721	2.721	2.037	$l_1 = l_2$		
	+1	1.451	1.451	$b_1 = b_2$	2.723	2.723	2.606	$l_1 = l_2$		
		b_1	b_2		b_3	b_4	b_5			
(c) $N_{CH}V_H$	0	1.393	1.474	$b_1 \neq b_2$	1.474	1.488	1.488	$b_4 = b_5$		
	−1	1.466	1.466	$b_1 = b_2$	1.449	1.491	1.491	$b_4 = b_5$		
	+1	1.509	1.509	$b_1 = b_2$	1.313	1.501	1.501	$b_4 = b_5$		
		b_1	b_2		l_1	l_2	l_3			
(d) $N_{CH}V_{CH}$	0	1.420	1.420	$b_1 = b_2$	2.680	2.680	2.220	$l_1 = l_2$		
	−1	1.412	1.412	$b_1 = b_2$	2.678	2.678	1.983	$l_1 = l_2$		
	+1	1.400	1.400	$b_1 = b_2$	2.814	2.814	2.343	$l_1 = l_2$		

The charge distribution around a point defect complex provides significant insights into some aspects of the complex's reactivity, physical and chemical properties. The charge distribution depicted by figure 2 shows an uneven spread of the charge around the nitrogen dopant. These point defects thus show polar traits- they have regions of low and high electron density. This has a significant bearing on how the systems interacts with other molecules in chemical reactions. We can thus put it forward that these point defect systems have low degree of symmetry or non-symmetric since there is an existence of regions that have varying electron density giving rise to sides that are partially positive as opposed to the other sides which are partially negative.

We again suggest that, generally the point defects brings about net dipole moments [63] and there is an existence of anisotropic characteristics for all the systems under our consideration. For all our point defect complexes, $N_C V_H$, $N_C V_{CH}$, $N_{CH} V_H$ and $N_{CH} V_{CH}$, we noted a substantial increase in the charge distribution around the nitrogen dopant as depicted by figure 2. This may be due to nitrogen atom introducing additional electrons into the system giving rise to localized regions that have considerable electron density.

3.3 Formation Energy

In this section we comprehensively explore the formation energies of the nitrogen-vacancy complexes of different charge states in graphane. For the three Fermi-level positions we explored, the formation energy of $N_C V_H$ ranges from 7.18 eV to 14.28 eV for all the charge states under consideration as shown by table 2. These values of formation energies are more or less similar to those for $N_{CH} V_H$ whose values are between 5.96 eV and 13.93 eV. $N_C V_{CH}$ and $N_{CH} V_{CH}$ point defect complexes yielded very high formation energies fluctuating from 16.23 eV to 25.14 eV for all the Fermi-level positions we explored. The high formation energies of these complexes is as a result of the combination of the isolated constituent point defects. A combination of N_C, N_{CH} and V_{CH} to form a particular complex will generally give rise to a high formation energy because the isolated point defects are energetically expensive to form [64][65]. However,

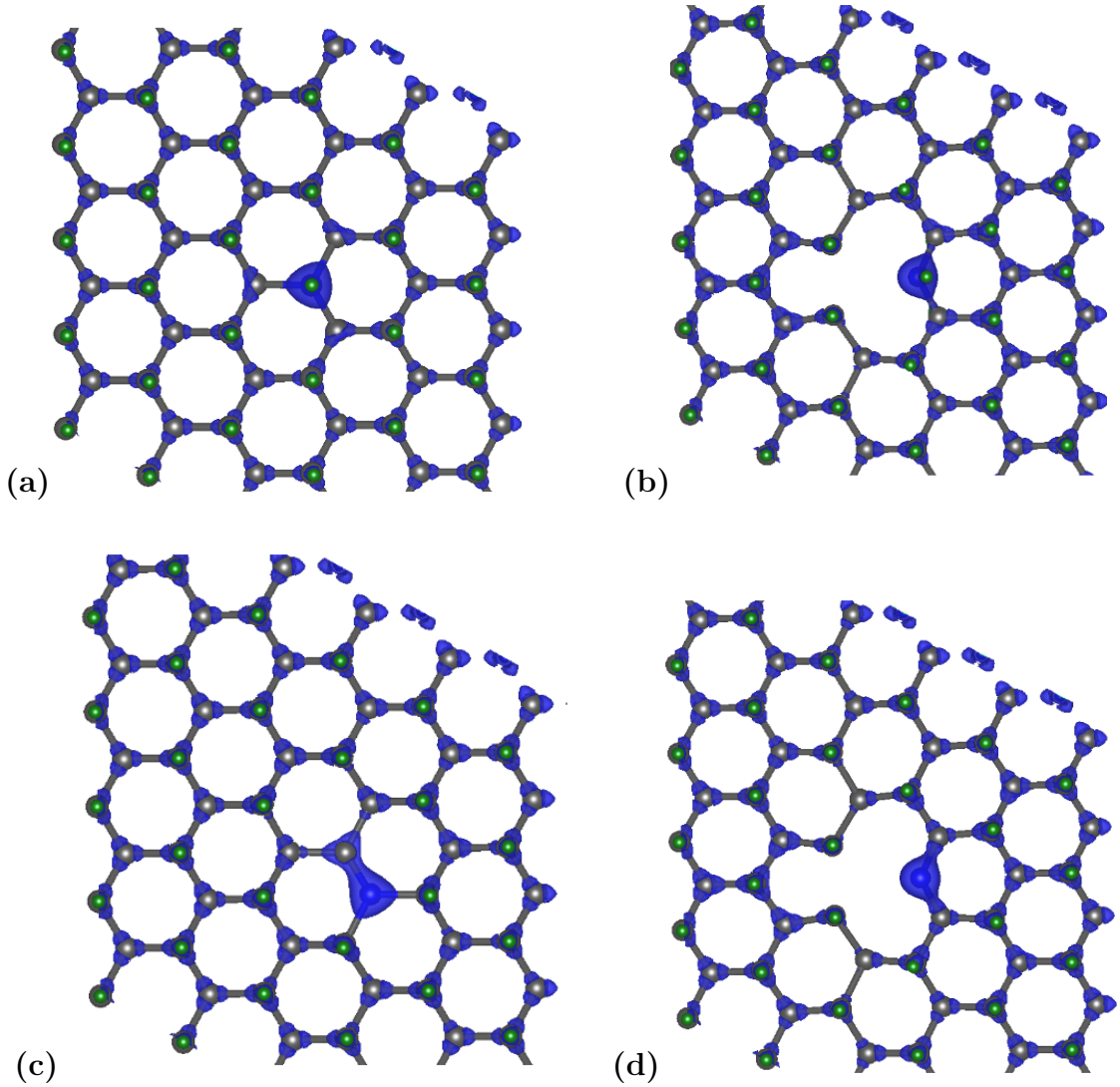

Fig 2: Charge distribution in the nitrogen dopant-vacancy defect complexes in graphane: (a) $N_C V_H$ and (b) $N_C V_{CH}$ (c) $N_{CH} V_H$ (d) $N_{CH} V_{CH}$ The grey and green spheres respectively represent carbon and hydrogen atoms. The dark blue non-uniform spheres shows the charge distribution which is more pronounced around the light blue nitrogen dopant atoms.

Table 2: Formation energy for nitrogen dopant-vacancy defect complexes in graphane: (a) $N_C V_H$, (b) $N_C V_{CH}$, (c) $N_{CH} V_H$ and (d) $N_{CH} V_{CH}$.

Defect complex	*Charge state*	*Formation energy when* $E_F = 0eV$	*Formation energy when* $E_F = -3.5eV$	*Formation energy when* $E_F = +3.5eV$
(a) $N_C V_H$	0	9.53	9.53	9.53
	-1	10.78	14.28	7.28
	$+1$	10.68	7.18	14.18
(b) $N_C V_{CH}$	0	18.52	18.52	18.52
	-1	19.73	23.23	16.23
	$+1$	19.83	16.23	23.33
(c) $N_{CH} V_H$	0	9.4	9.4	9.4
	-1	10.43	13.93	6.93
	$+1$	9.46	5.96	12.96
(d) $N_{CH} V_{CH}$	0	20.41	20.41	20.41
	-1	20.79	24.79	17.29
	$+1$	21.64	18.14	25.14

the high formation energy does not prevent the nitrogen-vacancy complexes formation in graphane [43].

For all the charge states under consideration, $N_{CH} V_{CH}$ has the highest values of formation energies. The formation energies of $N_C V_{CH}$ are also high but slightly lower than that of $N_{CH} V_{CH}$. In comparison with these two, $N_C V_H$ and $N_{CH} V_H$ have lower formation energies, albeit positive as shown in table 2. In the negative and neutral charge state, $N_C V_H$ has formation energies that are approximately equal to that of $N_{CH} V_H$. For the positive charge state, $N_{CH} V_H$ has the lowest formation energy.

3.4 Binding energy

The knowledge of binding energy concepts is of critical importance to material engineers in terms of controlling the formation of the defect complex as well as the dissociation of the complex into individual entities. The binding energy values we derived give an overview of the degree of stability of nitrogen-vacancy complexes in graphane. All the complexes yielded positive values of binding energies ranging from a minimum value of 0.47 eV for $N_{CH} V_H^0$ to a peak value of 5.14 eV for $N_C V_{CH}^{-1}$ as shown in table 3.

The positive binding energy values shows that more energy is needed to separate

Table 3: Binding energy, energy gap, defect level positions and U-parameter values for nitrogen-vacancy complexes in graphane: (a) $N_C V_H$, (b) $N_C V_{CH}$, (c) $N_{CH} V_H$ and (d) $N_{CH} V_{CH}$.

Defect complex	*Charge state*	*Binding energy* (*eV*)	*GGA energy gap* (*eV*)	*HSE energy gap* (*eV*)	*Defect level from VB* (*eV*)	*Defect level from CB* (*eV*)	$U-$*parameter value* (*eV*)
(*a*) $N_C V_H$	0	2.02	2.91	3.25	1.17	1.13	2.40
	−1	2.45	2.89	3.34	1.31	1.02	
	+1	1.17	2.96	3.89	–	–	
(*b*) $N_C V_{CH}$	0	4.14	3.23	3.32	0.72	1.90	2.52
	−1	5.14	3.02	3.25	0.51	1.95	
	+1	1.90	3.39	3.52	0.62	0.98	
(*c*) $N_{CH} V_H$	0	0.47	3.13	3.40	2.15	0.41	1.09
	−1	1.30	2.69	3.29	–	–	
	+1	4.11	3.37	3.42	1.77	1.33	
(*d*) $N_{CH} V_{CH}$	0	0.57	2.76	3.38	0.94	1.15	1.61
	−1	2.58	2.57	3.22	0.77	1.24	
	+1	1.81	3.41	3.45	0.46	0.56	

the components than the energy that is required during the phenomenon of complex formation. The separation of the defect complexes into their respective individual constituents is a non-spontaneous process. It is also worth noting that, a positive binding energy may also indicate that the components of the defect complex are relatively more stable in comparison to the parent complex.

The defect complexes of the type $N_C V_H^{+1}$ (1.17 eV), $N_C V_{CH}^{+1}$ (1.90 eV), $N_{CH} V_H^0$ (0.47 eV), $N_{CH} V_H^{-1}$ (1.30 eV), $N_{CH} V_{CH}^0$ (0.57 eV) and $N_{CH} V_{CH}^{+1}$ (1.81 eV) yielded low positive binding energies (shown in brackets) demonstrating the existence of weak interactions between the constituents of the defect complexes.

The second group of defect complexes comprising $N_C V_H^0$ (2.02 eV), $N_C V_H^{-1}$ (2.45 eV) and $N_{CH} V_{CH}^{-1}$ (2.58 eV), produced moderate binding energy values (shown in brackets) indicating relatively moderate strength of interaction and hence these complexes are stable in relationship to the former class of nitrogen-vacancy complexes. However, dissociation of these complexes into their separate components is still possible under certain external perturbations.

The third class of nitrogen-vacancy complexes made up of $N_C V_{CH}^0$ (4.14 eV), $N_{CH} V_H^{+1}$ (4.11 eV) and $N_C V_{CH}^{-1}$ (5.14 eV) gave rise to relatively high binding energies (shown in brackets) signifying the existence of strong bonds between the components. This group of nitrogen-vacancy defect complexes is relatively stable and unlikely to break-up into their respective components without the external application of energy or other apt perturbation factors.

We noted that for $N_C V_H$ and $N_C V_{CH}$, the addition of an electron to the complex increases the binding energy as opposed to the withdrawal of an electron that significantly reduces the binding energy. For $N_{CH} V_H$, an additional electron put into the system slightly increases the binding energy while the withdrawal of a single electron considerably increases the binding energy. Likewise, the addition and withdrawal of an electron for $N_{CH} V_{CH}$, more than doubles the binding energy of the neutral configuration.

3.5 U-parameter

The U-parameter values are pivotal in terms of the determination of the ability of a point defect to change from one charge state to another. The greater the U-parameter value, the less likely is the transition of the defect from an initial charge state to another. All the point defect complexes yielded positive values of U-parameter as illustrated by the recordings of table 3. $N_{CH}V_H$ gave rise to the lowest U-parameter value of 1.09 eV while N_CV_{CH} produced the highest U-parameter value of 2.52 eV as illustrated in table 3. It is thus easier for $N_{CH}V_H$ to undergo transition from one charge state to another as compared to N_CV_{CH}. A lower activation energy is required when $N_{CH}V_H$ changes from a given charge state to another as compared to N_CV_{CH}. The other two defect configurations, N_CV_H and $N_{CH}V_{CH}$ yielded U-parameter values of 2.40 eV and 1.61 eV respectively. Therefore, it is slightly easier for $N_{CH}V_{CH}$ to go through a charge state transition as compared to N_CV_H.

The positive U-parameter values of all the defect configuration considered also give an insight into the stability of the defects. Generally, the point defect complexes showed some degree of stability, since they permitted the formation of positive and negative charge states. We propose that, the acceptor levels of the point defect complexes, $(0/-)$, yielded higher values of energy relative to the energy values of the donor levels, $(+/0)$. In line with this perspective, we conclude that the thermodynamic transition states of all the point defects we considered are not inverted [54,66].

3.6 Defect transition level diagrams

The graphs of formation energy versus Fermi-level position give us a way of comprehensively assessing the charge transition levels which we use to derive the U-parameters. These graphs as shown by figure 3 also help to visualize the defect formation energy variation within the valence band, band gap and the conduction band. This information is critical in terms of defect migration implications in a given material. For N_CV_H, our calculations yielded the transition level values of -1.15 eV and 1.25 eV for $\varepsilon(+1/0)$ and $\varepsilon(0/-1)$ respectively. The point defect complex N_CV_{CH} gave rise to charge state

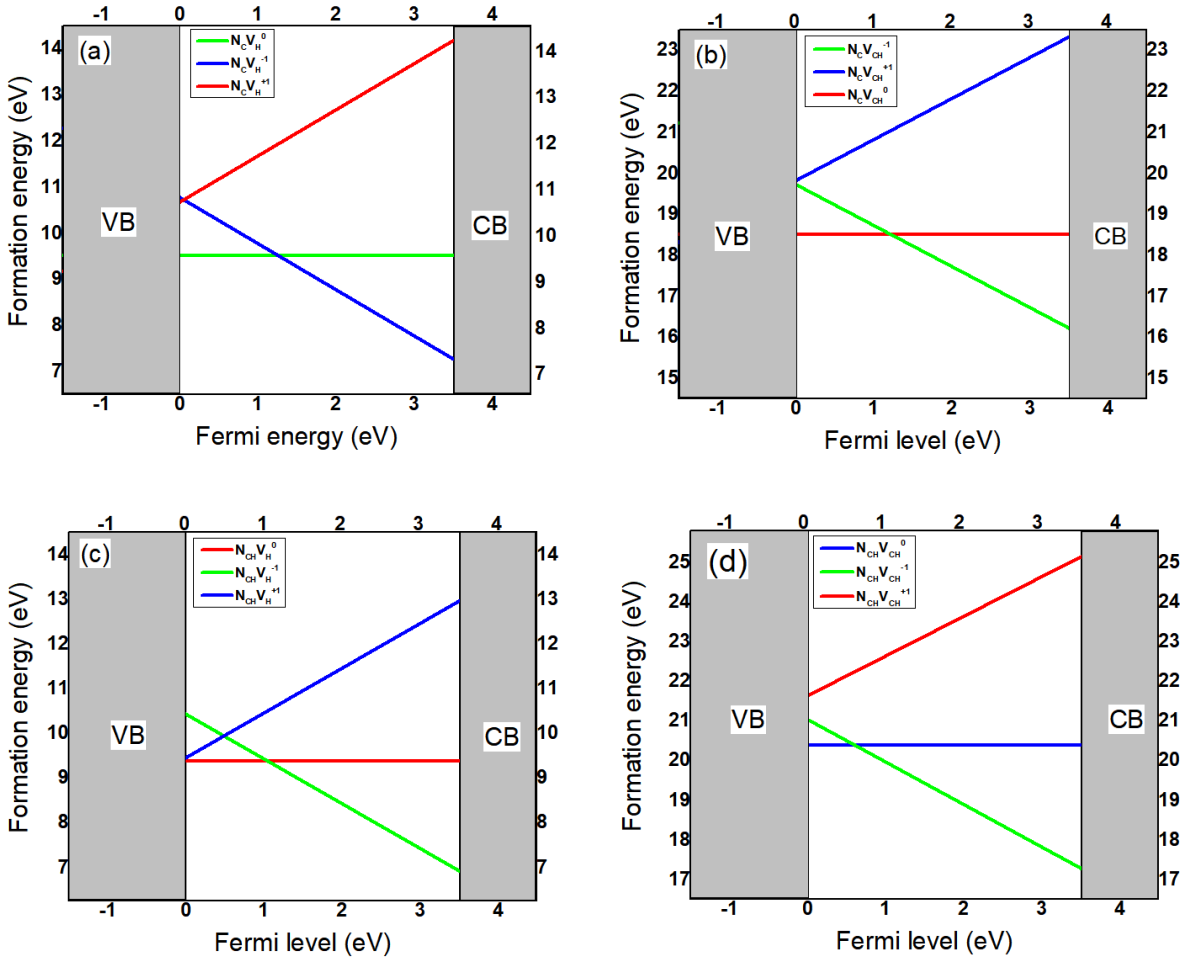

Fig 3: Transition level diagrams for nitrogen dopant-vacancy complexes in graphane: (a) N_CV_H (b) N_CV_{CH} (c) $N_{CH}V_H$ and (d) $N_{CH}V_{CH}$.

transition values of -1.31 eV and 1.21 eV for $\varepsilon(+1/0)$ and $\varepsilon(0/-1)$, taken in that order. $N_{CH}V_H$ transition level values decreased to -0.06 eV $[\varepsilon(+1/0)]$ and 1.03 eV $[\varepsilon(0/-1)]$, hence this point defect complex can easily transform from one charge state to another in comparison to N_CV_H and N_CV_{CH}. We derived charge transition energy level values of -1.23 eV $[\varepsilon(+1/0)]$ and 0.38 eV $[\varepsilon(+1/0)]$, for point defect complex, $N_{CH}V_{CH}$. These values are of paramount importance in terms of defect engineering implications.

3.7 Density of states

The plots depicted by figure 4 shows density of states (DOS) versus energy for all our defect configurations in the neutral, negative and positive charge states. The graphs

in black for all the point defect complexes show the majority spin-up states while the bold blue graphs show the minority spin-down states. On these plots, we represented the Fermi-level position with red dotted lines as depicted by figure 4. The Fermi-level position is important because among other aspects it influences material electronic properties such phase transitions, thermodynamic stability and conductivity. Moreover, it has a bearing on charge carrier concentration and it also separates unoccupied energy states from the occupied ones. For these and other reasons, the position of the Fermi-level on density of states plots is crucial in the prediction of 2-dimensional material properties. However, the precise prediction of the true Fermi-level position still remains a challenging aspect in first principles calculations. Among other factors, the Fermi-level position depends on the exchange-correlation functional that is being used to do the computational calculations. Therefore, in this contribution, the Fermi-level position depicted by the red dotted line denotes the highest occupied energy levels, rather than the true Fermi-level positions.

3.7.1 $N_C V_H$

The density of states graphs as depicted by figure 4 (a, b and c) shows that the majority spin-up energy states are perfectly aligned with the minority spin-down states, thus this point defect complex does not show traits of magnetism for the neutral, negative and positive defect states. $N_C V_H^0$ is electrically active as depicted by figure 4 (a). This defect induces deep defect energy states that are partially occupied in the middle of the band gap. We put it forward that the defect energy states are positioned approximately 1.13 eV from the conduction band edge and 1.17 eV from the valence band edge. Our calculated band gap values are 2.91 eV for GGA and 3.25 eV for HSE as shown by the values recorded in table 3. $N_C V_H^0$ pushes the Fermi level to the site of the defect states.

This defect in the negative charge state, $N_C V_H^{-1}$, give rise to energy states deep in the middle of the band gap. We propose that the states are positioned 1.31 eV from the VB edge and 1.02 eV from the CB edge as depicted by table 3. The Fermi-level is

pinned slightly into the CB but very close to the edge. Using GGA and HSE methods, we derived the band gap values of 2.89 eV and 3.34 eV respectively. Since there are no induced states within the band gap, $N_C V_H^{+1}$ is electrically inactive as shown by figure 4 (c). The Fermi-level is positioned near the VB edge showing traits of electron deficiency. This point defect therefore shows acceptor-type characteristics and may trap electrons creating holes in the valence band and causing the material to exhibit p-type behaviour. The GGA band gap is underestimated at a value of 2.96 eV, while HSE widens the band gap to a value of 3.89 eV.

3.7.2 $N_C V_{CH}$

For this defect complex, the bulk majority spin-up states are symmetric to the minority spin-down states. Non-magnetic traits were noted as illustrated by figure d (d, e and f). $N_C V_{CH}^0$ is electrically active and induces partially filled acceptor states close to the valence band. The defect states are positioned 0.72 eV from the valence band edge and 1.90 eV from the conduction band edge. The Fermi-level is intertwined with the induced defect states slightly close to the CB edge depicting n-type traits. Our derived band gap values are 3.23 eV and 3.32 eV for GGA and HSE methods respectively.

$N_C V_{CH}^{-1}$ is also electrically active and give rise to occupied acceptor states that are positioned 0.51 eV from the VB edge and 1.95 eV from the CB edge. We deduced band gap values of 3.02 eV (GGA) and 3.25 eV (HSE) for $N_C V_{CH}^{-1}$ as shown by table 3. $N_C V_{CH}^{+1}$ give rise to both acceptor and donor states between the band gap as shown by figure 4 (f). The acceptor states are partially occupied and they are separated from the unoccupied donor states by an energy value of 0.72 eV. The defect states close to the VB are positioned 0.62 eV from the VB edge while the states close to the CB are positioned 0.98 eV from the CB edge. Our calculated band gap values are 3.39 eV (GGA) and 3.52 eV (HSE).

3.7.3 $N_{CH} V_H$

The density of states are symmetric, hence the presence of the defect does not bring about any magnetic traits in this material. The point defect complex in the neutral

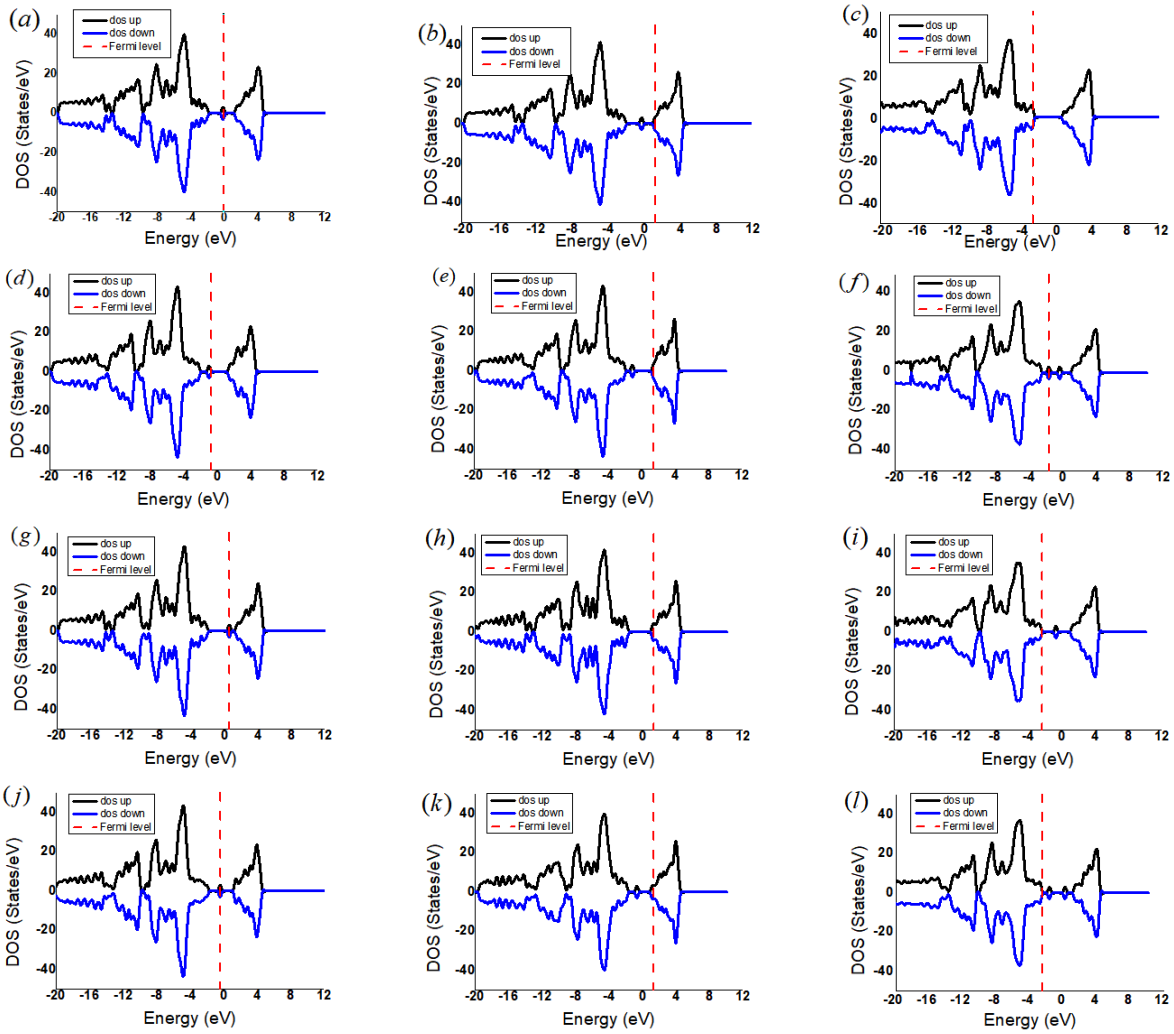

Fig 4: Total density of states for nitrogen dopant-vacancy complexes in graphane: (a) $N_C V_H^0$ (b) $N_C V_H^{-1}$ (c) $N_C V_H^{+1}$(d) $N_C V_{CH}^0$ (e) $N_C V_{CH}^{-1}$ (f) $N_C V_{CH}^{+1}$ (g) $N_{CH} V_H^0$ (h) $N_{CH} V_H^{-1}$ (i) $N_{CH} V_H^{+1}$ (j) $N_{CH} V_{CH}^0$ (k) $N_{CH} V_{CH}^{-1}$ and (l) $N_{CH} V_{CH}^{+1}$. The graphs in bold black and bold blue colours represents dos up and dos down respectively. The red dotted line shows the Fermi-level position.

state, $N_{CH}V_H^0$, is electrically active. We predict that this point defect induces partly filled donor energy states very close to the conduction band as shown by figure 4 (g). The states are positioned 0.41 eV from the conduction band edge and 2.15 eV from the valence band edge. We predict that the band gap values are 3.13 eV (GGA) and 3.40 eV (HSE).

For $N_{CH}V_H^{-1}$, we did not observe any defect electronic states in the band gap as shown by figure 4 (h). The Fermi level is pushed slightly deep into the conduction band depicting n-type characteristics. The defect in the negative charge state modifies the band gap to 2.69 eV (GGA) and 3.29 eV (HSE) as illustrated by the values recorded in table 3.

The withdrawal of an electron from this point defect complex to form $N_{CH}V_H^{+1}$ yields unoccupied energy states deep in the middle of the band gap - approximately 1.33 eV from the conduction band edge and 1.77 eV from the valence band edge as portrayed by figure 4 (i). The Fermi level is pinned on the valence band edge showing p-type characteristics. Our derived band gap values are 3.37 eV (GGA) and 3.42 eV (HSE).

3.7.4 $N_{CH}V_{CH}$

The symmetric density of states depicted by figure 4 (j, k and l) reveals that there is no magnetism induced by this point defect complex in graphane. The $N_{CH}V_{CH}^0$ DOS illustrated by 4 (j), shows that the Fermi-level is positioned in the middle of the band gap, very close to the site of the partially filled mid-gap induced defect states. These defect states are positioned 0.94 eV from the valence band edge and 1.15 eV from the conduction band edge. We suggest that the GGA band gap is 2.76 eV and the HSE method widens the band gap to a value of 3.38 eV for $N_{CH}V_{CH}^0$. Populating $N_{CH}V_{CH}$ with a single electron, shifts the defect states to a site close to the valence band - approximately 0.77 eV from the valence band edge and 1.24 eV away from the conduction band edge. We propose that the defect energy levels are acceptor states. $N_{CH}V_{CH}^{-1}$ pushes the Fermi-level slightly deeper into the conduction band indicating

Table 4: Comparison of the electronic properties of $N_CV_H^{-1}$ in graphane and NV^- in diamond

Property	$N_CV_H^{-1}$ *in graphane*	NV^- *in diamond* [ref 8–11]
Formation energy (eV)	7.28	$2.40 - 4.50$
Energy gap(HSE) (eV)	3.34	5.50
Binding energy (eV)	2.45	$4.40 - 5.40^{\#\#theoretical}$ $4.90 - 5.50^{**experimental}$
Defect level position	$1.31eV$ *from* VB $1.02eV$ *from* CB	$2.50 - 2.70eV$ *from* VB^a *acceptor* $1.70 - 1.90eV$ *from* CB^{donor}

n-type traits. This defect modulates the band gap to 2.57 eV (GGA) and 3.22 eV (HSE) as illustrated by the values indicated in table 3. The withdrawal of a single electron from $N_{CH}V_{CH}$ to form the positive charge state gave rise to the DOS plot shown by figure 4 (l). The unoccupied acceptor and donor states induced in the band gap are separated by 1.12 eV. The states close to the valence band are 0.46 eV from the valence band edge while the donor states are 0.56 eV from the conduction band edge.

3.8 $N_CV_H^{-1}$ in graphane and diamond

In this section we briefly compare the stability and some electronic properties of $N_CV_H^{-1}$ in graphane and NV^- in diamond. The formation energy of $N_CV_H^{-1}$ in graphane is relatively high compared to that of NV^- in diamond as shown by the recordings in table 4. Exploring different ways of reducing this formation energy in graphane may be an area of research interest. $N_CV_H^{-1}$ in graphane yields a band gap of 3.34 eV which is slightly lower than 5.50 eV of NV^-in diamond [8-11]. The theoretical and experimental values of the binding energy of the negatively charged nitrogen-vacancy center in diamond ranges from 4.40 eV to 5.50 eV [8-11] as illustrated in table 4. The value of 2.45 eV for the binding energy of $N_CV_H^{-1}$ in graphane is lower than the binding energy of NV^-in diamond, making the later point defect complex to be relatively more stable.

4. DISCUSSION OF RESULTS AND CONCLUSION

The formation energies of nitrogen-vacancy complexes in graphane give invaluable information on the stability as well as the electronic and opto-electronic properties of this group of point defects. The derived formation energies give critical insight into the interplay that exists between nitrogen dopant (N_C or N_{CH}) chemisorption, vacancy creation (V_C or V_{CH}) as well as the structural stability of graphane in the presence of nitrogen-vacancy complexes. Moreover, the comprehension of these formation energies is of paramount importance for tailoring graphane's electronic properties for targeted applications in the field of nano-technology. We also put it forward that the derived formation energies give material engineers the priceless information that this two-dimensional material is stable in the presence of nitrogen-vacancy complexes and hence we anticipate graphane to exhibit consistent and reliable operating performance over a period of time when used in nanotechnology applications.

We noted very low binding energy values for $N_{CH}V_H^0$ and $N_{CH}V_{CH}^0$, which are respectively 0.47 eV and 0.57 eV. These point defect complexes are thus relatively unstable and can easily break-up into the individual substituents point defects. The binding energies for $N_CV_H^{+1}$, $N_{CH}V_H^{-1}$, $N_{CH}V_{CH}^{+1}$ and $N_CV_{CH}^{+1}$ are slightly higher at values of 1.17 eV, 1.3 eV, 1.81 eV and 1.90 eV respectively. The defect configurations that have high binding energies of 4.11 eV, 4.14 eV and 5.14 eV are $N_{CH}V_H^{+1}$, $N_CV_{CH}^0$ and $N_CV_{CH}^{-1}$ taken in that order. These point defects exhibit stability and are thus energetically favourable. We noted that the defects that have almost the same binding energies, depict almost similar defect level states. For example, $N_CV_H^{+1}$ and $N_{CH}V_H^{-1}$, have no defect level states within their band gap and their binding energies are almost the same at values of 1.17 eV and 1.30 eV respectively. The same argument applies to $N_CV_{CH}^{+1}$ and $N_{CH}V_{CH}^{+1}$, whose binding energies are 1.90 eV and 1.81 eV taken in that order. They show nearly similar defect energy states in the middle of the graphane band gap.

The U-parameter values give material engineers invaluable insight into the ability of point defects to change from an initial charge state to another. All the defect config-

urations in our contribution yielded positive U-parameter values. N_CV_H and N_CV_{CH} produced relatively higher migration energy values of 2.40 eV and 2.52 eV respectively, showing that these point defect complex have to overcome a greater energy barrier in order to transition from one charge state to another. In contrast, the U-parameter values of 1.09 eV and 1.61 eV for $N_{CH}V_H$ as well as $N_{CH}V_{CH}$ taken in that order depicts a better ability for these point defect complexes to change their charge state. The derivation and comparison of the U-parameter values is of extreme importance because the change of charge state of point defects may also considerably influence the local properties of a material and this has a bearing on their performance.

One other imperative finding in this contribution is that the existence of nitrogen-vacancy complexes in graphane generally induce localized defect electronic energy states between the band gap of graphane. All the defect configurations in the neutral state induced partially filled defect states aligned with the Fermi-level position. The negatively charged defect configurations generally gave rise to occupied mid-gap states that pushed the Fermi-level to positions that are close to the conduction band edge exhibiting n-type traits. Generally the point defects in the positive charge state gave rise to unoccupied defect states and also pushed the Fermi-level close to the valence band edge showing p-type characteristics. These point defect complexes also fine-tune the magnitude of the band gap in such a way as to either narrow or widen it. The realization of this knowledge gives material engineers a window of opportunity for specific applications of graphane in band gap engineering.

In conclusion, it is interesting to ascertain whether some modifications of the two-dimensional material graphane can favourably influence the formation energies, binding energies as well as the U-parameter values of the dopant-vacancy complexes. As an area of future study, it is therefore worth investigating the effects of doping graphane with different impurities, other than nitrogen. Another sphere of interest will be investigating the presence of point defects in a graphane material that has been modified by way of increasing the material's pressure and temperature. Moreover, the incorporation of

various materials into graphane in order to form alloys as well as surface and strain modification of this material in the presence of point defects presents innovative areas of research.

Data Availability: The authors of this contribution will avail the source file and data upon reasonable request.

Funding Declarations: The authors declare that there was no funding for this project.

References

[1] Weber J.R, Koehl W.F, Varley J.B, Janotti A, Buckely B.B, Van de Walle C.G, Awschalom D.D.: Quantum computing with defects, Applied Physical Sciences vol 107, pp. 8513-8518 (2010)

[2] Deak P.: Calculating the optical. properties of defects and surfaces in wide band gap materials, Physica B 535, pp. 35-43 (2018)

[3] Choi S, Jain M, Louie S.G.: Mechanism for optical initialization of spin in NV center in diamond, Phys. Rev. B 86, pp. 041202 (2012)

[4] Lenef A, Rand S.C.: Electronic structure of the N-V center in diamond: Theory, Phys. Rev. B 53, pp. 13441 (1996)

[5] Capelli M, Heffernan A.H, Ohshima T, Abe H, Jeske J, Hope A, Greentree A.D, Reineck P, Gibson B.C.: Increased nitrogen-vacancy centre creation yield in diamond through electron beam irradiation at high temperature, Carbon 143, pp. 714-719 (2018)

[6] Gali A.: Ab initio theory of the nitrogen-vacancy center in diamond, Nanophotonics 8, pp. 1907-1943 (2019)

[7] Choi J, Choi S, Kucsko G, Maurer PC, Shields B.J, Sumiya H, Onoda S, Isoya J, Demler E, Jelezko F, Yao NY, Lukin M.D.: Depolarization Dynamics in a Strongly Interacting Solid-State Spin Ensemble, Phys. Rev. Lett. 118, pp. 093601 (2017)

[8] Schirhagl R, Chang K, Loretz M, Degen C.L.: Nitrogen-Vacancy Centers in Diamond: Nanoscale Sensors for Physics and Biology, Annu. Rev. Phys. Chem. 65, pp. 83-105 (2014)

[9] Gali A, Fayta M, Kaxiras E.: Ab initio supercell calculations on nitrogen-vacancy center in diamond: electronic structure and hyperfine tensors, Phys. Rev. B, pp. 155206 (2008)

[10] Doherty M.W, Manson N.B, Delaney P, Hollenberg L.C.L.: The negatively charged nitrogen-vacancy centre in diamond: the electronic solution, New J. Phys. 13, pp. 025019 (2011)

[11] Larsson J.A, Delaney P.: Electronic structure of the nitrogen-vacancy center in diamond from first principles theory, Phys. Rev. B 77, pp. 165201 (2008)

[12] Geim A.K.: Nobel Lecture: Random walk to graphene, Reviews of modern Physics 83, pp. 851-862 (2010)

[13] Geim A.K, Novoselov K.S.: The rise of graphene, Nature Mat. 6, pp. 183-191 (2007)

[14] Urade A.R, Lahiri I, Suresh K.S.: Graphene Properties, Synthesis and Applications: A Review, JOM 75, pp. 614-630 (2023)

[15] Zou L, Wang L, Wu Y, Ma C, Yu S.: Trends Analysis of Graphene Research and Development, Journal of Data and Information Science 3, pp. 82-100 (2018)

[16] Li C, Zheng C, Cao F, Zhang Y, Xia X.: The Development Trend of Graphene Derivatives, Journal of Electronic Materials 51, pp. 4107-4114 (2022)

[17] Jiang L, Fu W, Birdja Y, Koper M.T.M, Schneider GF.: Quantum and electrochemical interplays in hydrogenated graphene, Nat Commun 9, pp. 793 (2018)

[18] Carpenter J, Kim H, Suarez J, van der Zande A, Miljkovic N.: The Surface Energy of Hydrogenated and Fluorinated Graphene, ACS Appl. Mater. Interfaces 15, pp. 2429-2436 (2023)

[19] Worku A.K, Ayele D.W.: Recent advances of graphene-based materials for emerging technologies, Results in Chemistry 5, pp. 100971 (2023)

[20] Dietrich F, Guevara U.J, Tiutiunnyk A, Laroze D, Cisternas E.: Vacancies and Stone-Wales defects in twisted bilayer graphene - A comparative theoretical study, FlatChem 41, pp. 100541 (2023) [21] Xiang H. J, Kan E.J., Su-Huai Wei X, Gong G, Whangbo M.H.: "Thermodynamically stable single-side hydrogenated graphene", Phys. Rev. B 82, pp. 165425 (2010)

[22] Tiwari S.K, Pandey S.K, Pandey R, Wang Bystrzejewski NM, Mishra YK, Zhu Y.: Stone-Wales Defect in Graphene, Small 19, pp. 2303340 (2023)

[23] Whitener K.E.: Review Article: Hydrogenated graphene: A user's guide, J. Vac. Sci. Technol. A 36, pp. 1-15 (2018)

[24] Sofo J.O., Chaud[hari A.S, Barber G.D.: Graphane: a two-dimensional hydrocarbon, Phys. Rev. B 75, pp. 153401 (2007)

[25] Peaker C.V.: First principles study of point defects in diamond (2018)

[26] Dreyer C.E, Alkauskas A, Lyons J.L, Janotti A, Van de Walle C.G.: First-Principles Calculations of Point Defects for Quantum Technologies, Annu. Rev. Mater. Res., pp. 2.1-2.26 (2018)

[27] Zhou C, Chen S, Lou J, Wang J, Yang Q, Liu C, Huang D.: Graphene's cousin: the present and future of graphane, Nanoscale Research Letters 9, pp. 1-9 (2014)

[28] Yang C.K.: Graphane with defect or transition-metal impurity, Carbon 48, pp. 3901-3905 (2010)

[29] Wang Y, Ding Y, Shi S, Tang W.: Electronic structures of graphane sheets with foreign atom substitutions, American Institute of Physics 98, pp. 163104 (2011)

[30] Sluiter M.H.F, Kawazoe Y.: Cluster expansion method for adsorption: Application to hydrogen chemisorption on graphene, Phys. Rev. B 68, pp. 085410 (2003)

[31] Samarakoon D.K, Qian Wang X.: Structural and Electronic Properties of Hydrogenated Graphene, Physics and Applications of Graphene - Theory. InTech (2011)

[32] He C, Sun L.Z, Zhang C.X, Jiao N, Zhang K.W, Zhong J.: Structure, stability and electronic properties of tricycle type graphane, Research Letters 6, pp. 1-5 (2012)

[33] Chaoyu H, Sun L.Z, Zhang C.X, Jiao N, Zhang K.W, J. Zhong J.: Structure, stability and electronic properties of tricycle type graphane (2012)

[34] Carbonell-Coronado C, de Soto F, Cazorla C, Boronat J, Gordillo M.C.: H2 Physisorbed on Graphane, J Low Temp Phys 171, pp. 619-625 (2013)

[35] Reshak A.H, Auluck S.: Electronic and optical properties of chair-like and boat-like graphane, The Royal Society of Chemistry 4, pp. 37411-37418 (2014)

[36] Pujari B.S, Kanhere D.G.: Density functional investigations of defect induced mid-gap state in graphane, J Phys. Chem 113, pp. 21063-21067 (2009)

[37] Dicko M, Seydou M, Lamari F.D, Langlois P, Maurel F, Levesque D.: Hydrogen adsorption on graphane: An estimate using ab-initio interaction, International journal of hydrogen energy 42, pp. 10057 (2017)

[38] Podlivaev A.I, Openov L.A.: Elementary Defects in Graphane, Condensed Matter 106, pp. 110-115 (2017)

[39] Haldar S, Sanyal B.: Defects in Graphene and its Derivatives. InTech (2016)

[40] Kristoffel N, Rago K.: On the interband pairing in doped graphane, Physics Letters A 106, pp. 1003.5083v1 (2011)

[41] Sahin H, Leenaerts O, Singh S.K, Peeters F.M.: Graphane", WIREs Computational Molecular Science 5, pp. 255-272 (2015)

[42] Pumera M, Wong C.H.: Graphane and hydrogenated graphene, Chem. Soc. Rev. 42, pp. 5987-5995 (2013)

[43] Sahin H, Leenaerts O, Singh S.K, Peeters F.M.: GraphAne: From Synthesis to Applications, Condensed Matter Material Science, pp. 1-14 (2015)

[44] Lebegue S, Klintenberg M, Eriksson O, Katsnelson M.I.: Accurate electronic band gap of pure and functionalized graphane from GW calculations, Phys. Rev. 79, pp. 245117 (2009)

[45] Ilyin A.M, Nemkaeva R.R, Guseinov N.R, Tsyganov I.A, Beall G.W.: Computer Simulations and Experimental Study of Graphane-Like Materials Produced by Electrolytic Hydrogenation, NSTI- Nanotech, pp. 726-728 (2012)

[46] Giannozzi P, Baroni S, Bonini N, Calandra M, Car R, Cavazzoni C, Ceresoli D, Chiarotti G.L, Cococcioni M, Dabo I, Dal Corso A, Fabris S, Fratesi G, Gebauer R, Gerstmann U, Gougoussis C, Kokalji A, Lazzeri M, Martin-Samos L, Marzari N, Mauri F, Mazzarello R, Paolini S, Pasquarello A, Paulatto L, Sbraccia C, Scandolo S, Sclauzero G, Seitsonen A.P, Smogunov A, Umari P, Wentzcovitch R.M.: QUANTUM ESPRESSO: a modular and open-source software project for quantum simulations of materials, J. Phys. Condens. Matter 21, pp. 395502 (2009)

[47] Kohn W, Sham L.J.: Self-Consistent Equations Including Exchange and Correlation Effects, Phys. Rev. 140, pp. A1133-A1138 (1965)

[48] Perdew J.P, Burke K, Ernzerhorf M.: Generalized gradient approximation made simple, Phys. Rev. Lett. 77, pp. 3865 (1996)

[49] Heyd J, Scuseria G.E, Ernzerhorf M.: Hybrid Functionals Based on a Screened Coulomb Potential, The Journal of Chemical Physics 118, pp. 8207 (2003)

[50] Koch W, Holthausen M.C.: A Chemist's Guide to Density Functional Theory (E. J. Baerends, ed.). WILEY-VCH (2000)

[51] Monkhorst H.J, Pack J.D.: Special point for Brillouin-zone integrations., Rev. B 13, pp. 5188 (1976)

[52] Methfessel M, Paxton A.T.: High-precision sampling for Brillouin-zone integration in metals, Phys. Rev. B 40, pp. 3616 (1989)

[53] Gordienko A.B, Filippov S.I.: A modified version of the Methfessel-Paxton Method, Russian Physics Journal 52, pp. 668-673 (2009)

[54] Freysoldt C, Grabowski B, Hickel T, Neugebauer J, Kresse G, Janotti A, Van de Walle C.G.: First-principles calculations for point defects in solids, Reviews of Modern Physics 86, pp. 253-305 (2014)

[55] Thomas D.M, Asiri Y, Drummond N.D.: Point defect formation energies in graphene from diffusion quantum Monte Carlo and density functional theory, Phys. Rev. B 105, pp. 184114 (2022)

[56] Cherati N.G, Thiering G.A, Gali A.: Investigation of oxygen-vacancy complexes in diamond by means of ab-initio calculations, Journal of Physics: Condensed Matter 35, pp. 315502 (2023)

[57] Mapasha R.E, Molepo M.P, Chetty N.: Ab initio studies of isolated hydrogen vacancies in graphane, Physica E 79, pp. 52-58 (2015)

[58] Zhang S.B, Northrup J.E.: Chemical potential dependence of defect formation energies in GaAs: Application to Ga self-diffusion, Phys. Rev. Lett. 67, pp. 2339-2342 (1991)

[59] Van de Walle C.G, Laks D.B, Neumark G.F, Pantelides S.T.: First-principles calculations of solubilities and doping limits: Li, Na and N in ZnSe, Phys. Rev. B 47, pp. 9425-9434 (1993

[60] Payne M.C, Teter M.P, Allan D.C, Arias T.A, Joannopoulos J.D.: Iterative minimization techniques for ab initio total-energy calculations: molecular dynamics and conjugate gradients, Reviews of Modern Physics 64, pp. 1045-1097 (1992)

[61] Naik M.H, Jain M.: CoFFEE: Corrections For Formation Energy and Eigenvalues for charged defect simulations, Elsivier 226, pp. 114-126 (2018)

[62] Yu P.Y, Cardona M.: Fundamentals of Semiconductors: Physics and Materials Properties, Springer (1996)

[63] Rossi Fernandez A.C, Castellani N.J.: Dipole moment effects in dopamine N-doped-graphene systems, Surface Science, pp. 121546 (2020)

[64] H. Mapingire H, Mapasha R.E.: First principles characterization of nitrogen substitutional point defects in graphane (CH) (SAIP) (2023)

[65] Mapingire H, Mapasha R.E.: Thermodynamic stability and formation energies of hydrogen and carbon vacancy centres in hydrogenated graphene (SAIP) (2023)

[66] Watkins G. D.: Negative –U Properties for Defects in Solids, Mat. Science. Forum, vol 143-147, pp 1009-1014 (1994)

Chapter 7

Results and Discussion:

Published paper 4

This chapter is one of our contributions that was published in nanoenergy advances, as Refilwe Edwin Mapasha, Sentserere Phodisho Kgalema, Hezekia Mapingire and Emmanuel Igumbor. The article title is **"Lithium on CH Divacancy Self-Healed Graphane: AFirst-Principles Study."** In this contribution, we utilized density functional theory calculations to do an indepth study of the energetic stability as well as structural and electronic properties of Li on a graphane monolayer that has various CH divacancy configurations. This study is important in terms of the use of graphane as an electrode material.

Li on a CH divacancy self-healed graphane: A first - principles study

R. E. Mapasha[a,1,*], S. P. Kgalema[a], H. Mapingire[a], E. Igumbor[b]

[a]*Department of Physics, University of Pretoria, Hatfield campus, Pretoria 0002, RSA*
[b]*Department of Mechanical Engineering Science, University of Johannesburg, Johannesburg, South Africa*

Abstract

The possibility of using graphane monolayer crystals as the electrode material is becoming popular. Graphane is stable at room temperature and has large surface area, but its chemical inertness hinders its direct interactions with Li ions. In this study, we performed density functional theory calculations to study the energetic stability, structural and electronic properties of Li on graphane with various CH divacancy configurations (v_{12}, v_{13} and v_{14}). The results show that adsorption of Li atom reduces the formation energy of the CH divacancy configurations. The Li-v_{12} is most stable with the highest binding energy of 3.25 eV/Li and relaxes to in-plane with other C atoms. Altering the Li charge state to have Li^{-1}-v_{12} or Li^{+1}-v_{12} affects the energetic stability and electronic characters of Li-v_{12}. The Li^{-1}-v_{12} (Li^{+1}-v_{12}) enhances (reduces) the binding force between Li and v_{12} configuration, and furthermore it improves (deteriorates) the conductivity of the structure. Further investigation of graphane with vacancies is encouraged due to these intriguing observations, as it holds promise for potential utilization as an electrode material.

Keywords: Graphane; divacancy; lithiation; density functional theory, charge doping, conductivity

*Corresponding author
Email address: edwin.mapasha@up.ac.za (R. E. Mapasha)

1. Introduction

Lithium-ion batteries (LIBs) have been widely used as power sources for most of electronic devices[1]. The LIBs are known to be non-toxic, have long discharging rate, have high energy density etc[1, 2, 3]. The most used electrode in LIBs is graphite [1]. Nevertheless, many properties, such as the specific capacity, are unlikely to meet the increasing future demand for high energy. The search for alternative electrode materials with distinct properties from graphite is rapidly intensifying [4, 5, 6]. The two-dimensional (2D) materials are emerging as promising candidates to address future energy demands due to their high electrical conductivity, reduced dimensionality, high thermodynamic stability, large surface area etc., distinguishing them from their bulk counterpart [7, 8, 9]. These properties make 2D materials well suited to accommodate a greater number of Li atoms, among other advantages.

Graphane [10] monolayer material falls under materials belonging to the graphene derivatives were each carbon is bonded to hydrogen atom in an alternating pattern. The realization of graphane was first reported by Sluiter et al. [11], based on the density functional theory (DFT). Graphane was later synthesized [12, 13] by applying hydrogen plasma to graphene monolayer samples. The graphane samples were found to be stable at room temperatures [12]. Each carbon atom's bonding network takes on the form of sp^3 hybridization due to the presence of hydrogen atoms [13].

Experimental studies report that graphane has insulating characters [12]. This was supported by the theoretical studies which predicted the energy band gap of 3.50 eV (standard DFT) [10], 5.40 eV (GW)[14], 4.21 eV (HSE06)[15]. Graphane has a large surface area, high volumetric capacity, non-toxic samples [13, 16, 17]. These indicators suggest that a graphane monolayer could find utility in a range of technological application. The focus of this work is on the mechanisms of enchoring the Li ions on the graphane monolayer for electrode exploitation. Theoretically, an inertness [13, 16, 17] (under ambient conditions) of C atoms conjugating graphane monolayer due to the sp^3 bonding network could physisorb instead of chermisorbing Li ions, which will be a setback for encoring Li atoms. Watcharinyanon et al.[18] studied intercalation of Li ions on graphane using experimental techniques. They reported that instead of bonding with the substrate Li atoms form islands among themselves. The DFT studies by Yang et al.[19] revealed that Li ions are screened by H atoms, as such no chemisorption takes place.

The modification of graphane monolayer for possibility of enhancing Li interaction is necessary. Several methods are known for introducing reactive sites on graphane, potentially enhancing its interaction with Li ions.

These methods include structural modification like creating vacancies, doping, strain application, among others [13, 16, 17, 20]. Creation of vacancies in graphane can primarily be in different forms: hydrogen (H) vacancy, carbon (C) vacancy, carbon-hydrogen (CH) vacancy.The creation of multiple vacancies is also possible in graphane monolayer. H divacancy, trivacancy and CH divacancy, trivacancy have been created in graphane monolayer. These vacancies can be created by applying high or low ions bombardment, and they can also occur during synthetic processes [13, 16, 17, 20]. Numerous properties of these mentioned vacancies have been examined, ranging from their energetic stabilities to their magnetic properties [13, 16, 17, 20, 21, 22, 23, 24]. With the exception of the divacancy structure, all other types of vacancies introduce mid-gap states within the band gap and exhibit magnetic properties.

The structural and electronic behavior of CH divacancies in graphane have been studied using DFT [24]. The structural reconstruction of the two adjacent vacancies has been reported, which break the hexagonal symmetry and translates into the new 5-8-5 defect structure that is thermodynamically stable. Graphane with 5-8-5 defect structure is characterized as a wide band gap material [24]. Considering the potential of utilizing graphane with this defect structure as an electrode holds merit. Notably, the adsorption of Li ions onto the graphane with 5-8-5 defect structure remains unexplored. A comprehensive understanding of how Li anchors at different charge states on graphane is imperative. This helps to understand the energetic and electronic behavior of Li during charging and discharging. This study intends to understand the energetic stabilities (formation energy and binding energy), structural properties (bondlength) and electronic properties (density of states) of Li on the graphane with 5-8-5 defect structure at different Li charge states (+1 or -1). This study relies on a spin-polarized density functional theory approach, and the outcomes will serve as a reference for the experimentalists to corroborate their findings during practical synthesis and characterization processes.

This manuscript is arranged as follows: the computational details and equations for calculating formation and binding energies are presented in section 2. The results of Li on graphane monolayer with vacancies are summarized in section 3. Section 4 concludes the results.

2. Computational details

All the spin polarized calculations in this study have been performed using hybrid density functional theory (DFT) approach implemented within the Vienna *ab initio* simulation package (VASP) code [25]. The chosen hy-

brid exchange correlation functional is the Heyd, Scuseria, and Ernzerhof (HSE06) [26], which the PBE functional is mixed with the non-local Fock. The Fock mixing parameter used is 0.25 which it is known to give the correct band gap of 2D materials. In this study it was selected with the intention of enhancing the magnitude of the band gap and providing a more accurate description of the positions of electronic states induced by defects within the band gap. For the description of pseudopotentials, the projector augmented wave (PAW) methods [27] with C atoms represented as $2s^2 2p^2$, H atoms represented by $1s^1$ and Li adatom represented as $2s^1$ valence electrons.

The kinetic energy cut-off of 500 eV was used for the expansion of the plane wavefunctions. For sampling the Brillouin zone of graphane monolayer, the 6×6×1 k-mesh grid was used, employing the Monkhorst-Pack scheme [28] method. This k-mesh grid is doubled during the density of states calculations. The atomic positions were allowed to relaxe until their residual forces are less than 0.01 eVÅ^{-1} utilizing the Hellman-Feynman theorem. The total energies of the structures were allowed to converge to within 10^{-7} eV during the self-consistent field calculations of each relaxation. The 9×9 supercell of graphane was used for all our calculations. This supercell size was chosen to ensure that the divacancy interaction between the cell images along the x and y direction is minimal. The separation spacing between the layers was set to the converged 20 Å , to avoid unwanted interactions due to periodic images.

To study the energetic stability of Li on a graphane with various CH divacancy configurations (v_{12}, v_{13} and v_{14}), their formation energies were calculated employing the Zhang-Northrup expression [29] below:

$$E_f(CH) = E_{tot}(CH) - E_{tot}(G) - \sum_i n_i \mu_i, \tag{1}$$

where $E_{tot}(CH)$ is the total energy of Li on a CH divacancy configuration in a 6×6 graphane supercell and $E_{tot}(G)$ is the total energy of 6×6 pristine graphane. The μ_i in equation 1 represents the chemical potential of H, C and Li atoms calculated as the total energies per atom of isolated hydrogen molecules in a large box, graphene and Li in bulk body centered cube (BCC), respectively. n_i represents the number of atomic species (H, C and Li atoms) removed or adsorbed on the graphane monolayer system.

To assess the interactions between the Li adatoms and various configurations of CH divacancies in graphane monolayer, we calculated the binding energies as follows:

$$E_b = \frac{E_{tot}(CHLi) - E_{tot}(CH) - n_{Li} E_{tot}(Li)}{n_{Li}}, \tag{2}$$

where $E(CHLi)$ is the total energy of Li adatom on a CH divacancy in a 6×6 graphane supercell, $E(CH)$ is the total energy of 6×6 graphane with divacancy and $E(Li)$ is the total energy per adatom of Li in a bulk body centered cube (BCC).

3. Results and discussion

3.1. Proposed structures studied.

Firstly, we demonstrate how different CH pair divacancy configurations are identified on an isolated single hexagon in a graphane monolayer. A single hexagon in a graphane monolayer is shown in Fig. 1 circled with purple. The numbers 1-6, position around an isolated single hexagon, serve as labels for the CH pairs that should be removed during the vacancies creation in this study. These numbers 1-6 are also used to name different vacancy configurations. In this paper, we report a systematic study of different CH pair divacancy configurations presented in Fig. 1.

Three distinct configurations are identified as follows: (1) v_{12} configuration, this configuration consist of a CH divacancy where two CH pairs are adjacent to each other. It is denoted as v_{12} configuration, meaning that two adjacent CH pairs are removed from positions 1 and 2 of the single hexagon, as illustrated in Fig. 1. (2) v_{13} divacancy configuration, in this configuration there are two CH pairs vacancies at positions 1 and 3, with which CH pair at position 2 separate them. (3) v_{14} configuration, this configuration represents the two CH pair vacancies at positions 1 and 4, facing each other, and separated by the two CH adjacent pairs. These configurations describe different arrangements of CH pair vacancies within the hexagonal structure.

3.2. Thermodynamic stability and structural properties of different CH vacancy configurations

As a common practice in first-principles work, the relative stabilities of various vacancy defects configurations in the host materials are evaluated through the formation energy analysis. In this study, we conduct a comparative analysis of energetic stability of previously mentioned distinct divacancy configurations, namely v_{12}, v_{13} and v_{14}. This comparison is based on their calculated formation energies ($E_{Form}(v)$), as illustrated in Fig. 2 and indicated by the red circles. All calculations are computed at the same level of accuracy. As shown in Fig. 2(a), divacancy configuration v_{12} has the lowest formation energy of 2.71 eV/v_{CH}. This value is 2.21 eV/v_{CH} and 2.00 eV/v_{CH} lower than those of v_{13} and v_{14}, respectively. Perhaps this could be the reason the previous study [24] only report properties of v_{12} divacancy

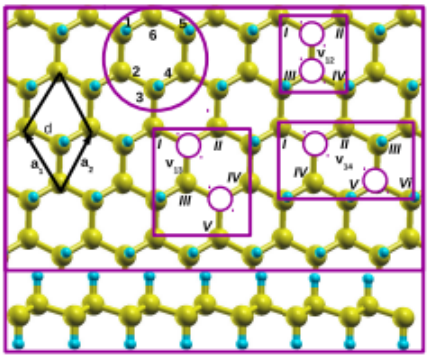

Figure 1: Top panel present top view of the ball-and-stick model of graphane structure, while bottom panel present side views of graphane structure. Different CH pair divacancy configurations v_{12}, v_{13} and v_{14} positions are shown. The white and purple circles hide the numerically labeled CH pair vacancies that are created. The rectangular shapes that enclose vacancy configurations primarily connect the carbon atoms through their potential dangling bonds before undergoing structural relaxation. These carbon atoms are labeled with the roman numbers. The black rhombus shape represents the primitive unit cell of graphane structure, consisting of two C and two H atoms. The vectors $\mathbf{a}_1$ and $\mathbf{a}_2$ correspond to its Bravais lattice vectors. The C and H atoms are represented by the yellow and light blue spheres respectively.

configuration. As is often observed in many material studies, we have observed that the thermodynamic stability of the v_{12}, v_{13} and v_{14} configurations is significantly influenced by the structural reconstruction and the behavior of dangling bonds around the vacancy within a graphane layered structure, after relaxation.

In v_{12} configuration (seen in Fig. 2(c)), the pair dangling C atoms I and II as well as the C atoms III and IV attract each other 'to a certain extent' forming a weak bondlength of $d_{I,II} = d_{III,IV} = 1.99$ Å after geometry optimization. This structural reconstruction or self-healing forms a 'peculiar' vacancy defect type of 5-8-5 divacancy structure as shown in Fig. 2(c), is in good agreement with the results of Ref [24]. Such type of defect has experimentally been realized in graphene, the mother of graphane, using the high-energy ion beams creating a stable carbon chain [30]. Fig 2(b) shows that v_{12} lacks a magnetic moment, indicating that structural reconstruction of the dangling C atoms suppresses any potential magnetic moment in agreement with Ref [24].

In a v_{13} divacancy configuration, a C atom III having possibly two unpaid electrons (based on electronic counting) relaxes towards another two C atoms II and IV. The equivalent bond distances $d_{III,II}$ and $d_{III,IV}$ of 2.42 Å are formed between C atoms III and II as well as between C atoms III and

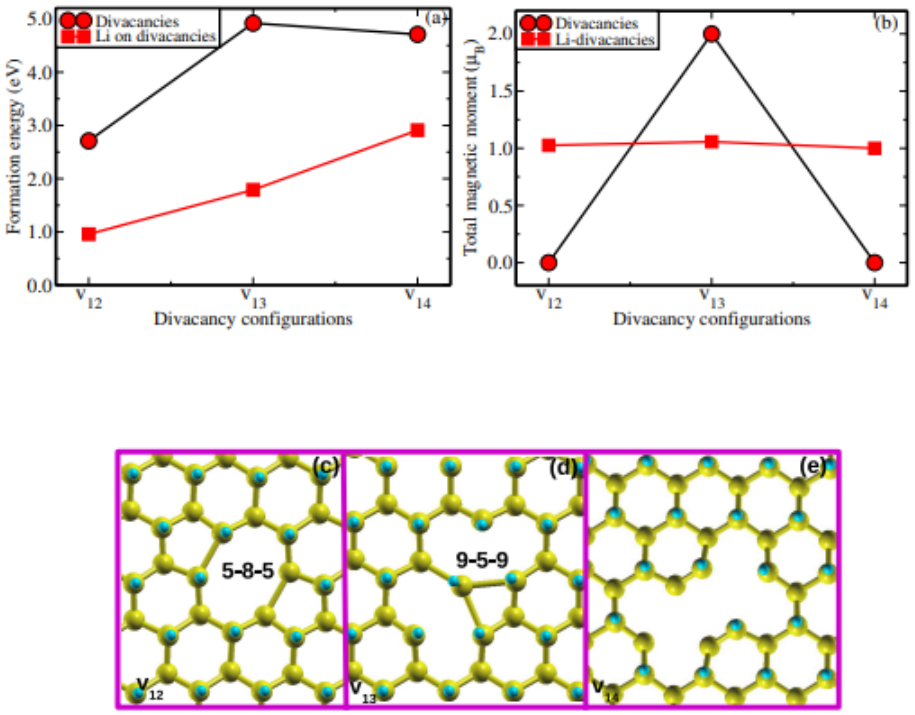

Figure 2: (a) The formation energies of different CH divacancy configurations (v_{12}, v_{13} and v_{14}) are indicated by the circle spheres while those of a Li atom on the different CH divacancy configurations (Li-v_{12}, Li-v_{13} and Li-v_{14}) are represented by the square shapes.(b) The total magnetic moments arising from the v_{12}, v_{13} and v_{14} configurations are indicated by the circle spheres while those influenced by a Li atom adsorption on the different CH divacancy configurations (Li-v_{12}, Li-v_{13} and Li-v_{14}) are represented by the square shapes. (c-e) The relaxed structures of different CH divacancy configurations (v_{12}, v_{13} and v_{14}) created in a 9×9 supercell. Each divacancy configuration reconstructs to form a peculiar type of a topology defect.

IV, respectively. This reconstruction of v_{13} divacancy configuration yields an unusual defect structure of 9-4-9 type (see Fig. 2(d)). It is possible that the construction of 9-4-9 defect structure does not saturates all the dangling bonds surrounding the vacancy, hence the magnetic moment of 1 μ_B has been achieved (Fig. 2(b)). This could be attributed to the C atoms *I* and *III* each still having an unpaired electron after structural relaxation. Fig. 2(e) presents the relaxed geometry of a v_{14} divacancy configuration. The C atoms I, II, III, IV, V and VI are unable to rearrange to form any typical vacancy defect. Based on electron counting, v_{14} remains with six unpaired electrons (one electron on each C atom I, II, III, IV, V and VI) after structural relaxation. The absent of total magnetic moment in this system (Fig. 2(b)) could be the result of the cancellation of opposite electronic spins.

3.3. Effect of Li on the energetic stability and structural properties of different CH vacancy configurations

We now examine the effects of Li atom on the energetic stabilities, structural and electronic properties of v_{12}, v_{13} and v_{14} configurations. Initially, we adsorbed Li atom on the biggest hollow site of each vacancy configuration, i.e v_{12} (octagon site), v_{13} (nanogon site) and v_{14}(largest site). Fig. 2(a) shows the effect of Li atom on the energetic stability of v_{12}, v_{13} and v_{14} configurations. It is noted that the Li atom energetically stabilizes the v_{12}, v_{13} and v_{14} configurations through reduction of their formation energies. The formation energy of Li-v_{12} configuration, which is 0.96 eV, suggests that although it is endothermic (requiring an input of energy), it can be relatively easily synthesized compared to the Li-v_{13} and Li-v_{14} configurations.

Figs 3(a), (b) and (c) present the relaxed structures of Li atom on the different CH divacancy configurations Li-v_{12}, Li-v_{13} and Li-v_{14}, respectively. In these configurations, the Li atom relaxes closer to the hollow site, which has an impact on the local vacancy structures. Fig 3(a) shows that in the case of Li-v_{12}, Li atom remains within the octagon hollow site leading to a height of 0.00 Å (insertion to remain in-plane with other C atoms). Consequently, this results in an increase in the bond distances $d_{III,II}$ and $d_{III,IV}$ to 2.63 Å equivalently. This has led to the high amount of the binding force (greater enchoring) between Li and the substrate with a binding energy of 3.25 eV. The Li-v_{12} interactions induced a magnetic moment of 1.00 μ_B as shown in Fig 2(b). Figs 3(b) shows that Li-v_{13} buckled up after relaxation, hence this leads to a height of 0.62 Å with a binding energy of 2.07 eV. Fig 2(b) shows that Li adsorption on a v_{13} reduces the magnetic moment from 2.00 μ_B to 1.00 μ_B. In this configuration, the vacancy defect structure of 9-4-9 reconstructs to create a penta ring and v_{CH} (closest to each other) separated by a newly formed bondlength $d_{III,II}$ of 1.72 Å. The latter value

is less than that of its counterpart in 5-8-5 defect without a Li atom. In the Li-v_{14} configuration, the Li atom relaxes to a height of 1.54 Å with a binding energy of 1.99 eV. Notably, there is no significant reconstruction observed in this configuration, as depicted in Figs 3(c).

The binding energies for Li-v_{12}, Li-v_{13} and Li-v_{14} configurations, respectively, are relatively larger than that of Li on pristine graphene (1.04) eV [31] and on a single vacancy (v_{CH}) in graphane [15], calculated on the same level of accuracy. The binding energies between Li and v_{12}, v_{13} and v_{14} configurations are more than the Li bulk cohesive energy (1.63 eV), suggesting no chances of Li clusters formation but possible short time Li charging.

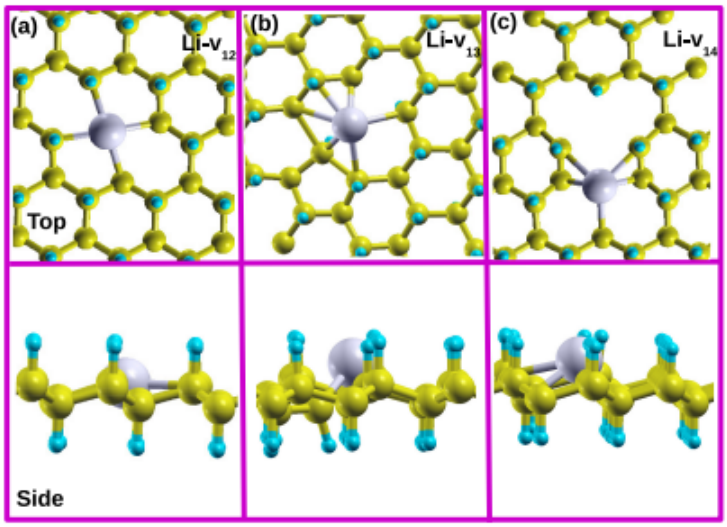

Figure 3: The relaxed structures of Li atom on the different CH divacancy configurations (a) Li-v_{12}, (b) Li-v_{13} and (c) Li-v_{14} created in a 9×9 supercell. In some configurations, Li atom enforces divacancy configuration reconstruction.

3.4. Influence of different charge states (-1, and +1) on the energetic stability, structural and electronic properties of Li-v_{12}

In this section, we examined the effects of Li charge state alteration on the energetics, local structure around the v_{12} vacancy and electronic properties (DOS) and make camprison with those of the uncharged structure. The charge states considered on Li-v_{12} are q = -1 and +1 of which their respective structures are denoted as Li^{-1}-v_{12} and Li^{+1}-v_{12}. The binding energies for Li^{-1}-v_{12} and Li^{+1}-v_{12} structures are 3.21 eV and 2.24 eV respectively. In

Table 1: Comparing the binding energies E_b (in eV) and distances between Li atom and graphane d_{Li} (in Å) for Li-v_{12}, Li-v_{13} and Li-v_{14} configurations with that of Li on graphene (Li-*graphene*).

Configurations	E_B	d_{Li}	Vacancy reconstruction
Li-v_{12}	3.25	0.00	5-8-5 changes to divacancy symmetry
Li-v_{13}	2.07	0.62	9-4-9 translates to penta ring and v_{CH}
Li-v_{14}	1.99	1.14	None
Li-v_{CH}	1.72^a	1.54^a	None
Li-*graphene*	1.10^b, 1.29^c	1.71^b 1.69^c	None

[a]Ref[15],[b]Ref[31] and [c]Ref[32]

comparison with the uncharged binding energy shown in Table 1, the charge doping reduces the binding force between the Li atom and v_{12} substrate, significantly in configuration Li^{+1}-v_{12}.

In the case of an addition of electron (Li^{-1}-v_{12}), a Li atom remains within the octagon hollow site, maintaining the same in-plane level with other C atoms leading to a height of 0.00 Å as shown in fig 4(a). Fig 4(a) shows that the bond distances $d_{III,II}$ and $d_{III,IV}$ increases slightly by 0.03 Å as compared to uncharged Li-v_{12} (Fig 4(b)), which is an indication that an addition of electron in to the system (Li^{-1}-v_{12}) increases the repulsion force between the C atoms surrounding the Li atom. For the removal of electron (Li^{+1}-v_{12}), Li atoms moves slightly upward to a height of 0.51 Å. Fig 4(b) shows that the bond distances $d_{III,II}$ and $d_{III,IV}$ decreases significantly by 0.25 Å as compared to uncharged Li-v_{12} (see Fig 4(b)). This is an indication that the removal of electron from the system (Li^{+1}-v_{12}) enhances the attraction force between the C atoms surrounding the Li atom.

Fig. 5 presents the density of states (DOS) for the most stable Li-v_{12} configuration, comparing with that of without Li counterpart (v_{12}). Fig. 5 (a) (top panel) shows that v_{12} has the insulating features with a wide band gap of 4.18 eV (HSE06) between the valence band maximum (VBM) and conduction band minimum (CBM). The VBM and CBM are mainly contributed by the carbon p orbital states as shown on Fig. 5 (a) (bottom panel). This is in agreement with Pujari *et al.*[24] reporting that the carbon atoms surrounding the divacancy rearrange to form two new σ bonds leading to the formation of 5-8-5 ringed structure with a band gap of 3.00 eV (GGA). Fig. 5 (b) (top panel) shows the effects of Li atoms on the DOS of v_{12}. It is noted that Li atom shifts the Fermi level from the VBM towards the middle of the band gap (suggesting an excess of electrons in the system). It also introduces the occupied and unoccupied states at distinct positions with some crossing the Fermi level in a spin up channel, suggesting metallic character. The

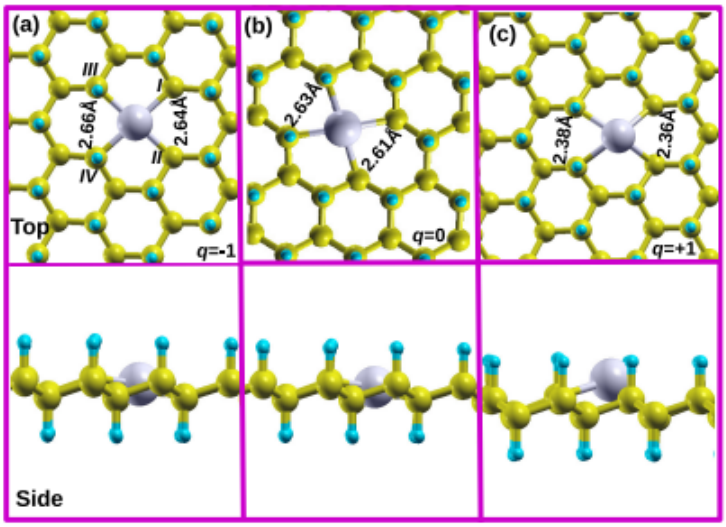

Figure 4: The relaxed structures of Li-v_{12} at different charge states; (a) Li^{-1}-v_{12}, (b) Li^{0}-v_{12} and Li^{+1}-v_{12}.

observed states are due to hybridization of carbon p orbital and Li s orbital states (Fig. 5 (b) (bottom panel)). An addition of electron into the system (Li^{-1}-v_{12}) shifts the Fermi level further towards the CBM Fig. 5 (c). It is interesting to realize that the partially filled mid gap states as shown in Fig. 5 (b) becomes fully occupied in Fig. 5 (c). The removal of electron from the system (Li^{+1}-v_{12}) shifts the Fermi level back towards the VBM (Fig. 5 (d)). Retaining the metallic character of the system with the partially filled states crossing the Fermi level. Alteration of charge states of Li atom changes the electronic behavior of Li-v_{12} structure. We propose that graphane with Li-v_{12} may serve as a suitable electrode material for LIBs. This suitability arises from the potential enhancement of electronic transmission performance mechanisms facilitated by the newly identified Li states.

4. Conclusions

The adsorption mechanisms of Li on graphane with various CH divacancy (v_{12}, v_{13} and v_{14}) configurations have been studied using DFT approach. Firstly, we compared the energetic stability (formation energies) and structural aspects (bond lengths) for v_{12}, v_{13} and v_{14} configurations. Employing structural optimization calculations, it was established that there is a vacancy reconstruction leading to a new defect configuration surrounded by

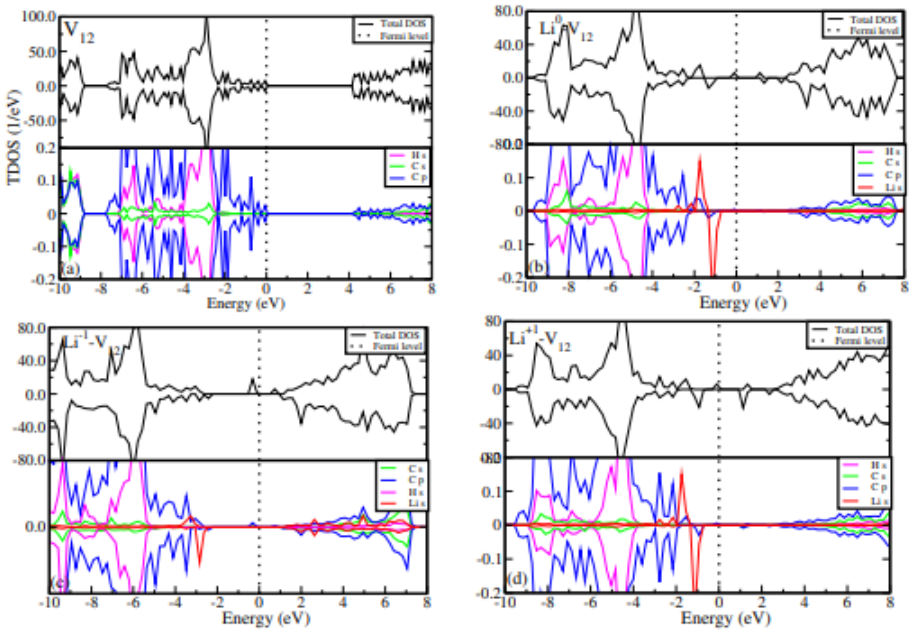

Figure 5: The calculated density of states for (a) v_{12}, (b) Li-v_{12}, (c) Li^{-1}-v_{12} and (d) Li^{+1}-v_{12}. For each sub figure, the top panel represents total density of states, while the bottom panel represents the partial density of states. The Fermi level is set to 0.00 eV and marked by the vertical dashed line.

the hexagonal rings in graphane. The v_{12} translated to 5-8-5 defect configuration and is the most stable CH divacancy configuration. Furthermore, we adsorbed Li on v_{12}, v_{13} and v_{14} configurations. The formation energy annalys revealed that Li tends to stabilizes these CH vacancies, with Li-v_{12} being most stable and Li atom relaxes to the same in-plane level with C atoms on the octagon ring. Li interacts strongly with v_{12} at a highest binding energy of 3.25 eV/Li, more than the Li bulk cohesive energy of 1.63 eV/Li. The charge doping Li^{-1}-v_{12} or Li^{+1}-v_{12} alters the energetic stability, structural properties and electronic characters of Li-v_{12}. The Li^{-1}-v_{12} configuration has more binding energy that Li^{+1}-v_{12} configuration. The electronic density of states plot for Li^{-1}-v_{12} reveals an abundance of electrons and increase in conductivity. These interesting observation encourages further studies on designing graphane with vacancies and its characterization for LIBs.

Acknowledgment

The authors acknowledge the University of Pretoria for financial support and availability of computational resources. We express gratitude to the National Institute for Theoretical and Computational Sciences (NITheCS) for funding. Center for high performance computing (CHPC) in cape town is acknowledged for state-of-the-art resources.

References

[1] J.M. Tarascon, M. Armand, *Nature* **414** 359 (2001).

[2] N. Oyama, T. Tatsuma, T. Sato, T. Sotomura, *Nature* **374** 196 (1995).

[3] D.P. Dubal, O. Ayyad, V. Ruiz, P. Gómezromero, *Chem. Soc. Rev.* **44** 1777 (2015).

[4] H. Wang, L.F. Cui, Y. Yang, C.H. Sanchez, J.T. Robinson, *J. Am. Chem. Soc.* **132** 13978 (2010).

[5] F. Zou, X. Hu, Z. Li, Q. Long, C. Hu, *Adv. Mater.* **26** 6622 (2014).

[6] X. Sun, W. Si, X. Liu, J. Deng, L. Xi, *Nano Energy* **9** 168 (2014).

[7] K-S. Chen, I. Balla, N. S. Luu, and M. C. Hersam. Emerging opportunities for two- dimensional materials in lithium-ion batteries.*ACS Energy Letters*, **2** (9):2026-2034, (2017). doi: 10.1021/ acsenergylett.7b00476. URL https://doi.org/10.1021/acsenergylett.7b00476.

[8] L. Peng, Y. Zhu, D. Chen, R. S. Ruoff, and G. Yu. Two-dimensional materials for beyond- lithium-ion batteries. *Adv. Energ Mater.*, *6* (11):1600025, (2016). doi: https://doi.org/10.1002/aenm. 201600025. URL https://onlinelibrary.wiley.com/doi/abs/10.1002/aenm.201600025.

[9] H. Li, Y. Shi, M-H. Chiu, and L-J. Li. Emerging energy applications of two-dimensional layered transition metal dichalcogenides. //doi.org/10.1016/j.nanoen.2015.10.023. *Nano Energy*, **18** :293-305, (2015). ISSN 2211-2855. doi: https: URL https://www.sciencedirect.com/science/article/pii/S2211285515004024.

[10] J. O. Sofo, A. S. Chaudhari, and G. D. Barber, *Phys. Rev. B* **75**, 153401 (2007).

[11] M.H.F. Sluiter, Y. Kawazoe, Cluster expansion method for adsorption: application to hydrogen chemisorption on graphene.[?]hys Rev B **68** 085410 (2003).

[12] D. C. Elias, R. R. Nair, T. M. G. Mohiuddin, S. V. Morozov, P. Blake, M. P. Halsall. A. C. Ferrari, D. W Boukhvalov, M. I. Katsnelson, A. K. Geim, and K. S. Novoselov, *Science* **323**, 610 (2009).

[13] C. Zhou, S. Chen, J. Lou, J. Wang, Q. Yang, C. Liu, D. Huang and T. Zhu, *Nanoscale Research Letters 9*, 26 (2014).

[14] S. Lebègue, M. Klintenberg, O. Eriksson, M. I. Katsnelson., *Phys Rev B* **79** (24), 245117, 1-5 (2009).

[15] R.E. Mapasha, M.P. Molepo, N. Chetty, *RSC Adv.* **7**, 63, 39748-39757 (2017).

[16] H. Sahin, O. Leenaerts, S. K. Singh, and F. M. Peeters, *Wires Comput. Mol. Sci.* **5**, 255 (2015).

[17] E. Keith, Jr. Whitener, *J. Vac. Sci. Technol. A* **36**, 05G401 (2018), https://doi.org/10.1116/1.5034433

[18] S. Watcharinyanon, C. Virojanadara, J. Osiecki, A. Zakharov, R. Yakimova, R. Uhrberg, and L. Johansson. Hydrogen interca-lation of graphene grown on 6h-sic(0001), *Surf. Scie.*, **605**:1662-1668, 09 (2011). doi: 10.1016/j.susc.2010.12.018.

[19] Y.E. Yang, Y. Xiao, and X.H. Yan. Charge distribution of lithium-doped graphane/graphene hybrid system: Role of nearly-free electronic states. *Sol. Stat. Commun.*, **229**:43-48, (2016). ISSN 0038-1098. doi: https://doi.org/10.1016/j.ssc.2015.12.011. URL https://www. sciencedirect.com/science/article/pii/S0038109815004366.

[20] Sahin H, Ataca C, Ciraci S. Electronic and magnetic properties of graphane nanoribbons. *Phys Rev B*, **81**:205417 (2010).

[21] H. Sahin, C. Ataca, and S. Ciraci, Magnetization of graphane by dehydrogenation. *Appl. Phys. Lett.* **95**, 222510 (2009).

[22] J. Berashevich, and T. Chakraborty, Sustained ferromagnetism induced by H-vacancies in graphane. *Nanotechnology* **21**: 355201 (2010).

[23] R E Mapasha, M P Molepo and N Chetty, *Phys. E.* **79**, 52-58 (2016).

[24] B. S. Pujari and D.G. Kanhere, *J. Phys. Chem. C* **113**, 21063 (2009).

[25] G. Kresse and J. Hafner, *Phys. Rev. B* **47**, 558 (1993).

[26] J. Heyd, G. E. Scuseria, and M. Ernzerhof, *J. Chem. Phys.* **118**, 8207 (2003); **124**, 219906 (2006).

[27] P. E. Blochl, *Phys. Rev. B* **50**, 17953 (1994).

[28] H. J. Monkhorst and J. D. Pack 1976, *Phys. Rev. B* **13**, 5188.

[29] S. B. Zhang and J. E. Northrup, *Phys. Rev. Lett.* **67**, 2339 (1991.)

[30] Jin C, Lan H, Peng L, Suenaga K, Iijima S. Phys Rev Lett, **102** 205501 (2009).

[31] K.T. Chan, J.B. Neaton, M.L. Cohen, Phys. Rev. 77 (2008) 235430.

[32] A. M. Garay-Tapia, A. H. Romero, V. Barone, J. Chem. Theory Comput. 8, 3, 1064-1071,(2012)

Chapter 8

Further Discussion and Conclusion

8.1 Formation energy

For the neutral, negative and positive charge states of V_H, the derived formation energy is generally low. V_H^0 formation phenomenon produced a formation energy of 2.64 eV for all the Fermi level positions we considered. The addition of an electron to form V_H^{-1}, slightly increased the formation energy to 3.14 eV. The difference between the formation energies of V_H^0 and V_H^{-1} is 0.5 eV. The withdrawal of an electron to give rise to V_H^{+1}, resulted in the formation energy increasing to 3.98 eV. These values of formation energy are in good agreement with the values derived by Mapasha et al [95]. The notable difference in formation energies between the neutral (V_H^0) and the positively charged state of the hydrogen vacancy (V_H^{+1}) is 1.34 eV. The phenomena of defect formation for all the three configurations (V_H^0, $V_H^{-1}$and V_H^{+1}) are endothermic, hence all the processes are non-spontaneous (require activation energy). The formation energy is dependent on the charge state of the defect, with the negative charge state / positive charge state being lower in energy at fermi levels close to the conduction/valance band, compared to the neutral charge state.

For the three Fermi-level positions, we considered (0 eV, -3.5 eV and 3.5 eV), the formation energy of a carbon vacancy in graphane ranged from a minimum value of 10.26 eV to a maximum value of 17.48 eV. It is therefore energetically expensive to form a carbon vacancy in the two-dimensional material-graphane. The formation energy of V_C^0 was 12.57 eV but after the addition of an electron to the system to form V_C^{-1}, the formation energy increased to 13.76 eV when the Fermi-level was fixed at 0 eV. The withdrawal of an electron to form V_C^{+1} also resulted in an increase in the formation energy to a value of 13.98 eV. There is a difference of 1.41 eV when compared with the formation energy of V_C^0.

The formation energy of the carbon-hydrogen vacancy ranged from 10.36 eV for V_{CH}^0 to a value of 18.28 eV for V_{CH}^{-1}. When the Fermi-level position was pinned at -3.5 eV, the formation energy was 10.36 eV for V_{CH}^{+}, but yielded a maximum value of 18.28 eV for the negatively charged defect, V_{CH}^{-1}. The formation energies of V_{CH}, fluctuated between 11.28 eV and 17.36 eV when the Fermi-level was positioned at 3.5 eV (close to the conduction band).

For the neutral and positive charge states of N_H, the formation energy is low. N_H^0 formation phenomenon produced a formation energy of 2.74 eV for all the Fermi level positions under consideration. The withdrawal of an electron to form N_H^{+1}, slightly decreased the formation energy to 2.37 eV. The slight difference in formation energies between N_H^0 and N_H^{+1} is 0.37 eV. The phenomena of defect formation for all the these point defect configurations ($N_H^0$and N_H^{+1}) are endothermic. Therefore these processes require activation energy to happen.

The formation energy of N_C^q in graphane ranged from a minimum value of 5.66 eV to a peak value of 8.91 eV. The formation energy of N_C^0 was 8.91 eV but after the addition of an electron to the system to form N_C^{-1}, the formation energy decreased to 8.64 eV. The withdrawal of an electron to form N_C^{+1} resulted in a further decrease in the formation energy to a value of 5.66 eV.

The formation energy of N_{CH} substitutional point defect ranged from 6.88 eV for

N_{CH}^{+} to a value of 7.23 eV for N_{CH}^{0}. This point defect in the positive charge state (N_{CH}^{+}), yielded the lowest formation energy value of 6.88 eV while the maximum value of 7.23 eV was produced by this point defect in the neutral charge (N_{CH}^{0}). This point defect in the negative charge state yielded a formation energy of 7.20 eV.

For the nitrogen-vacancy complexes, the formation energy of $N_C V_H$ varied from 7.18 eV to a maximum value of 14.28 eV for the three charge states under consideration as shown by figure 8.1. For $N_{CH}V_H$, we derived formation energy values that ranged between 5.96 eV and 13.93 eV. The other two defect complexes, $N_C V_{CH}$ and $N_{CH}V_{CH}$, yielded high formation energies that fluctuated from 16.23 eV to 25.14 eV for the Fermi-level positions we considered. The high formation energies of these point defect complexes emanate from the combination of the isolated constituent point defects (N_C, N_{CH}, V_C and V_{CH}). A combination of N_C, N_{CH}, V_C and V_{CH} resulted in the formation of complexes of high formation energies because the original isolated point defects are generally energetically expensive to form. Even though the formation energies are high, the nitrogen-vacancy complexes in graphane still form.

For the three charge states under consideration (-1,0 and +1), $N_{CH}V_{CH}$ formation process gave rise to the highest values of formation energies. The formation energy of $N_C V_{CH}$ is also high but but a little bit lower than that of $N_{CH}V_{CH}$. Relative to these two, $N_C V_H$ and $N_{CH}V_H$ have formation energies that are also slightly lower, as depicted by figure 8.1.

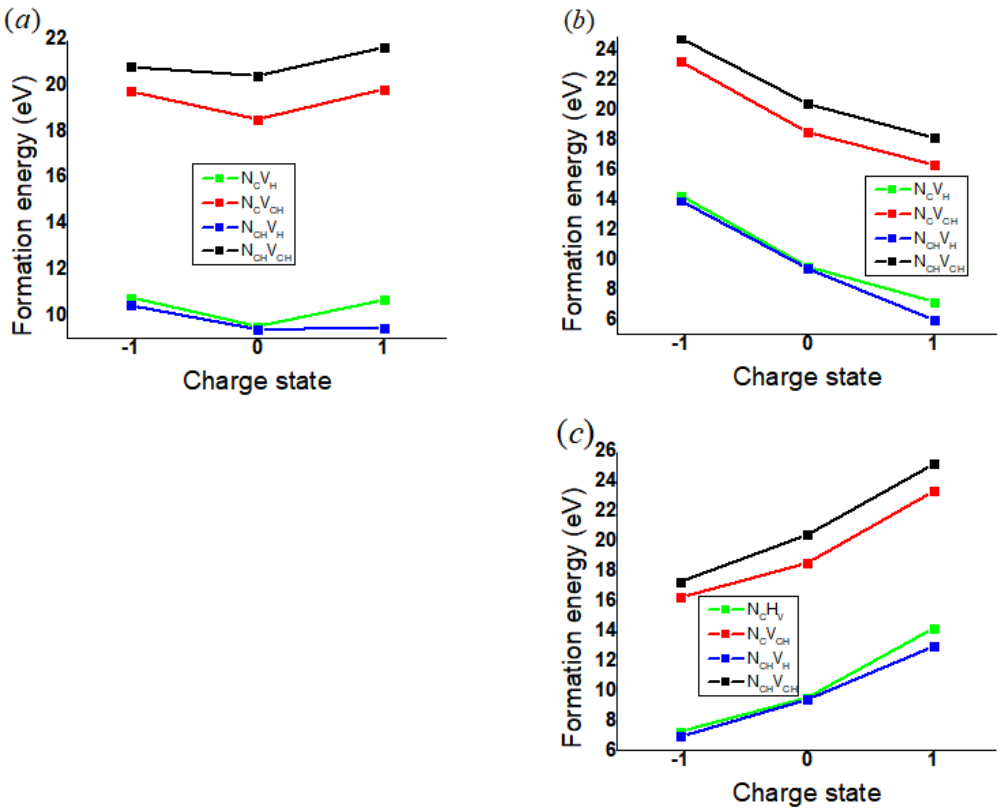

Figure 8.1: Formation energy for the point defect complexes of the type: N_CV_H, N_CV_{CH}, $N_{CH}V_H$ and $N_{CH}V_{CH}$ in the graphane two-dimensional material when the Fermi-level is (a) 0 eV (b) -3.5 eV and (c) 3.5 eV.

The calculated formation energies of the various nitrogen-vacancy complexes in graphane are generally higher than the formation energies of nitrogen-vacancy complexes in diamond. This, however, does not inihibit the fabrication of practical graphane based devices because these defects have notable stability. Moreover, the derived formation energies give material science engineers, critical insight into the relationship that exists between nitrogen dopant (N_C or N_{CH}) adsorption and vacancy creation (V_C or V_{CH}). The calculation of the formation energies has enabled exploration of the structural stability of graphane chair conformer . Furthermore, the comprehension of the nitrogen-vacancy complexes' formation energies is of critical importance in terms of the tailoring of graphane's electronic properties. This aspect is very important for targeted applications in the nano-technology field. In addition, the derived formation

energies provide material engineers with the information that graphane material is relatively stable in the presence of nitrogen-vacancy complexes. We therefore expect this two-dimensional material to have consistent and reliable operating performance over a given duration of time, when applied in nanotechnology.

8.2 U-parameter

The U-parameter or Hubbard correction is a fundamental concept that represents the difference in energy between two successive thermodynamic energy transition levels. This important parameter is used to derive information that relates to the activation energy which is required when a point defect or defect complex undergoes transition from an initial charge state to another.

The hydrogen vacancy yielded a positive U-parameter value of 1.84 eV. The significance of this value is that it gives us information that the acceptor level (-1/0) has a higher value of energy in comparison with the donor level (0/+1). We can thus deduce that the hydrogen vacancy in the neutral state (V_H^0) is stable and it allows the formation of both V_H^{-1} and V_H^{+1} without any traits of instability.

For the carbon vacancy we deduced a U-parameter value of 2.60 eV. This positive value also shows that the donor level energy value (0/+1) is lower when compared with the energy value of the acceptor level (-1/0). We can also thus put it forward that the thermodynamic transition states for V_C point defect are not inverted. This point defect is therefore stable and allows the formation of the singly positive and singly negative charged states. The U-parameter value for V_C (2.60 eV) is considerably high as compared to the U-parameter for V_H (1.84 eV). The migration energy for V_C is thus significantly larger than that of V_H. It is easier for V_H to transition from one energy level to another as compared to V_C. Just like V_H and V_C, our U-parameter value for V_{CH} is positive (+1.14 eV) showing that this point defect is also stable and permits the formation of both the singly positive and singly negative charged states. It is relatively easy for V_{CH} to undergo transition from one state to another, therefore this defect can

diffuse through graphane easily as compared to its two counterparts- V_H and V_C.

N_C yielded a positive U-parameter value of 0.14 eV. The importance of this value is that it shows that the acceptor level for N_C (-1/0) has a bigger value of energy relative to the donor level (0/+1). We can thus put it forward that N_C^0 is stable and it permits the formation of both N_C^{-1} and N_C^{+1} without notable instability. For N_{CH} we determined a U-parameter value of 3.72 eV. Just like N_C, the donor level energy value for N_{CH} (0/+1), is lower in comparison with the energy value of the acceptor level (-1/0). We can also thus predict that the thermodynamic transition states for N_{CH} point defect are also not inverted. Thus, N_{CH} point defect is relatively stable and permits the formation of the singly negative and singly positive charged states. The U-parameter value for N_{CH} (3.72 eV) is bigger relative to the U-parameter value for N_C (0.14 eV). We put it forward that the energy of migration for N_{CH} is considerably larger than that of N_C. It is therefore easier for N_C to undergo transition from one energy state to another as compared to N_{CH}.

The nitrogen-vacancy point defect complexes yielded positive values of U-parameter. We got the lowest U-parameter value of 1.09 eV for $N_{CH}V_H$. In contrast, N_CV_{CH} yielded the highest U-parameter value of 2.52 eV. From these values, we can deduce that it is easier for $N_{CH}V_H$ to transition from an initial charge state to another as compared to N_CV_{CH}. This is because a smaller activation energy is needed when $N_{CH}V_H$ transitions from a given charge state to another in comparison to N_CV_{CH}. N_CV_H and $N_{CH}V_{CH}$ gave rise to U-parameter values of 2.40 eV and 1.61 eV taken in that order. We thus propose that, it is a little bit easier for $N_{CH}V_{CH}$ to go through a charge state change as compared to its counterpart, N_CV_H. The derived positive U-parameter values of the four groups of the point defect complexes also give an indication of how stable the point defect systems are. We can deduce that, these point defect complexes depicted notable degree of stability, because they allowed the formation of negative and positive charge states. We thus put it forward that, the acceptor energy levels of these point defect complexes, $(0/-)$, produced higher energy values compared to the energy values of the

donor levels, (+/0). We can thus deduce that the thermodynamic transition states of N_CV_H, N_CV_{CH}, $N_{CH}V_H$ and $N_{CH}V_{CH}$ are not inverted.

8.3 Charge transition levels

Charge transition levels are of extreme importance because they have a bearing on the electrical and optical properties of a material. The charge transition levels show the energy level at which a point defect is likely to change its charge state. At these energy levels, the point defect can either emit or capture an electron. The transition energy levels are calculated relative to the valence band maximum ($E_F = 0$ eV). The calculated charge transition levels for the hydrogen vacancy, V_H, are respectively -1.34 eV and 0.5 eV. The negative charge transition state shows that V_H becomes more stable by way of trapping an electron. Conversely, the positive charge transition level shows that this point defect becomes more stable by way of releasing an electron. The charge transition levels for the carbon vacancy, V_C, are -1.41 eV and 1.19 eV for $\varepsilon(+1 \mid 0)$ and $\varepsilon(0 \mid -1)$ respectively. For, V_{CH}, the values we calculated are -0.11 eV and 1.03 eV for $\varepsilon(+1 \mid 0)$ and $\varepsilon(0 \mid -1)$ respectively.

The calculated charge transition level for N_H, is -2.31 eV. The negative value shows that N_H is more stable when it traps an electron. In contrast, a positive charge transition level shows that a point defect under consideration becomes more stable if it releases an electron. The charge transition states for, N_C, are 1.04 eV and 1.18 eV for $\varepsilon(+1 \mid 0)$ and $\varepsilon(0 \mid -1)$ taken in that order. The derived charge transition states for, N_{CH}, are -2.34 eV and 1.34 eV for $\varepsilon(+1 \mid 0)$ and $\varepsilon(0 \mid -1)$ respectively. We also put it forward that, the $\varepsilon(+1 \mid 0)$ transition occurs within the valence band (i.e below the valence band maximum) for all the various vacancy defect complexes considered in this study. The implication of these is that such transitions will not be observed experimentally, since they do not occur within the band gap.

N_CV_H, yielded transition level values of -1.15 eV and 1.25 eV respectively for $\varepsilon(+1/0)$ and $\varepsilon(0/-1)$. N_CV_{CH} produced charge transition energy states values of -1.31 eV and

1.21 eV for $\varepsilon(+1/0)$ and $\varepsilon(0/-1)$, respectively. $N_{CH}V_H$ produced transition level states of -0.06 eV [$\varepsilon(+1/0)$] and 1.03 eV [$\varepsilon(0/-1)$]. We propose that this point defect complex is able to easily transform from one charge state to another relative to N_CV_H and N_CV_{CH}. We calculated charge transition energy level values of -1.23 eV [$\varepsilon(+1/0)$] and 0.38 eV [$\varepsilon(0/-1)$], for $N_{CH}V_{CH}$.

8.4 Density of states

The presence of vacancies, V_H, V_C and V_{CH} in graphane seems to induce defect states within the band gap. Some defect states are not clearly distinct as they seem to be intertwined with the bulk majority states. The bulk states for these point defects:V_H^0, V_H^{-1}, V_C^{+1} and V_{CH}^{+1}, show symmetric traits. Conversely, point defect configurations such as V_H^{+1}, V_C^{-1}, V_{CH}^0 and V_{CH}^{-1}, depict non-symmetric traits of the bulk majority energy states. These point defects push the Fermi-level to the conduction or valence band edge except for V_H^0 and V_C^{+1} whereby the Fermi level is positioned deep in the middle of the band gap. One notable outcome of the presence vacancy point defects in graphane is the inducing of distinct spin-up (spin-down) polarised defect states showing that these point defects are electrically active. Some of these defect energy levels are donor states while others are acceptor states. Some states are unoccupied while others are either partially or completely occupied. These findings are in line with the report by Mapasha et al [27].

Nitrogen substitutional point defects in graphane do not seem to induce magnetism in the graphane monolayer. The bulk majority states are perfecly aligned to the minority states for all the point defects we considered except for N_H^{-1} that seems to show partial variation for some energy states. The point defects generally pushes the Fermi level to the valence (conduction) band edges. Nitrogen substitutional point defects in graphane seems to fine-tune the size of the band gap. These point defects also seem to induce states in the band gap, but some defect states are not clearly distinct since they are intertwined with the bulk states. The defect states are more pronounced for

the configurations: N_C^{+1}, N_H^{-1} and N_H^{+1}.

The density of states for the four groups of point defect complexes we considered (N_CV_H, N_CV_{CH}, $N_{CH}V_H$ and $N_{CH}V_{CH}$), showed that the minority spin-down states are symmetric to the majority spin-up energy states. We thus propose that these point defects as well as their charge states (neutral, negative and positive) do not depict magnetic traits in graphane. Generally, these point defect complexes induce energy states in the middle of the band gap. The induced band gap values ranged from 2.57 eV ($N_{CH}V_{CH}^{-1}$) to a peak value of 3.41 eV ($N_{CH}V_{CH}^{+1}$) for GGA method. HSE method produced energy gap values ranging from a value of 3.22 eV ($N_{CH}V_{CH}^{-1}$) to a maximum value of 3.89 eV ($N_CV_H^{+1}$).

8.5 Charge distribution for nitrogen-vacancy complexes

All the point defect complexes (N_CV_H, N_CV_{CH}, $N_{CH}V_H$ and $N_{CH}V_{CH}$) depicted polar traits. They have regions of high and low electron density as shown by figure 8.2. We can thus propose that these point defect complexes show a low degree of symmetry which is caused by regions that have non-uniform electron density. Our considered point defect systems have sides that are partially negative and other sides which are slightly positive. Generally these point defects in graphane give rise to net dipole moments and there is a presence of anisotropic characteristics for the point defect complexes: N_CV_H, N_CV_{CH}, $N_{CH}V_H$ and $N_{CH}V_{CH}$. We noted a considerable increase in the charge distribution in the vicinity of the nitrogen dopant. We attributed this observation to the fact that the nitrogen atom introduced additional electrons into the system, forming localized regions that have varying electron density as depicted by figure 8.2.

8.6 Nitrogen-vacancy complexes binding energy

For easier illustration, we plotted a graph of binding energy versus point defect complex as shown by 8.3 (a). The four groups of point defect complexes, N_CV_H, N_CV_{CH}, $N_{CH}V_H$

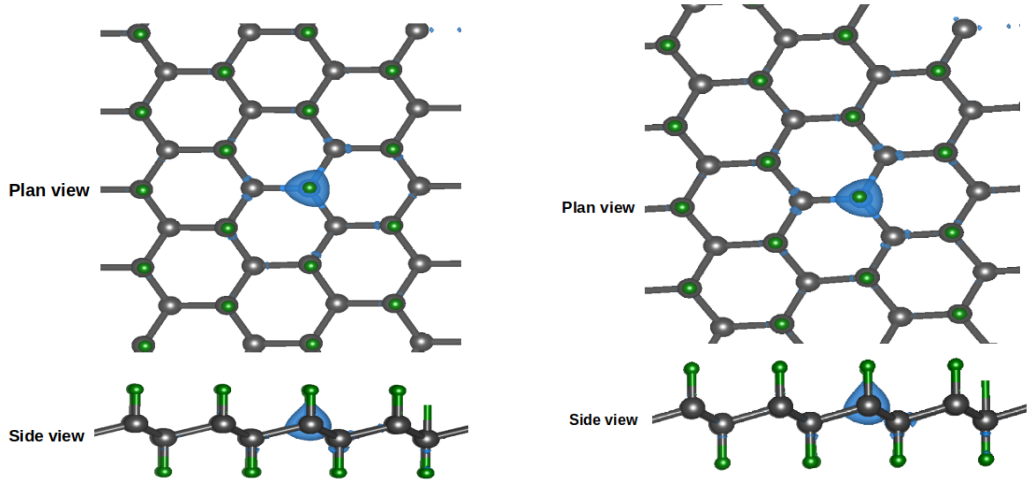

Figure 8.2: Charge distribution in the nitrogen dopant-vacancy defect complexes in graphane: (a) $N_C V_H^0$ and (b) $N_C V_H^{+1}$. The grey and green spheres respectively represent carbon and hydrogen atoms. The dark blue non-uniform spheres shows the charge distribution which is more pronounced around the light blue nitrogen dopant atoms.

and $N_{CH}V_{CH}$ are represented by the letters A, B, C and D respectively as depicted by both 8.3 (a) and (b). We denoted the neutral, negative and positive charge of each point defect configuration by the numbers 1, 2 and 3 respectively. All the complexes we considered yielded binding energy values ranging from 0.47 eV for $N_{CH}V_H^0$ to a maximum value of 5.14 eV for $N_C V_{CH}^{-1}$. The binding energy values of 1.17 eV ($N_C V_H^{+1}$), 1.90 eV ($N_C V_{CH}^{+1}$), 0.47 eV ($N_{CH}V_H^0$), 1.30 eV ($N_{CH}V_H^{-1}$), 0.57 eV ($N_{CH}V_{CH}^0$), and 1.81 eV ($N_{CH}V_{CH}^{+1}$) generally show the presence of weak interactions that exist between the constituents of the point defect complexes under considerations (shown in brackets). The second group of binding energy values of 2.02 eV ($N_C V_H^0$), 2.45 eV ($N_C V_H^{-1}$) and 2.58 eV ($N_{CH}V_{CH}^{-1}$), depict moderate strength of interaction relative to the former. The third group of binding energy values of 4.14 eV ($N_C V_{CH}^0$), 4.11 eV ($N_{CH}V_H^{+1}$) and 5.14 eV ($N_C V_{CH}^{-1}$) for the configurations shown in brackets shows the existence of relatively strong bonds between the parent components. These point defect defect complexes ($N_C V_{CH}^0$, $N_{CH}V_H^{+1}$and $N_C V_{CH}^{-1}$) are considerably stable and are unlikely to decompose into their isolated components without the presence of external perturbations. Positive

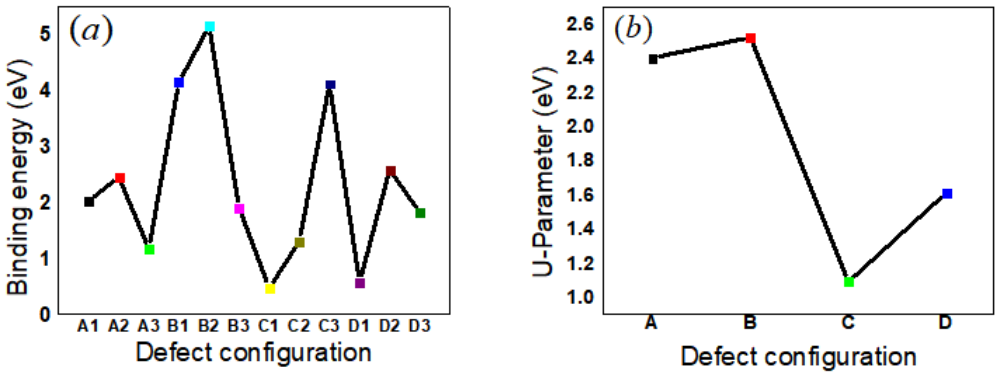

Figure 8.3: Binding energy and U-parameter values for nitrogen-vacancy complexes in graphane

binding energy values depicts that more energy is required to separate the components relative to the energy that is needed during the process of complex formation. The processes of separation of the point defect complexes into their isolated constituencies are non-spontaneous.

We observed that for the point defect configurations, $N_C V_H$ and $N_C V_{CH}$, an extra electron increased the binding energy as depicted by figure 8.3 (a). In contrast, the withdrawal of a single electron from both $N_C V_H$ and $N_C V_{CH}$, considerably decreases the binding energy. However, for $N_{CH} V_H$, an extra electron put into the configuration, increases the binding energy slightly, while the removal of one electron increases the binding energy as depicted by figure 8.3 (a). For the point defect complex, $N_{CH} V_{CH}$, both the addition and withdrawal of an electron increases the binding energy when compared to that of the neutral system.

In the sub-section that follow, we briefly explore the Li-doped divacancies in graphane.

8.7 Li-doped divacancies in graphane

Our results depict that, the adsorption of the Li dopant atoms decreases the formation energy of the carbon-hydrogen divacancy configurations. The most stable configuration is the Li-v12. The calculated binding energy of this configuration is 3.25 eV/Li and it relaxes to in-plane with other carbon atoms. The adjustment of the Li charge state to

Li−1-v12 or alternatively to Li+1-v12 distorts the energetic stability of these configurations. We noted that, the Li−1-v12 structure, decreases the binding force between the Li and v12 configuration to a lesser extent. Conversely, Li+1-v12 structure, considerably decreases the binding force between Li and v12. Moreover, the conductivity of the graphane material is also distorted by the adsorption of Li dopant atoms. As a result of these intriguing observations, we believe that graphane with Li-doped divacancies has the potential for utilization as an electrode material.

8.8 Summary

With the help of first-principles computations we characterised hydrogen and carbon vacancies of the type V_H, V_C and V_{CH} in the graphane two-dimensional material. These three types of vacancy point defects gave rise to relatively high positive formation energies in a monolayer of hydrogenated graphene. The direct implication of our finding is that the hydrogen and carbon vacancies require activation energy in order to form. The hydrogen vacancy,V_H, yielded lower formation energies relative to both V_C and V_{CH}. V_H is therefore most likely to form relative to V_C and V_{CH}. One of our findings is that hydrogen and carbon vacancies in a monolayer of graphane distort the electronic structure of this material because of the formation of defect energy states between the bandgap. We therefore propose that these point defects may find utilization in bandgap engineering. We also put it forward that V_H, V_C and V_{CH} point defects in graphane alter the chemical and electronic properties of this material, raising the likelihood of using them in the field of nano-technology.

Moreover, we also found out that, V_H, V_C and V_{CH} point defects in hydrogenated graphene are subject to the Jahn-Teller distortions. These point defects reduce their symmetry from C_{3v} to C_s giving rise to the loss of the three-fold rotation axis. The symmetry breaking is brought about by the change in the structural and electronic configuration of the point defect-modified graphane. The Jahn-teller distortion (electronic reconfiguration) cause this spontaneous symmetry breaking. The distortion happens as

a result of orbital degeneracy (double or triple degeneracy) or alternatively symmetry protected degeneracy. This degeneracy is lifted by the Jahn-Teller distortion, giving rise to symmetry-lowering effect, (C_{3v} to C_s) that changes the degenerate energy states into non-degenerate energy states. The pseudo Jahn-Teller effect, happens in a system whereby the non-degenerate energy states undergoes some kind of structural distortion because of the coupling of the system's electronic states. First-order coupling of the electronic energy states results in the Jahn-Teller effect, while second-order coupling of energy states give rise to the pseudo Jahn-Teller effect.

V_H, V_C and V_{CH} yielded positive U-parameter values. We can thus conclude that these point defects in graphane allow the formation of their respective charged states without any traits of instability. One result of this finding is that we can conclude that, the acceptor levels $(0/-)$ of V_H, V_C and V_{CH} point defects have higher values of energy relative to the donor levels $(+/0)$.

We also used first principles calculations to study nitrogen substitutional dopants, N_H, N_C and N_{CH} in graphane. These point defects yielded positive formation energies. In order for these defects to form in graphane, they need activation energy. We also propose that, N_H, N_C and N_{CH} substitutional point defects are subject to the Jahn-Teller effect. N_H, N_C and N_{CH} embedded in graphane monolayer fine-tuned band gap and induced donor (acceptor) energy states. We therefore propose that nitrogen substitutional point defects in graphane can be exploited for a variety of targeted applications, which among others include nano-electronic and band gap engineering. N_C and N_{CH} yielded positive U-parameter values. We can thus deduce that nitrogen substitutional point defects in a single layer of graphane show stability and generally permits formation of positive and negative charged states. We put it forward that the thermodynamic transition states of N_H, N_C and N_{CH} are not inverted and hence these defects are relatively stable.

In the last part of this research project, we employed quantum espresso first principles calculations to systematically investigate the energetic stabilities and apt electronic

properties of nitrogen dopant-vacancy complexes in graphane (hydrogenated graphene). We extensively investigated nitrogen-vacancy complexes of the type, $N_C V_H$, $N_C V_{CH}$, $N_{CH} V_H$ and $N_{CH} V_{CH}$ in the graphane two-dimensional material. Analysis of the formation energies shows that $N_C V_H$ and $N_{CH} V_H$ complexes require smaller values of energy to form relative to $N_C V_{CH}$ and $N_{CH} V_{CH}$. The calculated binding energies for the four groups of the nitrogen-vacancy complexes show that, these complexes are stable relative to the isolated point defects that forms them. Analysis of the U-parameter values derived, depicts that, it is easy for $N_{CH} V_H$ complex to change from one charge state to another relative to $N_C V_{CH}$. The nitrogen-vacancy complexes in graphane induce acceptor and donor states between the band gap.

Table 8.8 shows a comparison of the electronic properties of $N_{CH} V_H^{-1}$ in graphane and NV^- in diamond. The depicted properties show that N-V complexes in graphane may have similar or slightly altered applications in comparison to the N-V center in diamond. This contribution has provided possibilities of using nitrogen-vacancy complexes in graphane for nano-technology tailored applications. Among others, the potential applications are: band gap engineering, quantum sensing, quantum imaging and opto-electronics. In band gap engineering, nitrogen-vacancy centers can be used to tune the band gap in such a way as to create two-dimensional materials that have tailored electronic properties. Band gap engineering, can enhance the fabrication of advanced nano-electronic devices like sensors and transistors. The use of nitrogen-vacancy centers in graphane, to make nano-scale sensors and nano-scale imaging devices is of paramount importance as far as the detection of temperature, electric fields and magnetic fields parameters is concerned. Nitrogen-vacancy centers in graphane can also find potential applications in the making of light emmitting diodes as well as nano-lasers that have novel optical properties.

Comparison of the electronic properties of $N_{CH}V_H^{-1}$ in graphane and NV^- in diamond

Property	$N_{CH}V_H^{-1}$ *in graphane*	NV^- *in diamond* [ref 10,11,12,47,51,52]
Formation energy (eV)	5.96	$2.40 - 4.50$
Energy gap(HSE) (eV)	3.29	5.50
Binding energy (eV)	1.30	$4.40 - 5.40^{\#\#theoretical}$ $4.90 - 5.50^{**experimental}$

8.9 Challenges

We have some challenges that are associated with the creation of N-V centers in graphane. Among others, the creation of nitrogen-vacancy centers in graphane is still a complex process and the operation of N-V point defects in graphane, may be affected by factors such as temperature and humidity. Moreover, mantaining defect stability can be a notable challenge in some nano-scale devices.

We also have some challenges and limitations that are associated with the Quantum Espresso computational approach we used in this study. For instance, one can have limitations in terms of: scalability, convergence testing, basis set choice, exchange-correlation functionals and pseudo-potential accuracy. Quantum Espresso may also require significant computational resources in order to run large simulations that require substantial storage and memory capacity. Therefore, this computational approach may be time-consuming as it requires accurate and carefull consideration of the parameters at play. The 144-atom supercell increased the computational cost because of the large number of atoms and electrons simulated. We used a 15-layer vacuum gap in order to reduce the artificial periodicity errors (defect-defect interaction) introduced by the supercell but it is not possible to totally eliminate the finite size effects. We also noted that the large supercell size may also affect the proper relaxation (optimization) of the supercell under consideration.

8.10 Future work

First principles study ofAl_CV_H and Si_CV_H and other related point defect complexes is worth pursuing. Intensive characterization of these point defect complexes in graphane is an area of interest for future studies since there is a possibility of their usefulness in band gap engineering and other nanotechnology applications.

Appendix A

CoFFEE corrections

In order to correct the artificial interaction between the point defects and their periodic images, we used the CoFFEE scheme (Corrections For Formation Energy and Eigenvalues for charged defect simulations). This scheme has the advantage of being able to be used alongside various density functional theory packages to get an *a posteriori* correction for the formation energy as well as the defect level position within a given band gap [96]. The utilization of the CoFFEE scheme commences from the derivation of the formation energy for a defect that has a charge state q. The determination of the formation energy is done using the equation 8.1

$$E_q^f[R_q](\epsilon_F) = \{E_q^{tot}[R_q] + E_q^{corr}\} - E_{pristine} + q\{\epsilon_{vbm}^{pristine} + \epsilon_F - \triangle V_{0/p}\} - n_x\mu_x \quad (8.1)$$

where ϵ_F is the Fermi level of the system under consideration. The Fermi level is given relative to the valence band maximum of the pristine structure;

$E_q^{tot}[R_q]$ represents the total energy of the system in which a defect of charge state q and position R_q is embedded;

$E_{pristine}$ is the total energy of the pristine supercell of equal magnitude;

n_x represents the number of atoms of type x, that have either been removed from the system (negative) or added to the system (positive);

μ_x denotes the chemical potential of the atom(s) under consideration and

E_q^{corr} represents the correction term of finite size.

The correction term, E_q^{corr}, is given by the equation 8.2

$$E_q^{corr} = E_q^{lat} - q\triangle V_{q-0/m} \tag{8.2}$$

where E_q^{lat} is derived from the calculation done using equation 8.3

$$E_q^{lat} = E_q^{iso,m} - E_q^{per,m} \tag{8.3}$$

and $q\triangle V_{q-0/m}$ is a term that represents potential alignment. This term is deduced by comparing the model potential to the difference in potential of DFT, i.e.

$$\triangle V_{q-0/m} = (V_q^{DFT} - V_0^{DFT})/_{far} - V_q^{per,m}/_{far} \tag{8.4}$$

where $\triangle V_{0/p}$ is a second potential alignment term, which is given by $\triangle V_{0/p} = V_0/_{far} - V_p$.

The computation of the correction term is done by the DFT code in conjuction with the CoFFEE code as hereby outlined [96]. The first step is the determination of the energy of the pristine supercell. We then derive the total energy of the supercell that has a neutral defect. The third step is the computation of the total energy of the supercell that contains the charged defect. These initial three steps are done using the DFT code.

Using the CoFFEE code, we calculate the E_q^{lat} term. The next stage is the determination of the model energy for different supercell sizes before extrapolating to derive $E_q^{iso,m}$. The term E_q^{lat}, will then be given by the equation 8.3

$$E_q^{lat} = E_q^{iso,m} - E_q^{per,m}(n \times n \times n)$$

whereby $(n \times n \times n)$ represents the supercell size. Lastly, the potential alignment terms, $\triangle V_{0/p}$ and $\triangle V_{q-0/m}$ are derived [96].

Bibliography

[1] C. He, L. Z. Sun, C. X. Zhang, N. Jiao, K. W. Zhang & J. Zhong, *"Structure, stability and electronic properties of tricycle type graphane"*, Research Letters **6**, 1 (2012)

[2] C. K. Yang, *"Graphane with defect or transition-metal impurity"*, Carbon **48**, 3901 (2010)

[3] K. E. Whitener, *"Review Article: Hydrogenated graphene: A user's guide"*, J. Vac. Sci. Technol. A **36**, 1 (2018)

[4] Y. Wang, Y. Ding, S. Shi & W. Tang, *"Electronic structures of graphane sheets with foreign atom substitutions"*, American Institute of Physics **98**, 163104 (2011)

[5] D. Sholl & J. A. Steckel, *"Density functional theory : a practical Introduction"*, John Wiley & Sons, Inc (2011)

[6] P. Rani & R. Bhandari, *"DFT Study of Defects in Graphene"*, in *"Proceedings of the "International Conference on Advanced Nanomaterials & Emerging Engineering Technologies" (ICANMEET-2013)"*

[7] J. R. Weber, W. F. Koehl, J. B. Varley, A. Janotti, B. B. Buckely, C. G. V. de Walle & D. D. Awschalom, *"Quantum computing with defects"*, Applied Physical Sciences **107**, 8513 (2010)

[8] A. Steane, *"Quantum computing"*, Rep. **61**, 117 (1998)

[9] N. academies of Sciences, *"Quantum Computing: Progress and Prospects"*, The national academic press (2019)

[10] B. K. Ridley, *"Quantum Processes in Semiconductors"*, Oxford University Press, New York (1988)

[11] R. Schirhagl, K. Chang, M. Loretz & C. L. Degen, *"Nitrogen-Vacancy Centers in Diamond: Nanoscale Sensors for Physics and Biology"*, Annu. Rev. Phys. Chem. **65**, 83 (2014)

[12] A. Gali, *"Ab initio theory of the nitrogen-vacancy center in diamond"*, Nanophotonics **8**, 1907 (2019)

[13] A. Gali, M. Fayta & E. Kaxiras, *"Ab initio supercell calculations on nitrogen-vacancy center in diamond: electronic structure and hyperfine tensors"*, Phys. Rev. B **77**, 155206 (2008)

[14] A. Lenef & S. C. Rand, *"Electronic structure of the N-V center in diamond: Theory"*, Phys. Rev. B **53**, 13441 (1996)

[15] C. E. Dreyer, A. Alkauskas, J. L. Lyons, A. janotti & C. G. V. de Walle, *"First-Principles Calculations of Point Defects for Quantum Technologies"*, Annu. Rev. Mater. Res. **48**, 2.1 (2018)

[16] C. Freysoldt, B. Grabowski, T. Hickel, J. Neugebauer, G. Kresse, A. Janotti & C. G. V. de Walle, *"First-principles calculations for point defects in solids"*, Reviews of Modern Physics **86**, 253 (2014)

[17] A. M. Ilyin, R. R. Nemkaeva, N. R. Guseinov, I. A. Tsyganov & G. W. Beall, *"Computer Simulations and Experimental Study of Graphane-Like Materials Produced by Electrolytic Hydrogenation"*, NSTI-Nanotech **1**, 726 (2012)

[18] N. G. Cherati, G. A. Thiering & A. Gali, *"Investigation of oxygen-vacancy complexes in diamond by means of ab-initio calculations"*, Journal of Physics: Condensed Matter **35**, 315502 (2023)

[19] K. S. Novoselov, A. K. Geim, S. V. Morozov, D. Jiang, Y. Zhang, S. V. Dubonos, I. V. Grigorieva & A. A. Firsov, *"Electric Field Effect In Atomically Thin Carbon Films"*, Science **35**, A. A. Firsov (2004)

[20] H. Sahin, O. Leenaerts, S. K. Singh & F. M. Peeters, *"GraphAne: From Synthesis to Applications"*, Condensed Matter Material Science **arXiv**, 1 (2015)

[21] A. K. Geim & K. S. Novoselov, *"The rise of graphene"*, Nature Mat. **6**, 183 (2007)

[22] A. K. Geim, *"Nobel Lecture: Random walk to graphene"*, Reviews of modern Physics **83**, 851 (2010)

[23] L. Sun, G. Yuan, L. Gao, J. Yang, M. Chhowalla, M. H. Gharahcheshmeh, K. K. Gleason, Y. S. Choi, B. H. Hong & Z. Liu, *"Chemical Vapour Deposition"*, Nature Reviews Methods **1**, 5 (2021)

[24] A. K. Worku & D. W. Ayele, *"Recent advances of graphene-based materials for emerging technologies"*, Results in Chemistry **5**, 100971 (2023)

[25] A. R. Urade, I. Lahiri & K. S. Suresh, *"Graphene Properties, Synthesis and Applications: A Review"*, JOM **75**, 614 (2023)

[26] D. K. Samarakoon & X. Q. Wang, *"Structural and Electronic Properties of Hydrogenated Graphene, Physics and Applications of Graphene - Theory"*, ", ed: S. Mikhailov, 113-132, InTech (2011)

[27] R. E. Mapasha, M. P. Molepo & N. Chetty, *"Ab initio studies of isolated hydrogen vacancies in graphane"*, Physica E **79**, 52 (2015)

[28] J. O. Sofo, A. S. Chaudhari & G. D. Barber, *"Graphane: a two-dimensional hydrocarbon"*, Phys. Rev. B **75**, 153401 (2007)

[29] M. H. F. Sluiter & Y. Kawazoe, *"Cluster expansion method for adsorption: Application to hydrogen chemisorption on graphene"*, Phys. Rev. B **68**, 085410 (2003)

[30] H. Sahin, O. Leenaerts, S. K. Singh & F. M. Peeters, *"Graphane"*, WIREs Computational Molecular Science **5**, 255 (2015)

[31] J. P. Perdew, K. Burke & M. Ernzerhorf, *"Generalized gradient approximation made simple"*, Phys. Rev. Lett. **77**, 3865 (1996)

[32] J. P. Perdew, *"Generalized gradient approximations for exchange and correlation : A look backward and forward"*, Physica B: Condensed Matter **172**, 1 (1991)

[33] M. Pumera & C. H. A. Wong, *"Graphane and hydrogenated graphene"*, Chem. Soc. Rev. **42**, 5987 (2013)

[34] A. H. Reshak & S. Auluck, *"Electronic and optical properties of chair-like and boat-like graphane"*, The Royal Society of Chemistry **4**, 37411 (2014)

[35] P. Blaha, K. Schwarz, G. K. H. Madsen, D. Kvasnicka, J. Luitz, R. Laskowsk, F. Tran, L. Marks & L. Marks, *"WIEN2k: An Augmented Plane Wave plus Local Orbitals Program for Calculating Crystal Properties"*, Techn. Universitat (2019)

[36] D. M. Ceperley & B. J. Alder, *"Ground state of the electron gas by a stochastic method"*, Phys. Rev. Lett. **45**, 566 (1980)

[37] P. Dufek, P. Blaha & K. Schwarz, *"Applications of Engel and Vosko's generalized gradient approximation in solids"*, Phys. Rev. B **50**, 7279 (1994)

[38] C. Zhou, S. Chen, J. Lou, J. Wang, Q. Yang, C. Liu & D. Huang, *"Graphene's cousin: the present and future of graphane"*, Nanoscale Research Letters **9**, 1 (2014)

[39] G. Sun, J. Kurti, P. Rajczy, M. Kertesz, J. Hafner & G. Kresse, *"Perfomance of the Vienna ab initio Simulation Package (VASP) in Chemical Applications"*, Journal of Molecular Structure: THEOCHEM **624**, 37 (2003)

[40] N. W. Ashcroft, N. D. Mermin & D. Wei, *"Solid State Physics"*, Cengage Learning (2016)

[41] J. McKelvey, *"Solid-State and Semiconductor Physics"*, Harper and Row (1966)

[42] P. Y. Yu & M. Cardona, *"Fundamentals of Semiconductors: Physics and Materials Properties."*, Springer (1996)

[43] J. Patterson & B. Bailey, *"Solid-State Physics"*, Springer (2010)

[44] H. P. Myers, *"Introductory Solid State Physics"*, Taylor & Francis (1997)

[45] C. Kittel, *"Introduction to Solid State Physics"*, John Wiley & Sons, Inc (2005)

[46] X. Tao, H. Chen, Y. Zhou, Q. Peng & Y. Ouyang, *"The formation energy and interaction energy of point defects in ZrC"*, Journal of Nuclear Materials **557**, 153235 (2021)

[47] S. Lebegue, M. Klintenberg, O. Eriksson & M. I. Katsnelson, *"Accurate electronic band gap of pure and functionalized graphane from GW calculations"*, Phys. Rev. **79**, 245117 (2009)

[48] P. Deak, B. Aradi, T. Frauenheim & E. Janzen, *"Accurate defect levels obtained from HSE06 range-separated hybrid functional"*, Phys. Rev. B **81**, 153203 (2010)

[49] P. Deak, *"Calculating the optical properties of defects and surfaces in wide band gap materials"*, Physica B **535**, 35 (2018)

[50] G. Thiering & A. Gali., *"Characterization of oxygen defects in diamond by means of density functional theory calculations"*, Phys. Rev. B **94**, 125202 (2016)

[51] M. Capelli, A. H. Heffernan, T. Ohshima, H. Abe, J. Jeske, A. Hope, A. D. Greentree, P. Reineck & B. C. Gibson, *"Increased nitrogen-vacancy centre creation yield in diamond through electron beam irradiation at high temperature"*, Carbon **143**, 714 (2018)

[52] J. A. Larsson & P. Delaney, *"Electronic structure of the nitrogen-vacancy center in diamond from first principles theory"*, Phys. Rev. B **77**, 165201 (2008)

[53] M. W. Doherty, N. B. Manson, P. Delaney & L. C. L. Hollenberg, *"The negatively charged nitrogen-vacancy centre in diamond: the electronic solution"*, New J. Phys **13**, 025019 (2011)

[54] J. C. Slater, *"Note on Hartree's Method"*, Phy **35**, 210 (1930)

[55] J. C. Slater, *"A Simplification of the Hartree-Fock Method"*, Phys. Rev. **81**, 385 (1950)

[56] P. E. Blochl, *"Projector augmented-wave method"*, Phys. Rev. B **50**, 17953 (1994)

[57] G. Burns, *"Solid State Physics"*, Academic Press Publishers (1985)

[58] J. L. Basdevant, *"Variational principles in physics"*, Springer nature (2023)

[59] C. Lanczos, *"The variational principles of mechanics"*, Courier Corporation (2012)

[60] M. C. Payne, M. P. Teter, D. C. Allan, T. A. Arias & J. D. Joannopoulos, *"Iterative minimization techniques for ab initio total-energy calculations: molecular dynamics and conjugate gradients"*, Reviews of Modern Physics **64**, 1045 (1992)

[61] R. M. Martin, *"Electronic Structure: Basic Theory and Practical Methods"*, Cambridge University Press (2004)

[62] J. MacDonald, *"Successive Approximations by the Rayleigh-Ritz Variation Method"*, Phys. Rev. **43**, 830 (1933)

[63] R. G. Parr & W. Yang, *"Density-Functional Theory of Atoms and Molecules"*, Oxford University Press, New York (1989)

[64] M. Born & R. Oppenheimer, *"Zur quantentheorie der molekeln"*, Annalen der physik **389**, 457 (1927)

[65] D. R. Hartree, *"The Wave Mechanics of an Atom with a Non-coulomb Central Field. Part 1. Theory And Methods"*, Mathematical Proceedings of the Cambridge Philosophical Society **24**, 89 (1928)

[66] V. Fock, *"Naherungsmethode zur Losung des quantenmechanischen Mehrkorperproblems"*, Zeitschrift fur Physik **61**, 126 (1930)

[67] E. H. Lieb & B. Simon, *"The Hartree-Fock Theory for Coulomb Systems"*, ", ed: W. Thirring, 299-308, Springer (1997)

[68] E. H. Lieb, *"Thomas-Fermi and related theories of atoms and molecules"*, Rev. Mod. Phys. **53**, 603 (1981)

[69] E. H. Lieb & B. Simon, *"The Thomas-Fermi theory of atoms, molecules and solids"*, Adv. in Math **23**, 22 (1977)

[70] P. Hohenberg & W. Kohn, *"Inhomogeneous electron gas"*, Phy **136**, B864 (1964)

[71] R. O. Jones & O. Gunnarsson, *"The density functional formalism, its applications and prospects"*, Rev. Mod. Phys. **61**, 689 (1989)

[72] C. D. Novaes, *"Reductio ad absurdum from a dialogical perspective"*, Philos. Stud. **173**, 2605 (2016)

[73] W. Kohn & L. J. Sham, *"Self-Consistent Equations Including Exchange and Correlation Effects"*, Phys. Rev. **140**, A1133 (1965)

[74] K. Burke, *"Kohn-Sham Equations: Teaching the Theory in Density Functional Theory"*, in *"CECAM-HQ-EPFL"*

[75] W. Koch & M. C. Holthausen, *"A Chemist's Guide to Density Functional Theory"*, WILEY-VCH (2000)

[76] G. F. Koster, *"Solid State Physics: Advances in Research and Applications"*, Academic Press Inc., New York (1957)

[77] M. Hamermesh, *"Group Theory and its Application to Physical Problems"*, Dover, Inc. New York (1962)

[78] H. Watanabe, *"A Proof of the Bloch Theorem for Lattice Models"*, Stat. Phys. **177**, 717 (2019)

[79] M. Cohen & J. Chelikowsky, *"Electronic Structure and Optical Properties of Semiconductors"*, Springer, Berlin (1989)

[80] E. Antonicik, *"A new formulation of the method of nearly free electrons"*, Czech. J. Phys. **4**, 439 (1954)

[81] J. C. Phillips & L. Kleinman, *"New method for calculating wave functions in crystals and molecules"*, Phys. Rev. **116**, L. Kleinman (1959)

[82] N. F. Andriambelaza, *"Band gap engineering of a MoS2 monolayer through transition metal and chalcogen alloying: an ab initio study"*

[83] C. V. Peaker, *"First principles study of point defects in diamond"*

[84] R. A. S. AL-Hamadany, *"Quantum Mechanical Study of Point and Molecular Defects in Perovskite Nano-systems."*

[85] A. Montanaro, *"Quantum speed up of Monte Carlo methods"*, Proc. Roy. Soc. Ser. A **471**, A. Montanaro (2015)

[86] P. F. Loos & P. M. W. Gill, *"The uniform electron gas"*, Computational Molecular Science **6**, 410 (2016)

[87] S. H. Vosko, L. Wilk & M. Nusair, *"Accurate spin-dependent electron liquid correlation energies for local spin density calculations: a critical analysis"*, Canadian Journal of Physics **58**, 80 (1980)

[88] U. von Barth & L. Hedin, *"A local exchange-correlation potential for the spin polarized case"*, Phys. C: Solid State Phys. **5**, 1629 (1972)

[89] D. C. Langreth & M. J. Mehl, *"Beyond the local-density approximation in calculations of ground-state electronic properties"*, Phys. Rev. B **28**, M. J. Mehl (1983)

[90] W. Yang, R. G. Parr & C. Lee, *"Various functionals for the kinetic energy density of an atom or molecule"*, Phys. Rev. A **34**, 4586 (1986)

[91] A. D. Becke, *"Density-functional thermochemistry III: The role of exact exchange"*, J. Chem. Phys **98**, 5648 (1993)

[92] A. D. Becke & E. R. Johnson, *"A simple effective potential for exchange"*, J. Chem. Phys **124**, 221101 (2006)

[93] A. D. Becke, *"Perspective: Fifty years of density-functional theory in chemical physics"*, J. Chem. Phys **140**, 301 (2014)

[94] S. Smiga & L. A. Constantin, *"Unveiling the Physics Behind Hybrid Functionals"*, J. Phys. Chem. A **124**, 5606 (2020)

[95] R. E. Mapasha, E. Igumbor, N. F. Andriambelaza & N. Chetty, *"Electronic properties of vacancies in bilayer graphane"*, Physica B **573**, 67 (2019)

[96] M. H. Naik & M. Jain, *"CoFFEE: Corrections For Formation Energy and Eigenvalues for charged defect simulations"*, Elsivier **226**, 114 (2018)